Dynamics of magnetic vortices and antivortices

Dissertation
zur Erlangung des Doktorgrades
des Fachbereichs Physik
der Universität Hamburg

vorgelegt von
André Drews

Hamburg
2009

Gutachter der Dissertation:	PD. Dr. Guido Meier Prof. Dr. Dietmar P. F. Möller
Gutachter der Disputation:	PD. Dr. Guido Meier Prof. Dr. D. Heitmann
Datum der Disputation:	08.04.2009
Vorsitzender des Prüfungsausschusses:	Dr. Tobias Kipp
Vorsitzender des Promotionsausschusses:	Prof. Dr. Robert Klanner
Dekan der MIN-Fakultät:	Prof. Dr. Heinrich Graener

Abstract

The dynamics of magnetic vortices and antivortices in ferromagnetic thin-film elements is investigated by numerical simulations and analytical calculations. For the numerical calculations the Landau-Lifshitz-Gilbert equation is solved by the Object Oriented Micromagnetic Framework (OOMMF). For the analytical calculations a two-dimensional oscillator model is used. The response of vortices and antivortices to external fields and spin-polarized currents is studied for increasing amplitudes of the exciting alternating magnetic fields and currents, which result in vortex motions in the linear, non-linear, and in the highly non-linear regime of vortex creation.

In the linear regime vortex dynamics is described by a harmonic oscillator model. Micromagnetic simulations yield the eigenfrequency and the damping of gyration in dependence on the size of the sample. The oscillator model is compared to the simulations. The elliptical shape of the trajectories and the phase between gyration and alternating excitation show good accordance. Resonance curves illustrate the dependence of the semiaxes and the phase on the exciting frequency. The harmonic oscillator model can be extended to a nonlinear oscillator model. The nonlinear equation of motion is solved by a Runge-Kutta-method. A comparison of the trajectories from this model with the trajectories from micromagnetic simulations yields the strength of the nonlinearities in dependence on the size of the sample. The limit between nonlinear gyration and the onset of the creation of vortices is estimated by a characteristic velocity of the vortex. In the highly non-linear regime of core gyration micromagnetic simulations reach their limits due to the formation of a magnetic singularity, the so-called Bloch point, where the polarization of the vortex core switches. A general description is used to explain the occurance of intermediate states at vortex formation.

Finally a possible application of vortices in memory cells is illustrated using the insights from the investigations of the linear and the highly non-linear regime. The write and the read process in the vortex random access memory (VRAM) or antivortex random access memory (AVRAM) are implemented by vortex core switching and gyration.

Zusammenfassung

In dieser Arbeit wird die Bewegung magnetischer Vortices und Antivortices in ferromagnetischen dünnen Schichten mit Hilfe von numerischen Simulationen und analytischen Rechnungen untersucht. Das verwendete mikromagnetische Simulationsprogramm Object Oriented Micromagnetic Framework (OOMMF) löst die Landau-Lifshitz-Gilbert Gleichung numerisch. Die analytischen Rechnungen werden mit einem zweidimensionalen Oszillatormodell durchgeführt. Dabei wird das dynamische Ansprechverhalten von Vortices und Antivortices auf externe Felder und spinpolarsierte Ströme betrachtet. Eine Anregung mit steigender Amplitude bewirkt eine Bewegung im linearen, nicht linearen und hochgradig nichtlinearen Bereich der Vortexentstehung.

Im linearen Bereich wird die Vortexbewegung mit einem harmonischen Oszillatormodell beschrieben. Mikromagnetische Simulationen ergeben die Eigenfrequenz und die Dämpfung der Gyration in Abhängigkeit von der Probengröße. Das Oszillatormodell und die Simulationen werden miteinander verglichen. Die elliptische Form der Trajektorien und die Phase zwischen Gyration und alternierender Anregung zeigen gute Übereinstimmung. Resonanzkurven stellen die Abhängigkeit der Halbachsen und der Phase von der Anregungsfrequenz dar. Das harmonische Oszillatormodell läßt sich auf ein nichtlineares Oszillatormodell erweitern. Die nichtlineare Bewegungsgleichung wird mit einem Runge-Kutta Verfahren gelöst. Ein Vergleich der Trajektorien des nichtlinearen Oszillatormodells mit den Trajektorieren der mikromagnetischen Simulationen ergibt die Stärke der Nichtlinearitäten in Abhängigkeit von der Probengröße. Die Grenze zwischen nichtlinearer Gyration und Vortexentstehung wird durch eine charakteristische Vortexgeschwindigkeit bestimmt. Im hochgradig nichtlinearen Bereich erreicht das mikromagnetische Modell seine Grenzen aufgrund der Entstehung einer magnetischen Singularität, des Bloch-Punkts, bei dem die Polarization des Vortexkerns umschaltet. Ein allgemeiner Formalismus beschreibt die Ursache für die Bildung der Zwischenzustände beim Vortexschalten.

Abschließend wird eine mögliche Anwendung von Vortices in Speicherzellen präsentiert. Dabei werden die Erkenntnisse über die Vortexdynamik aus den vorherigen Kapiteln benutzt. Der Schreib- und Leseprozess sind in dem Vortex Random Access Memory (VRAM) oder dem Antivortex Random Access Memory (AVRAM) über das Vortexschalten und die Vortexgyration realisiert.

Contents

1 Introduction **7**

2 Theoretical background **9**
2.1 Ferromagnetism 9
2.1.1 Spontaneous magnetization and Heisenberg model 10
2.2 Micromagnetic model 11
2.2.1 Landau-Lifshitz-Gilbert equation 12
2.2.2 Effective fields 12
2.2.3 Spin torque 14
2.3 Micromagnetic simulations 14
2.3.1 Numerical time integration of the magnetization 15

3 Static properties of vortices and antivortices **17**
3.1 Magnetic configurations 18
3.2 Geometrical and energetical considerations 20
3.2.1 Vortex-core radius and domain-wall width 21

4 Dynamics in the linear and non-linear regime **23**
4.1 Linear regime of vortex motion 23
4.1.1 Thiele equation and equation of motion of vortices 26
4.1.2 Vortices as harmonic oscillators 33
Publication 1 35
Publication 2 43
Publication 3 49
4.1.3 Amplitude of core gyration 55
Publication 4 57
4.2 Nonlinear dynamics of vortices and antivortices 65
4.2.1 Origin of nonlinear vortex gyration 65
4.2.2 Nonlinear equation of motion of vortices 66
4.2.3 Vortices as nonlinear oscillators 69
4.3 Switching of vortex and antivortex cores in the highly non-linear regime . 70
4.3.1 Intermediate states at core switching 70
4.3.2 Topological considerations 70
4.3.3 Critical velocities at switching 72
4.3.4 Limits of the micromagnetic model 73

5 Vortices in storage devices **75**
5.1 Logical states represented in vortices 75
5.2 Read and write process 76
5.3 Storage devices 77
Publication 5 79
Publication 6 85

6 Conclusion and Outlook **91**

7 Publications **93**

Bibliography **95**

8 Acknowledgments **101**

1 Introduction

Elements like nickel, iron, and cobalt as well as a great variety of alloys exhibit a collective interaction between the electron spins. This phenomenon causes a permanent magnetic moment leading to ferromagnetism that is of great interest concerning basic physics and technical applications. Industrial development of novel non-volatile storage devices like the Magnetoresistive Random Access Memory (MRAM) or the Racetrack Memory (RM) fuels magnetism on the micro- and nanometer scale.

A significant advance of the fundamental understanding of ferromagnetism was gained in 1928 by Heisenberg at the beginning of quantum mechanics when he proposed the exchange energy as the reason for the parallel alignment of electron spins in a ferromagnet. Since then different models besides the Heisenberg model such as the semiclassical micromagnetic model have been introduced to describe ferromagnetism in a simplified and phenomenological but solvable way.

In the past decades different developments allowed to study ferromagnetism in detail. Experimentally, new observation techniques like the magnetic-force microscope (MFM) or the spin-polarized scanning-tunneling microscope (SP-STM) made it possible to scrutinize ferromagnetic materials spatially resolved on the nanometer or subnanometer scale. X-ray microscopy based on the X-ray magnetic circular dichroism (XMCD) allowed to detect the dynamics of the magnetic moments in a ferromagnet with a high spatial and temporal resolution. Novel ferromagnetic alloys were fabricated to design ferromagnets with desired properties. For example, alloys with a high permeability like permalloy, which is considered in this work, strongly react to external fields. Numerically, the growth of computer power made it possible to simulate statics and dynamics of ferromagnetic microstructures with a resolution in the nanometer and subnanometer range by micromagnetic simulations.

Beside external magnetic fields, spin currents traversing ferromagnetic samples interact with their magnetic moments. This spin-torque effect gained high interest in recent years. While magnetoresistance effects like the giant magnetoresistance (GMR), the anisotropic magnetoresistance (AMR) or the tunneling magnetoresistance (TMR) have been technically utilized for decades, a theoretical description of the interaction between spin currents and the magnetic moments in ferromagnets was first proposed by Berger in 2002 and extended by Zhang and Li in 2004.

Magnetic vortices provide a fascinating field of research. These magnetic configurations possess magnetization cores with a diameter of a few nanometers pointing out-of-plane with a surrounding in-plane magnetization pattern. They occur in ferromagnetic thin-film elements. The flux-closured in-plane magnetization of vortices, called Landau pattern, was already theoretically predicted 1946 by Kittel [1] and experimentally observed 1957 by Coleman [2]. In general, vortices or similar structures are found in many different systems like in superfluids or Bose-Einstein condensates but also on large length scales in meteorology as tornados or in astrophysics as accretation discs or spiral galaxies. The dynamics of magnetic vortices can be studied in a controlable and reproducable way because the core moves in a confined potential when an external magnetic field or a spin current is applied. The magnetization of the vortex core is either up or down and is called polarization. Independent of the polarization, the orientation of the in-plane magnetization is either clockwise or anticlockwise. These magnetization orientations have been proposed to store binary data. Hence beside new fundamental physics, magnetic vortices and antivortices provide new technical possibilities for the realization of novel non-volatile storage devices.

In this thesis the dynamics of vortices and their topological counterparts, the antivortices, is investigated. A novel theoretical description of the core trajectory in the linear and nonlinear regime of excitation is outlined. The switching process of the orientation of the core magnetization is described and possible applications of a vortex as vortex random access memory (VRAM) or of an antivortex as antivortex random access memory (AVRAM) are presented.

2 Theoretical background

The Heisenberg model and the micromagnetic model are described in this chapter. The electron spins are assumed to be classical vectors. The focus of this work is on soft magnetic materials like permalloy.

2.1 Ferromagnetism

The fundamental object in ferromagnetism is the electron spin. The resulting elementary magnetic moment $\mathbf{m} = -\gamma\mathbf{S}$ lies along the same direction as the spin $\mathbf{S}$ and is proportional to it by the gyromagnetic ratio γ. The neglect of the orbital momentum $\mathbf{L}$ in the magnetic moment is a reasonable approximation for most of the transition metals [3]. The electron spins align parallel to each other due to the exchange interaction [4]. In competition to that they also orient into those directions, which avoid surface and volume charges of the magnetic moments to reduce the demagnetization energy. In soft magnets crystalline anisotropies caused by spin-orbit interaction are negligible and are not discussed in this thesis. In samples with a size smaller than some ten nanometers the exchange interaction dominates the interaction by the demagnetization field and a single magnetic domain [5] of parallel aligned magnetic moments is formed. Above a size of a few hundred nanometers the larger the ferromagnet the higher is the number of magnetic domains. In domain walls [6], the boundaries between the domains, the magnetic moments change their angles smoothly. If an external magnetic field $\mathbf{H}$ is applied to a soft magnetic material, the magnetic moments orient towards the direction of the field and the number of domains decreases in dependence on the strength of the field, see Figs. 2.1 (a) and 2.1 (b). The resetting of the domains and the domain walls proceeds in discrete Barkhausen jumps [7].

Ferromagnets can be classified by their response to an external field, the magnetic susceptibility [8]

$$\chi = \frac{\partial M_H}{\partial H}. \tag{2.1}$$

The magnetization $\mathbf{M}$ is the sum over the magnetic moments $\mathbf{m}$ times their density and M_H is the component of the magnetization in the direction of the applied field $\mathbf{H}$. The larger the susceptibility the stronger the field couples to the magnetic moments and the softer is the ferromagnet. The permeability $\mu_r = [1 + M_H(\chi, H)/H]$ describes the response of the magnetic flux density $\mathbf{B}$ in a sample to an external field $\mathbf{H}$. Permalloy ($Fe_{20}Ni_{80}$)

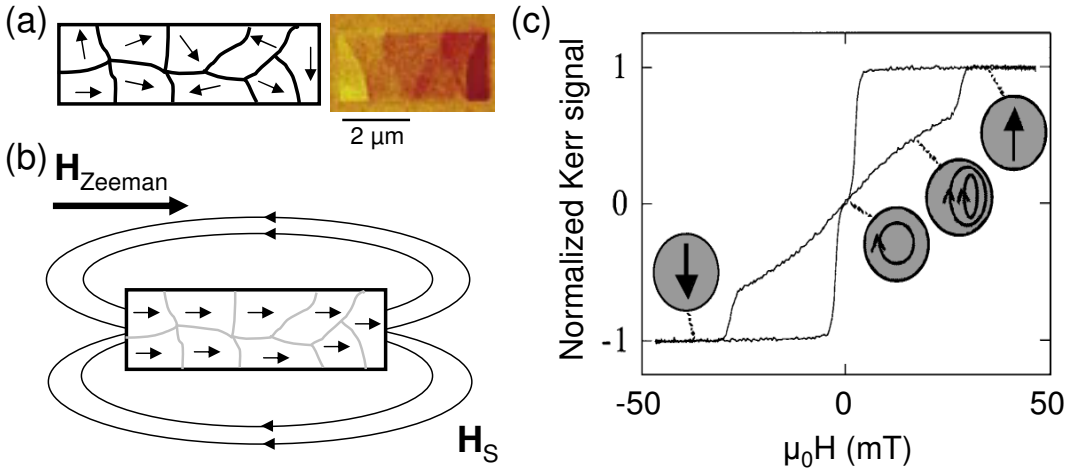

Fig. 2.1: (a) Sketch and magnetic-force micrograph [11] of the magnetic domains in a ferromagnetic rectangle. (b) Orientation of the magnetic moments of the domains into the direction of an external field **H**. The parallel aligned magnetic moments generate a stray field $\mathbf{H}_s$ due to the magnetic surface charges. (c) Kerr measurement of a hysteresis loop of a soft magnetic disk [10]. The sketches show the magnetic configurations.

possesses a permeability of $\mu_r = 8000$ for a magnetic flux density of $B = 2$ mT, which is larger than that of other ferromagnets like iron ($\mu_r = 200$) or nickel ($\mu_r = 100$) [9]. Another common way to classify ferromagnets is the hysteresis, as illustrated in Fig. 2.1 (c). An irreversible hysteresis loop $M_H(H)$ can be obtained by a cycle of first increasing an applied field until it is large enough to saturate the ferromagnet, then decreasing it to zero and increasing it in the opposite direction until the ferromagnet is saturated again. Different magnetic configurations occur during a hysteresis loop. They depend on the geometry and on the material. In permalloy squares of a lateral size of a few hundred nanometers a vortex state occurs in the absence of a field, in the so-called remanence state [10].

2.1.1 Spontaneous magnetization and Heisenberg model

The parallel alignment of electron spins is due to the exchange interaction [4], which follows from the Pauli principle and the Coulomb repulsion between electrons. A simple example are two electrons with the spins $s = 1/2$, which add to the $S = 0$ singlet state or the $S = 1$ triplet states. The total spin states are $2S+1$ fold degenerate. The fact of antisymmetric wavefunctions of the electrons leads to different eigenfunctions for the singlet and triplet states. The exchange integral

$$J_{ij} = (E_S - E_T)/2 = \frac{1}{4\pi\varepsilon_0} \int \psi_i(\mathbf{r}_1)^* \psi_j(\mathbf{r}_2)^* \frac{e^2}{|\mathbf{r}_1 - \mathbf{r}_2|} \psi_i(\mathbf{r}_2) \psi_j(\mathbf{r}_1) d\mathbf{r}_1 d\mathbf{r}_2 \tag{2.2}$$

is defined as the difference between the energies of the singlet state E_s and the triplet states E_T. According to the Heisenberg Hamiltonian $\widehat{H} = -J_{ij}\mathbf{S}_i \cdot \mathbf{S}_j$ for the exchange interaction between two neighboring spins $\mathbf{S}_i$ and $\mathbf{S}_j$ the exchange integral for a ferromagnet $J_{ij} > 0$ as $E_S > E_T$. Then a parallel spin configuration is favored [3, 12]. For an antiferromagnet $J_{ij} < 0$ and the spins align antiparallel to each other.

Generalizing the exchange interaction between two electron spins to the exchange interactions between many spins on a crystal lattice leads to the Heisenberg model [3, 13]. The Heisenberg Hamiltonian reads

$$\widehat{H} = -J_{ij}\sum_{i,j}\mathbf{S}_i \cdot \mathbf{S}_j, \tag{2.3}$$

where J_{ij} is the exchange integral between the spins $\mathbf{S}_i$ and $\mathbf{S}_j$. As the exchange interaction is of short range the indices i, j run over the next neighbors only. Starting with the time evolution of the spin $\mathbf{S}_i$ in the Heisenberg picture, evaluating the commutator in a Taylor expansion, and using the commutation relations of the spin operator yields [14]

$$\frac{d\mathbf{S}_i}{dt} = -\frac{1}{\hbar}\mathbf{S}_i \times \frac{d\widehat{H}}{d\mathbf{S}_i}. \tag{2.4}$$

The term on the right $d\widehat{H}/d\mathbf{S}_i = -J_{ij}\sum_j \mathbf{S}_j$ can be considered as an effective field of neighboring spins around which the spin $\mathbf{S}_i$ gyrates. The extended Heisenberg model, which includes the coupling of the magnetic moments to their dipole fields and to an external field with a magnetic flux density $\mathbf{B}$, reads

$$\widehat{H} = -J_{ij}\sum_{i,j}\mathbf{S}_i \cdot \mathbf{S}_j - \frac{d}{2}\sum_{i,j}\frac{3(\mathbf{S}_i \cdot \mathbf{e}_{ij}) \cdot \mathbf{e}_{ij} \cdot \mathbf{S}_j - \mathbf{S}_i \cdot \mathbf{S}_j}{\mathbf{r}_{ij}^3} - |\mathbf{m}|\mathbf{B} \cdot \sum_i \mathbf{S}_i. \tag{2.5}$$

Here d is the strength of the dipole coupling between the spins and $\mathbf{e}_{ij}$ is the unit vector that points into the direction of the distance vector $\mathbf{r}_{ij}$ between the spins.

2.2 Micromagnetic model

Micromagnetism describes a ferromagnetic body by a continuous vector field of classical magnetization vectors $\mathbf{M}$ [15, 16]. The magnetization vectors are spatial averages over the discrete elementary magnetic moments $\mathbf{m}$ of the electron spins. The micromagnetic model is used to describe ferromagnetism semiclassically on length scales of some ten nanometers to some hundred microns, which would be too complex to be calculated quantum mechanically. The interaction between the magnetization vectors is modeled by effective fields, which have their origin in internal forces like the exchange coupling or the demagnetization coupling and external fields like the Zeeman field.

2.2.1 Landau-Lifshitz-Gilbert equation

An external field $\mathbf{H}$ exerts a torque $d\mathbf{S}/dt = -\gamma^{-1} d\mathbf{m}/dt$ on the magnetic moment $\mathbf{m}$ if the direction of the magnetic moment is non-collinear to the field. This leads to a gyroscopic motion of the magnetic moment around the field according to the equation

$$\frac{d\mathbf{m}}{dt} = -\gamma \mathbf{m} \times \mathbf{H}. \tag{2.6}$$

The gyroscopic term

$$\frac{d\mathbf{M}}{dt} = -\gamma \mathbf{M} \times \mathbf{H}_{\mathsf{eff}} \tag{2.7}$$

of the Landau-Lifshitz-Gilbert equation describes the motion of the magnetization in an effective field H_{eff}. Gilbert introduced a phenomenological damping which encounters the gyration for example due to crystal impurities [17, 18]. In the Gilbert form of the Landau-Lifshitz equation

$$\frac{d\mathbf{M}}{dt} = -\gamma \mathbf{M} \times \mathbf{H}_{\mathsf{eff}} + \frac{\alpha}{M_s} \mathbf{M} \times \frac{d\mathbf{M}}{dt}. \tag{2.8}$$

the damping term leads to a motion of the magnetization, perpendicular to the velocity of the magnetization due to the gyroscopic term, into the direction of the effective field. In this equation the Gilbert damping parameter α determines the strength of the damping. At equilibrium both terms vanish to get a vanishing torque, which is the case for a collinear alignment of magnetization and effective field.

2.2.2 Effective fields

The effective field $\mathbf{H}_{\mathsf{eff}} = \mathbf{H}_{ex} + \mathbf{H}_d + \mathbf{H}_{Zeeman}$ in the Landau-Lifshitz-Gilbert equation is a sum of internal effective fields like the exchange and the demagnetization field as well as external fields like the Zeeman field. The internal anisotropy field, which describes the coupling between the magnetization vectors due to lattice symmetries [16], is not mentioned here because it is generally small in soft magnetic materials and negligible in permalloy.

The exchange energy between two magnetization vectors can be derived by starting from the Heisenberg Hamiltonian of two spins $\mathbf{S}_i$ and $\mathbf{S}_j$

$$\widehat{H} = -J\mathbf{S}_i \cdot \mathbf{S}_j = -J|\mathbf{S}_i||\mathbf{S}_j|\cos(\phi). \tag{2.9}$$

When the cosine is expanded into a Taylor series assuming only small angles between the spins and the zero of the total energy is shifted by the constant term $-J|\mathbf{S}_i||\mathbf{S}_j|$ the

exchange energy density reads

$$\widehat{H} = \frac{J}{a^3}|\mathbf{S}_i||\mathbf{S}_j|(\frac{\phi^2}{2}) \approx \frac{J}{2M_s^2 \cdot a}(\nabla \mathbf{M})^2 = \frac{A}{M_s^2}(\nabla \mathbf{M})^2. \tag{2.10}$$

Here a is the lattice constant, $\phi \approx |a\nabla \mathbf{M}|/M_s$ the angle between the spins, M_s the saturation magnetization, and $A = J/2a$ the exchange constant. The exchange energy of a ferromagnetic body results from a volume integration of Eqn. 2.10

$$E_{ex} = \frac{A}{M_s^2}\int (\nabla \mathbf{M})^2 dV. \tag{2.11}$$

The exchange field $\mathbf{H}_{ex}$ follows from the variational derivative of the exchange energy [14, 16]

$$\mathbf{H}_{ex} = -\frac{1}{\mu_0}\frac{\delta E_{ex}}{\delta \mathbf{M}} = \frac{2A}{\mu_0 M_s^2}\nabla^2 \mathbf{M}. \tag{2.12}$$

The demagnetization field can be derived from the Maxwell equations $\nabla \times \mathbf{H}_d = 0$ and $\nabla \cdot \mathbf{B}_d = 0$ in a ferromagnetic body [19]. Therefore the magnetic field is a gradient of a potential $\mathbf{H}_d = -\nabla \Phi_M(\mathbf{r})$, where

$$\Phi_M(\mathbf{r}) = \frac{1}{4\pi}\int \mathbf{M}(\mathbf{r}') \cdot \nabla'(\frac{1}{|\mathbf{r}-\mathbf{r}'|})dV'. \tag{2.13}$$

When a demagnetization tensor

$$\mathbf{N}_{ij} = \frac{1}{4\pi}\nabla_i \nabla'_j(\frac{1}{|\mathbf{r}-\mathbf{r}'|}) \tag{2.14}$$

is introduced [20], the demagnetization field becomes

$$\mathbf{H}_d = -\int \mathbf{N}(\mathbf{r}-\mathbf{r}')\mathbf{M}(\mathbf{r}')dV' \tag{2.15}$$

and the demagnetization energy is

$$E_d = \frac{\mu_0}{2}\int\int \mathbf{M}(\mathbf{r})\mathbf{N}(\mathbf{r}-\mathbf{r}')\mathbf{M}(\mathbf{r}')dV'dV = -\frac{\mu_0}{2}\int \mathbf{H}_d \cdot \mathbf{M}(\mathbf{r})dV. \tag{2.16}$$

With the Zeeman field $\mathbf{H}_{Zeeman}$ the Zeeman energy reads

$$E_{Zeeman} = -\mu_0 \int \mathbf{H}_{Zeeman} \cdot \mathbf{M}dV. \tag{2.17}$$

2.2.3 Spin torque

Itinerant spin-polarized electrons exert a torque on a nonuniform magnetization [21, 22]. This spin-torque can be derived from the exchange interaction

$$\widehat{H}_{sd} = \frac{|\mathbf{S}|J}{M_s}\mathbf{s}\cdot\mathbf{M}(\mathbf{r},t) \tag{2.18}$$

between an itinerant electron spin $\mathbf{s}$ and the localized electron spin $\mathbf{S}$, where $|\mathbf{S}|$ is the magnitude of the localized spin in the ferromagnet and J is the exchange integral. The localized spin $\mathbf{S} = -\mathbf{M}(\mathbf{r},t)|\mathbf{S}|/M_s$ is described by the magnetization. The itinerant spins $\mathbf{s}$ satisfy the continuity equation

$$\frac{d\mathbf{s}}{dt} + \nabla\cdot\widehat{\mathbf{j}} = -\frac{1}{ih}([\mathbf{s},\widehat{H}_{sd}] + [\mathbf{s},\widehat{H}_{scat}]), \tag{2.19}$$

where $\widehat{\mathbf{j}}$ is the spin-current operator, $[\mathbf{s},\widehat{H}_{sd}]$ is the torque due to the exchange interaction and $[\mathbf{s},\widehat{H}_{scat}]$ represents the torque due to the spin relaxation as a consequence of scattering at impurities. Some conversions of Eqn. 2.18 and Eqn. 2.19 and approximations yield the extended Landau-Lifshitz-Gilbert equation [21]

$$\begin{aligned}\frac{d\mathbf{M}}{dt} = -\gamma\mathbf{M}\times\mathbf{H}_{\text{eff}} + \frac{\alpha}{M_s}\mathbf{M}\times\frac{d\mathbf{M}}{dt} - \frac{b_j}{M_s^2}\mathbf{M}\times(\mathbf{M}\times(\mathbf{j}\cdot\nabla)\mathbf{M}) \\ -\frac{\xi b_j}{M_s}\mathbf{M}\times(\mathbf{j}\cdot\nabla)\mathbf{M},\end{aligned} \tag{2.20}$$

where $b_j = \mu_B P/[eM_s(1+\xi^2)]$ is the coupling constant between the itinerant spins and the magnetization, μ_B the Bohr magneton, P the spin polarization of the current, $\xi = \tau_{ex}/\tau_{sf}$ the ratio between the exchange relaxation time τ_{ex} and the spin flip relaxation time τ_{sf}, and $\mathbf{j}$ the electrical current density. The third term in Eqn. 2.20 describes the adiabatic spin torque, where the electron spin is assumed to be parallel to the magnetization. The fourth term, the non-adiabatic spin torque, includes deviations from the parallel alignment between electron spin and magnetization. The focus of this work lies on the spin torques generated by the nonuniform magnetization, temporal spin torques are not considered further like in Ref. [21].

2.3 Micromagnetic simulations

Usually the nonlinear Landau-Lifshitz-Gilbert equation can only be solved numerically. In the numerical calculations the continuous magnetization $\mathbf{M}(\mathbf{r},t)$ and the effective fields $\mathbf{H}(\mathbf{r},t)$ are discretized in space $\mathbf{r}_i$ and time t_i by mapping them onto grids of simulation cells, which represent the ferromagnetic body. In the finite difference method (FDM), as employed in the Object Oriented Micromagnetic Framework (OOMMF), equidistant simulation cells with a rectangular shape are used. In the numerical integration of the

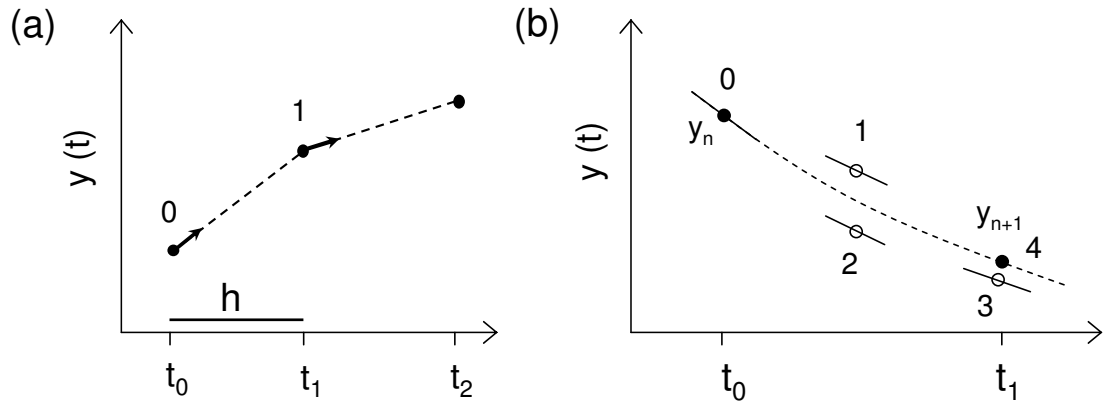

Fig. 2.2: (a) Runge-Kutta method of first order, also called Euler method. It extrapolates by the derivative of the function from the initial point 0 to the next simulation step: $y_{n+1} = y_n + hf(t_i, y_n)$. (b) Runge-Kutta method of fourth order. For each time step the derivative is evaluated four times: at the initial point 0, twice at the trial midpoints 1, 2, and at the trial endpoint 3. The final function values are shown as filled dots, the function values that are discarded once their derivatives have been calculated as open dots.

Landau-Lifshitz-Gilbert equation the magnetization evolves in discete time steps Δt by the interaction with the effective field.

2.3.1 Numerical time integration of the magnetization

The numerical time integration of the magnetization is partitioned into two parts. Before each time step Δt the effective field $\mathbf{H}_{\text{eff}}$ is calculated and inserted into the discrete Landau-Lifshitz-Gilbert equation. Then the solution of the Landau-Lifshitz-Gilbert equation yields the magnetization for the next time step $\mathbf{M}(\mathbf{r}_i, t_i + \Delta t)$.

The Laplace operator of the exchange field in Eqn. 2.12 in the finite difference method is represented by [23]

$$\mathbf{H}_{ex} = \frac{2A}{\mu_0 M_s^2 \, (\Delta \mathbf{r})^2} (\mathbf{M}_{i+1,j,k} + \mathbf{M}_{i-1,j,k} + \mathbf{M}_{i,j+1,k} + \mathbf{M}_{i,j-1,k} + \mathbf{M}_{i,j,k+1} + \mathbf{M}_{i,j,k-1} - 6\mathbf{M}_{i,j,k}). \tag{2.21}$$

where i, j, k are the indices of the simulation cells and $\Delta \mathbf{r}$ denotes the distance between the simulation cells in the direction of the coordinates. The algorithm for the calculation of the exchange field has a time complexity of O(n)=n. In OOMMF simulations the calculation of the exchange field needs less than 10 % of the calculation time. To calculate the demagnetization field a fast Fourier transformation (FFT) is performed to transform the convolution in Eqn. 2.15 to a product

$$\mathbf{H}_{d_i} = \sum_j N_{ij} M_j = \mathbf{N}_{ij} * \mathbf{M}_j = \text{iFFT}[\text{FFT}(\mathbf{N}_{ij}) \cdot \text{FFT}(\mathbf{M}_j)]. \tag{2.22}$$

This decreases the time complexity from O(n^2) to O(nlog(n)) since the multiplication has a complexity of O(n) and the fast Fourier transformation has a complexity of O(log(n)). An inverse fast Fourier transformation (iFFT) gives the spatially resolved demagnetization field. Despite the acceleration by the fast Fourier transformation the demagnetization field needs about 80% of the calculation time [24].

The discrete explicit Landau-Lifshitz-Gilbert equation including the spin-torque effect reads

$$\begin{aligned}\frac{\Delta\mathbf{M}(\mathbf{r}_i,t_i)}{\Delta t_i} &= -\frac{\gamma}{(1+\alpha^2)}\mathbf{M}(\mathbf{r}_i,t_i)\times\mathbf{H}_{\text{eff}}(\mathbf{r}_i,t_i) - \\ &\frac{\alpha\gamma}{M_s(1+\alpha^2)}\mathbf{M}(\mathbf{r}_i,t_i)\times[\mathbf{M}(\mathbf{r}_i,t_i)\times\mathbf{H}_{\text{eff}}(\mathbf{r}_i,t_i)] - \\ \frac{b_j}{M_s^2(1+\alpha^2)}(1+\alpha\xi)\mathbf{M}(\mathbf{r}_i,t_i)\times[\mathbf{M}(\mathbf{r}_i,t_i)\times(\mathbf{j}\cdot\frac{\Delta}{\Delta\mathbf{r}_i})\mathbf{M}(\mathbf{r}_i,t_i)] - \\ &\frac{b_j}{M_s(1+\alpha^2)}(\xi-\alpha)\mathbf{M}(\mathbf{r}_i,t_i)\times(\mathbf{j}\cdot\frac{\Delta}{\Delta\mathbf{r}_i})\mathbf{M}(\mathbf{r}_i,t_i).\end{aligned} \tag{2.23}$$

After the calculation of the effective fields Eqn. 2.23 is integrated [25]. To solve a differential equation by a Runge-Kutta method of fourth order [26], a Taylor expansion of the function $y(t)$ in time is performed until the fourth order as shown in Fig. 2.2 (b). This expansion is numerically realized by an interpolation

$$y(t_{i+1}) = y(t_i) + \frac{k_1}{6} + \frac{k_2}{3} + \frac{k_3}{3} + \frac{k_4}{6} + O(h^5) \tag{2.24}$$

with the four evaluating points $k_1 = h\ f(t_i, y(t_i))$, $k_2 = h\ f(t_i + \frac{h}{2}, y(t_i) + \frac{k_1}{2})$, $k_3 = h\ f(t_i + \frac{h}{2}, y(t_i) + \frac{k_2}{2})$, and $k_4 = h\ f(t_i + h, y(t_i) + k_3)$. The step size is h. After each time step the result $y(t_{i+1})$ can be compared to the result of a fifth order Runge-Kutta method to adapt the step size h. Step size control is used to reduce the calculation time by a maximum step size for a given error limit. In OOMMF the Runge-Kutta method is used to determine the time dependence of the magnetization $\mathbf{M}(\mathbf{r}_i,t_i)$ by the integration of Eqn. 2.23.

The micromagnetic model is limited. It cannot describe ferromagnetism quantum-mechanically because it is a semiclassical continuum theory. Due to the spatial average over the elementary magnetic moments of the magnetization large angles between the magnetization vectors are forbidden. In micromagnetic simulations the simulation cell size must be smaller than the exchange length $l = \sqrt{2A/\mu_0 M_s^2}$, which for permalloy is about 6 nm. Only then micromagnetic structures can be resolved properly. The temporal resolution is restricted by the numerical inaccuracy. The main memory of the employed computer restricts the number of simulation cells.

3 Static properties of vortices and antivortices

Magnetic vortices are magnetic configurations with an in-plane magnetization and an out-of-plane core of the magnetization [27]. They are formed in soft magnetic thin-film elements with a lateral size of a few hundred nanometers to some microns when the demagnetization energy forces the magnetization to align parallel to the sample's surface, which for thin films is the in-plane direction. At the vortex's center region, where magnetization vectors would align antiparallel to each other, the exchange energy leads to an alignment of the magnetization vectors out-of-plane either up or down and thus forms the magnetization core. Magnetic vortices possess a rotationally symmetrical in-plane magnetization with the vortex core as symmetry axis. They occur for example in permalloy squares, see Fig. 3.1 (a), or in disks [28]. The in-plane magnetization of a magnetic antivortex has a two-fold symmetry with the antivortex core as symmetry axis. Antivortices appear for example in infinity-shaped or clover-shaped samples [29]. Such a structure is shown in Fig. 3.1 (c), (d).

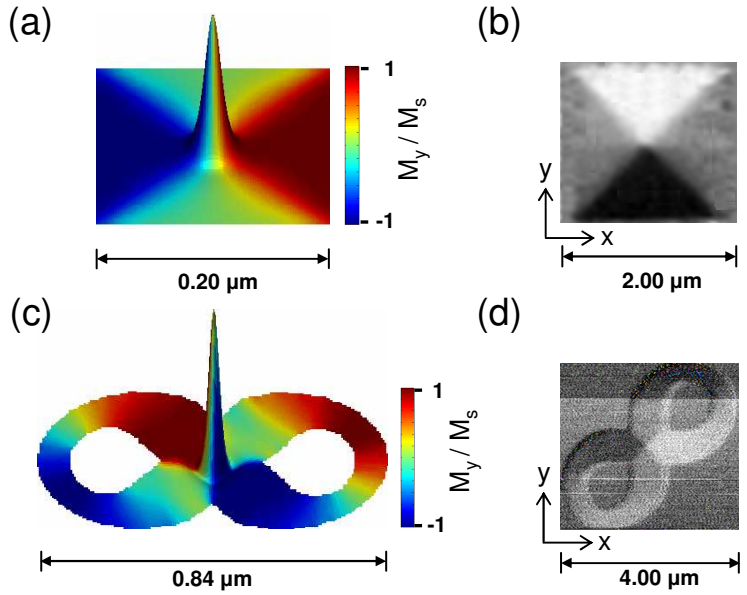

Fig. 3.1: (a) Simulation and (b) soft x-ray micrograph of a Landau pattern in a permalloy square [30]. The vortex core is at the center of the structure. (c) Simulation and (d) soft x-ray micrograph [31] of an antivortex at the center of an infinity-shaped sample. The colorbars show the y-component of the magnetization.

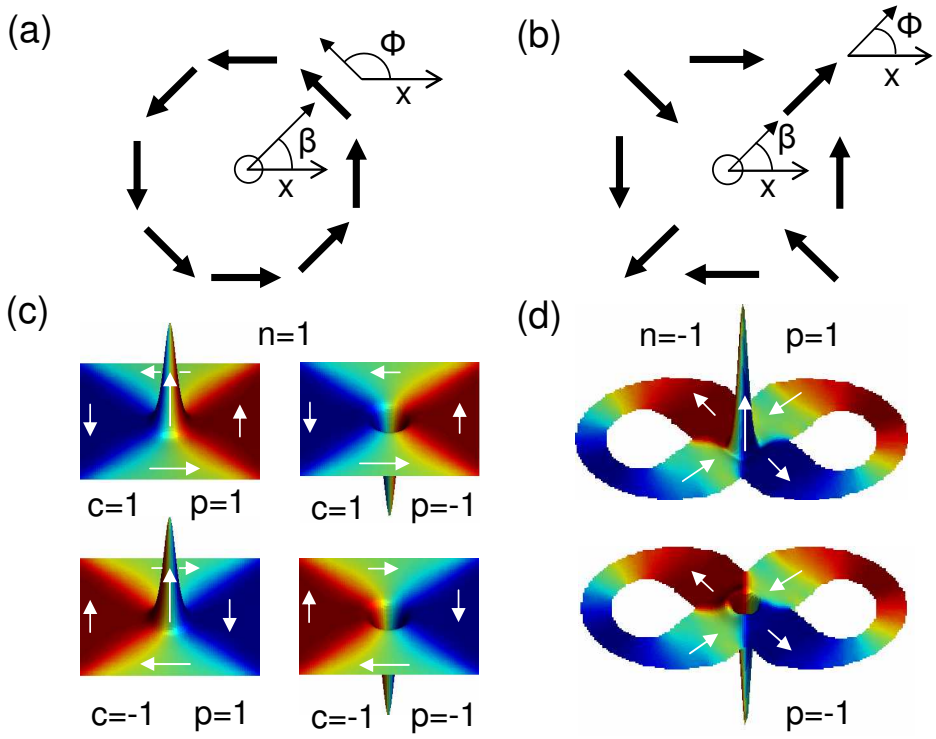

Fig. 3.2: (a) Vortex ($n = 1$) and (b) antivortex ($n = -1$) with chirality $c = (\phi - \beta)\frac{\pi}{2} = 1$ and c-value $c = (\phi + \beta)\frac{\pi}{2} = 1$, respectively. (c) Vortex ground states in a square and (d) antivortex ground states in an infinity-shaped sample.

3.1 Magnetic configurations

The magnetic configurations of vortices and antivortices are characterized by the winding number n, the chirality c for vortices or the c-value for antivortices, and the polarization p as illustrated in Fig. 3.2. To consider the characteristics of vortices and antivortices, we put their cores at the origin of a cartesian coordinate system and choose the x-axis as the axis of reference, see Figs. 3.2 (a) and 3.2 (b). The in-plane magnetization can be described by the relation

$$\phi(\beta) = n\beta + \frac{c\pi}{2}, \tag{3.1}$$

where ϕ is the angle between the local magnetization and the x-axis and β is the angle between the position vector, that points to the local magnetization, and the x-axis. The winding number describes the curling magnetization of vortices (n = 1), as shown in Fig. 3.2 (c), or the crossing magnetization of antivortices (n = -1), as illustrated in Fig. 3.2 (d). The chirality c gives the orientation of the in-plane magnetization for a vortex curling either clockwise (c = -1) or anticlockwise (c = 1) around the core. In case of antivortices the orientation of the in-plane magnetization varies when the sample is rotated. Therefore the distinct x-axis is chosen to define an unambiguous c-value for antivortices [32]. The c-value can assume values between c = -2 and c = 2.

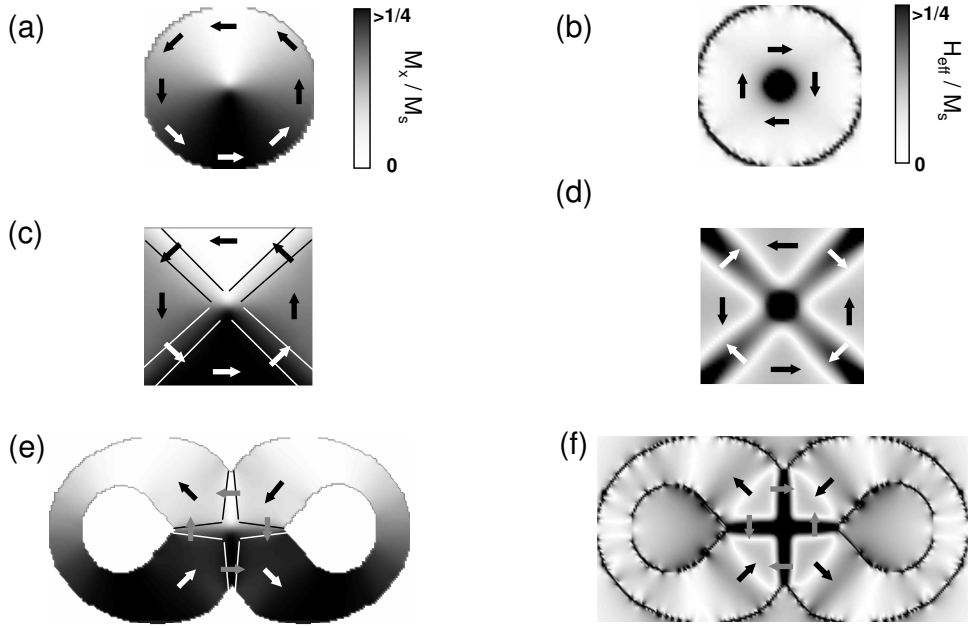

Fig. 3.3: Simulated magnetization configurations of a vortex in (a) a disk, (c) a square, and (e) of an antivortex in an infinity-shaped sample. (b), (d), and (f) corresponding effective fields. The colorbars show the strength of the x-component of the magnetization and the effective field. The arrows denote magnetization vectors. Black and white lines illustrate the domain walls.

The polarization p describes the magnetization direction of a vortex or antivortex core pointing up (p = 1) or down (p = -1) out-of-plane, as illustrated in Figs. 3.2 (c) and 3.2 (d).

The whole magnetization of a vortex state can be described by minimizing the total energy

$$E_{tot} = E_{ex} + E_d = \int \left\{ A \sum_{i=1}^{3} \frac{1}{M_s^2} [\nabla \mathbf{M}_i(\mathbf{r})]^2 - \frac{\mu_0}{2} \mathbf{H}_d \cdot \mathbf{M}(\mathbf{r}) \right\} dV. \tag{3.2}$$

The index i runs over the components of the magnetization, A is the exchange constant and $\mathbf{H}_d$ is the demagnetization field. In general the magnetization is given in spherical coordinates $\mathbf{M}(M_s, \phi, \theta)$ and the angles $\phi(\mathbf{r})$, $\theta(\mathbf{r})$ are functions of the position vector $\mathbf{r}$. In case of a disk it is most convenient to choose cylindrical coordinates ρ, ϕ, z. Additionally to these coordinates the out-of-plane component of the magnetization is described by the out-of-plane angle θ. Then the components of the magnetization $\mathbf{M}$ read $M_\rho = 0$, $M_\phi = \mathbf{M}_s \sin(\theta)$ and $M_z = \mathbf{M}_s \cos(\theta)$ [33]. The total energy is given by [34]

$$E_{tot} = 2\pi t \int_0^R \left\{ A \left[\left(\frac{d\theta}{d\rho} \right)^2 + \frac{\sin^2 \theta}{\rho^2} \right] + K_1 \sin^2 \theta \right\} \rho \, d\rho, \tag{3.3}$$

where t is the thickness of the sample. The last term $K_1 \sin^2 \theta$ approximates the demagnetization energy by an energetical penalty for magnetization vectors pointing out-of-plane,

where K_1 is similar to an anisotropy constant. The Euler-Lagrange equation applied to Eqn. 3.3 leads to the differential equation

$$-\frac{1}{\rho}\frac{d}{d\rho}\left(\rho\frac{d\theta}{d\rho}\right)+\frac{\sin\theta\cos\theta}{\rho^2}+\frac{K_1}{A}\sin\theta\cos\theta=0. \tag{3.4}$$

The solution of Eqn. 3.4 gives the out-of-plane angle of the magnetization θ, which reads

$$\theta = 2\arctan(\rho/r_{vc}) \tag{3.5}$$

when the term $\frac{K_1}{A}\sin\theta\cos\theta$ is neglected [34]. Here r_{vc} is the radius of the vortex core.
For a vortex in a square cartesian coordinates can be chosen for the position vectors. To include the edges of the square additional energy penalty terms have to be considered. Usually the resulting differential equation gets nonlinear and can only be solved numerically.
Micromagnetic simulations yield an exact solution for the magnetization pattern of vortices. Here exact means that no further assumptions are made and numerical inaccuracies are ignored. In a disk the in-plane magnetization isotropically surrounds the vortex core as shown in Fig. 3.3 (a). In a square there are four domains and four 90° domain walls as illustrated in Fig. 3.3 (c). The antivortex also contains, in addition to the antivortex core, four domains and four 90° domain walls, which is a result of the crossing in-plane magnetization, see Fig. 3.3 (e).
The effective fields follow from the magnetic configurations. Micromagnetic simulations show that for vortices in squares and antivortices in infinity-shaped samples the effective field in the domain walls points opposite to the direction of the magnetization. This is a consequence of the relation div$\mathbf{H}_d$=− div$\mathbf{M}$ between the demagnetization field and the magnetization. In the domains the effective field points into the same direction as the magnetization as shown in Fig. 3.3. The strength of the field in the domain walls is about one magnitude larger than that in the domains. In a disk the effective field always points into the direction opposite to the magnetization.

3.2 Geometrical and energetical considerations

The formation of vortices depends on the size and shape of the sample because the demagnetization energy [16]

$$E_d = M_s\int\lambda(\mathbf{r})\Phi_d(\mathbf{r})dV+\int\sigma(\mathbf{r})\Phi_d(\mathbf{r})dS \tag{3.6}$$

depends on the sample's geometry due to the surface charges $\sigma=\mathbf{n}\cdot\mathbf{M}$ and the volume charges λ =div$\mathbf{M}$. The potential of the demagnetization field is Φ_d. The larger the lateral size of a sample, the higher the number of possible surface charges and thus the stronger the demagnetization energy contribution to the total energy. To minimize the

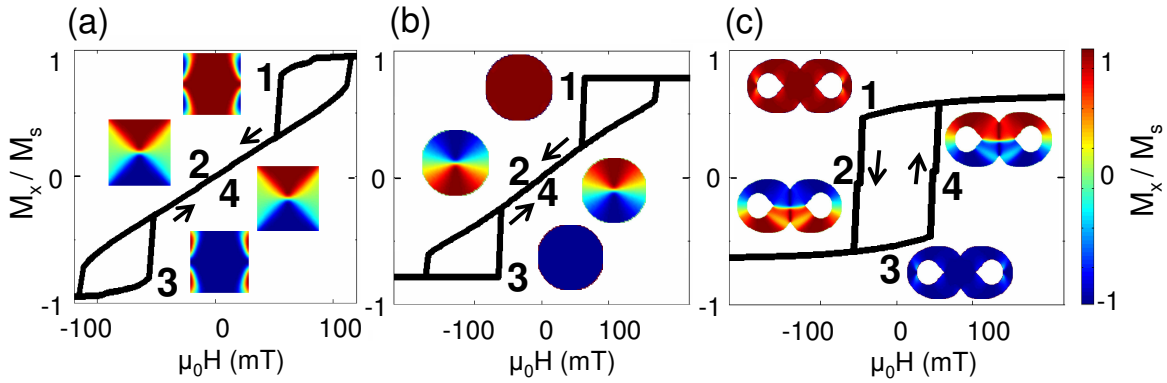

Fig. 3.4: Simulated hysteresis of (a) a square ($200 \times 200 \times 60$ nm^3), (b) a disk ($200 \times 200 \times 60$ nm^3), and (c) an infinity-shaped sample ($840 \times 400 \times 70$ nm^3). The field is applied in the x-direction in steps of $\mu_0 \Delta H = 4$ mT. The numbers denote the positions of the magnetic configurations shown on the hysteresis loop.

number of magnetic charges non-uniform magnetization configurations like vortices are preferred. The exchange energy tries to avoid a gradient of the magnetization and hence only depends on the sample geometry when there is a large gradient. Below a critical length of the sample the exchange energy overcomes the demagnetization energy and a monodomain is formed [35]. Above the critical radius of a disk the vortex represents the global energetical minimum. In squares the vortex is an energetical minimum as well. However, due to the edges, magnetic configurations like flower states or S-states are more prominent than in a disk, as shown in Figs. 3.4 (a) and 3.4 (b). The magnetic configurations in a sample of a certain geometry can be obtained from its hysteresis as illustrated in Fig. 3.4. The magnetic configurations at remanence for varying thicknesses and lengths of a certain sample shape are summarized in a phase diagram [10].

3.2.1 Vortex-core radius and domain-wall width

From the analytical result of the out-of-plane component M_z of the magnetization of a vortex core in Eqn. 3.5 the relation $r_{vc} \propto t^{1/3}$ between the vortex-core radius and the sample thickness follows [34]. Micromagnetic simulations of the core radius r_{vc} in disks as well as in squares for different lengths and thicknesses depicted in Fig. 3.5 (b) confirm this result. The out-of-plane component of the magnetization M_z is fitted by a spline interpolation and the core radius is defined for magnetization vectors with an out-of-plane component M_s/e, where M_s is the saturation magnetization and e is Euler's constant, see Fig. 3.5 (a).

Micromagnetic simulations in Fig. 3.5 (c) show an increase of the widths of the domain walls for an increase of the lateral size of the squares. A decrease of the sample thickness leads to an increase of the domain-wall width. It is much smaller than the one due to the variation of the lateral size illustrated in Fig. 3.5 (c). The borders of a domain wall are defined as lines where the deviation of the angles from the magnetization in the wall

differs by more than 22.5° from the angles of the magnetization vectors in the adjacent domains.

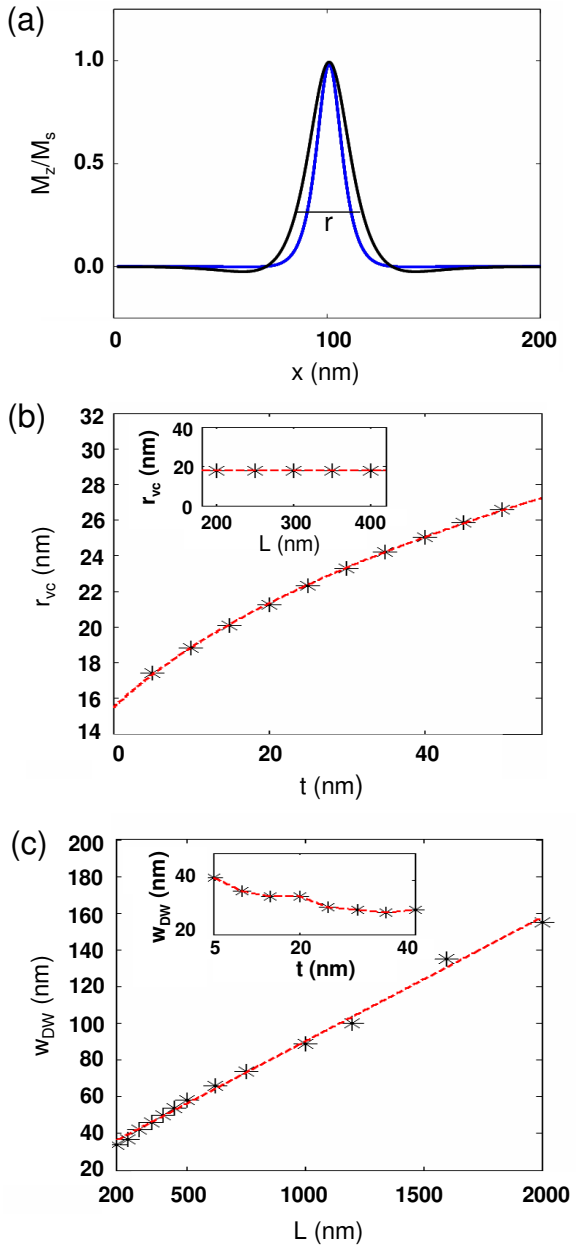

Fig. 3.5: (a) Magnetization component M_z of a vortex core in a $200 \times 200 \times 5$ nm^3 (blue line) and in a $200 \times 200 \times 50$ nm^3 (black line) square. (b) Vortex core radius in dependence on the thickness t of squares with a fixed lateral size $L = 200$ nm. Asterisks represent numerical results, the red line is a fit $r_{vc} = 6.69nm^{2/3}(t + 12.31nm)^{1/3}$. The asterisks in the inset denote the radius of the vortex core in dependence on the lateral sizes for a fixed thickness of $t = 10$ nm. The red line in the inset is a constant function. (c) Asterisks denote the domain-wall widths w_{DW} for different lengths for a fixed thickness $t = 20$ nm. The red line is a linear fit. In the inset the asterisks illustrate the domain-wall width in dependence on the thickness for a fixed lateral size of $L = 200$ nm. The red line is a guide to the eyes.

4 Dynamics in the linear and non-linear regime

External magnetic fields and spin currents couple to the magnetic moments of a vortex leading to a motion of the vortex core away from its equilibrium position. In addition to the external forces the displaced vortex core experiences an internal force due to the demagnetization field of the non-equilibrium magnetization pattern. This force is perpendicular to the velocity of the vortex core and causes a vortex gyration. For increasing and small amplitudes of excitation the internal force increases linearly. For increasing and large amplitudes of excitation the internal force increases nonlinearly, which results in a nonlinear vortex motion and in the highly nonlinear regime in the creation of new vortices.

4.1 Linear regime of vortex motion

First the gyroscopic vortex motion is described qualitatively by the Landau-Lifshitz-Gilbert equation. Then a linear equation of motion is derived from the Thiele equation. The dynamical characteristics of a vortex as a harmonic oscillator are presented and the response of the vortex to different forms of excitations is shown. Finally the amplitude variation of the core gyration for simultaneous excitation by a magnetic field and an electrical current or by a single rotating field or current is outlined.

To study the influence of the demagnetization field on the magnetization vectors that form the vortex core, the explicit Landau-Lifshitz-Gilbert equation [14]

$$\frac{d\mathbf{M}}{dt} = -\frac{\gamma}{(1+\alpha^2)}\mathbf{M}\times\mathbf{H}_{\text{eff}} - \frac{\gamma\alpha}{M_s(1+\alpha^2)}\mathbf{M}\times(\mathbf{M}\times\mathbf{H}_{\text{eff}}) \tag{4.1}$$

with the effective field $\mathbf{H}_{\text{eff}} = \mathbf{H}_{ex} + \mathbf{H}_D$ can be considered. In case of a disk the enlarged magnetic domain of a displaced vortex generates a demagnetization field at the vortex core which points antiparallel to the orientation of the enlarged domain, see Figs. 4.1 (a) and 4.1 (b). Then the first term of Eqn. 4.1, the gyration term, yields time derivatives of the magnetization vectors of the core that point into the disk's center or into the opposite direction. A vortex gyration follows with a counterclockwise (clockwise) gyration for a positive (negative) core polarization. A change of the chirality inherently changes the orientation of the demagnetization field at the core. Hence the gyration depends only on

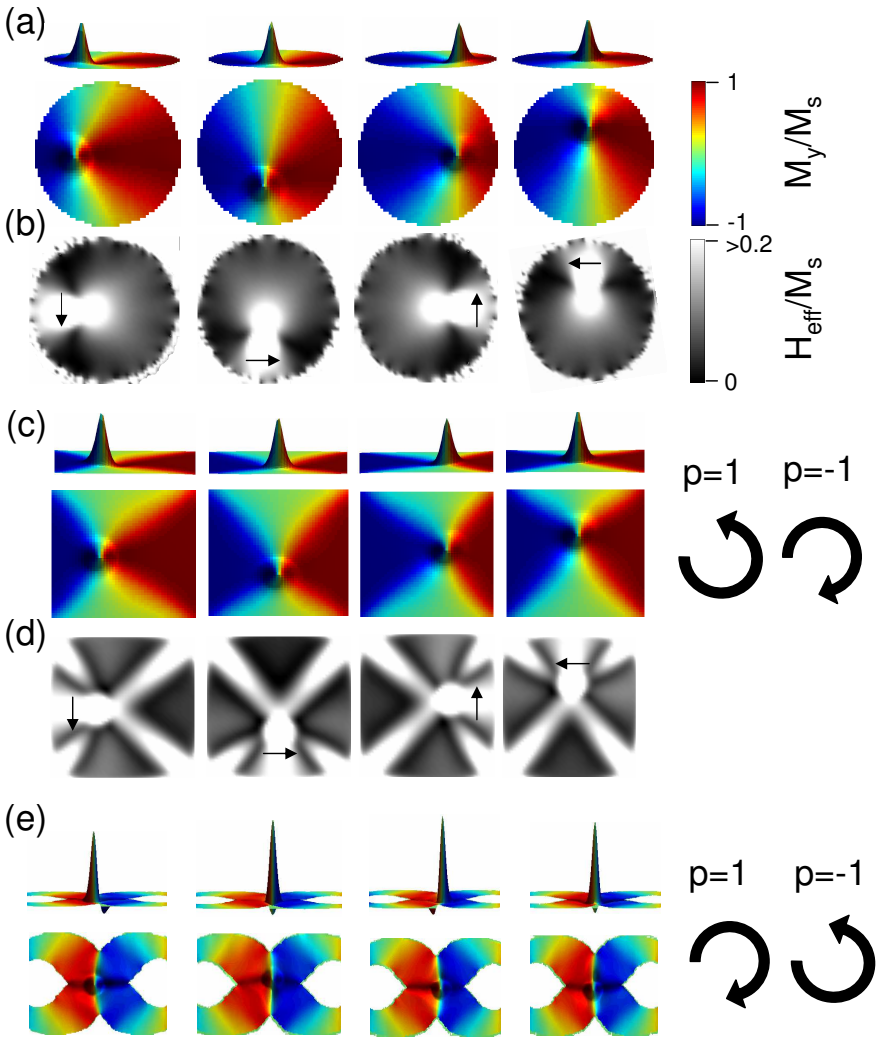

Fig. 4.1: Magnetic vortices in permalloy samples. The displaced core performs free damped gyrations induced by the demagnetization field. One gyration period of a vortex (c=1, p=1) in (a) and (b) a disk of radius 100 nm and thickness 20 nm with the free frequency $\omega_f = 4.95 \cdot 10^9$ 1/s, (c) and (d) in a square ($200 \times 200 \times 20$ nm^3) with the free frequency $\omega_f = 4.40 \cdot 10^9$ 1/s, (e) of an antivortex (c=0, p=1) in an infinity-shaped sample ($840 \times 400 \times 50$ nm^3) with the free frequency $\omega_f = 5.74 \cdot 10^9$ 1/s. (a), (c) and (e) depict the magnetizations, (b) and (d) the effective fields. The color bars illustrate the normalized y-component of the magnetization and the normalized strength of the effective field. The black arrows in (b) and (d) denote the direction of the effective field at the core. The circular black arrows denote the sense of gyration in dependence on the polarization.

the polarization and not on the chirality. The second term of Eqn. 4.1, the damping term, causes time derivatives of the magnetization vectors of the vortex core that point perpendicular to the time derivative due to the gyration term. It leads to a motion of the vortex into the direction of the equilibrium position and thus to a damped gyration.
In case of a square the core gyration is driven by the demagnetization field of the domain walls in the vicinity of the vortex core. It is much higher than that in the magnetic do-

mains as illustrated in Figs. 4.1 (c) and 4.1 (d).
In case of an antivortex the demagnetization field of the domain walls at the antivortex core results in an opposite sense of gyration in comparison to the vortex gyration, as shown in Fig. 4.1 (e). This is due to the two-fold symmetry of the in-plane magnetization of an antivortex. In general, for a vortex and an antivortex, the sense of the core's gyration is given by the product of the winding number n due to the symmetry of the in-plane magnetization and the polarization p due to the orientation of the out-of-plane magnetization. The product $np = 1 (np = -1)$ means a positive (negative) mathematical sense of gyration.
The vortex core can be displaced by an external spin current and an external magnetic field. This can be described by an additional spin-current and Zeeman field term. When excited by an alternating current at resonance the core gyrates on a circular orbit in the

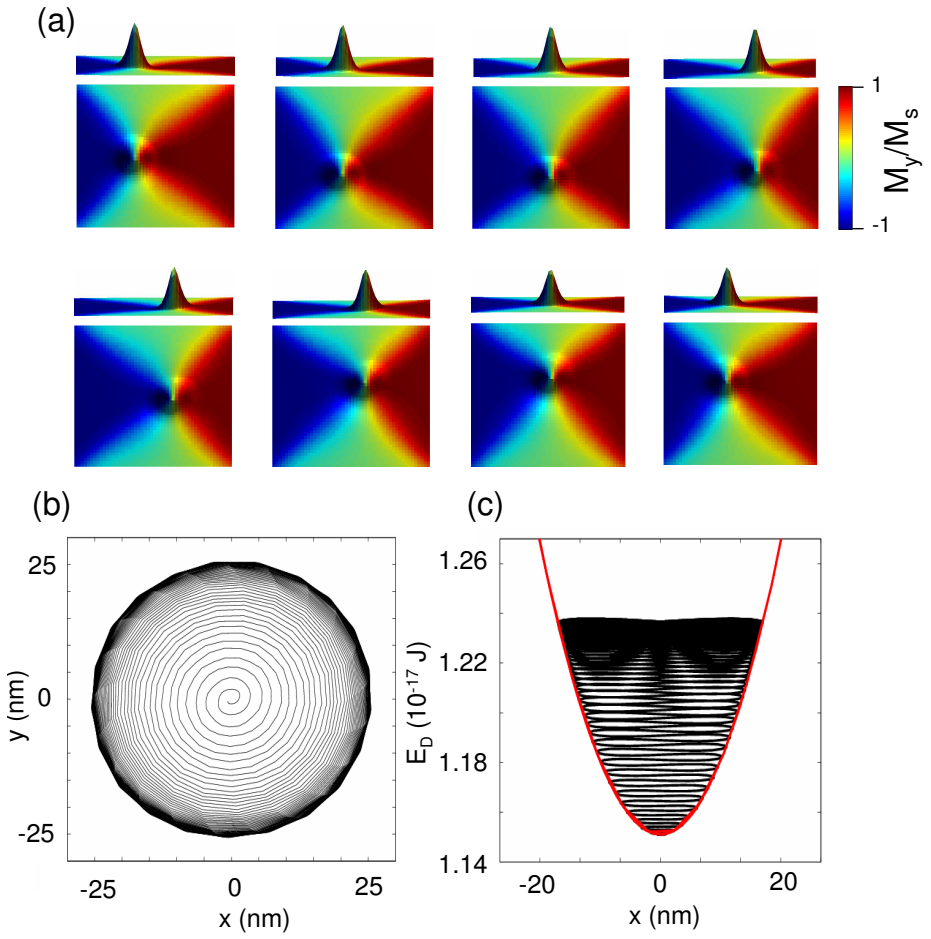

Fig. 4.2: (a) One simulated gyration period of a vortex (c=1, p=1) in the steady state. The vortex is excited in a square of permalloy ($200 \times 200 \times 20$ nm^3) by an alternating current density of amplitude $j \cdot P = 5 \cdot 10^{10}$ A/m^2 in x-direction at the free frequency $\omega_f = 4.4 \cdot 10^9$ 1/s. (b) Corresponding spiral trajectory that becomes circular when the steady state is reached. (c) The black curve illustrates the demagnetization energy in dependence on the displacement of the excited vortex core. The red line is a parabolic fit of the demagnetization energy.

steady state. Figure 4.2 (a) depicts the magnetization of a square excited by an alternating current density of amplitude $j \cdot P = 5 \cdot 10^{10}$ A/m^2 in x-direction. The domain walls are undistorted and the core performs a spiral trajectory starting from the equilibrium position in the center of the sample until a steady state with a circular trajectory is reached. This spiral trajectory is illustrated in Fig. 4.2 (b). The steady state is reached when the forces due to the external excitation and due to the demagnetization field are in equilibrium.
Since the core gyration is induced by the demagnetization field the demagnetization energy establishes the potential for the vortex core. Figure 4.2 (c) shows the demagnetization energy of the excited vortex in dependence on the core displacement. The fit shows that for small core displacements a parabolic potential can be assumed for the vortex gyration. Then the vortex gyration can be described by a harmonic oscillator model.

4.1.1 Thiele equation and equation of motion of vortices

The forces acting on a magnetic vortex can be derived starting from the implicit Landau-Lifshitz-Gilbert equation with the spin-torque terms [21]

$$\begin{aligned}\frac{d\mathbf{M}}{dt} =& -\gamma\mathbf{M}\times\mathbf{H}_{\text{eff}} + \frac{\alpha}{M_s}\mathbf{M}\times\frac{d\mathbf{M}}{dt} - \frac{b_j}{M_s^2}\mathbf{M}\times[\mathbf{M}\times(\mathbf{j}\cdot\nabla)\mathbf{M}] \\ & - \frac{\xi b_j}{M_s}\mathbf{M}\times(\mathbf{j}\cdot\nabla)\mathbf{M}.\end{aligned} \tag{4.2}$$

The absolute values of the magnetization vectors are assumed to be spatially constant and equal to the saturation magnetization $M_s = 8 \cdot 10^5$ A/m of permalloy. Then the derivatives of the squared magnetization $\frac{d}{dr}\mathbf{M}^2 = 2\mathbf{M}\cdot\frac{d}{dr}\mathbf{M} = 0$ and $\frac{d}{dt}\mathbf{M}^2 = 2\mathbf{M}\cdot\frac{d}{dt}\mathbf{M} = 0$ vanish. Hence the derivatives $d\mathbf{M}/dr$ and $d\mathbf{M}/dt$ point perpendicular to the magnetization $\mathbf{M}$. A cross product of Eqn. 4.2 from the left-hand side by the magnetization $\mathbf{M}$ and an evaluation of the resulting equation by employing the identity $\mathbf{a}\times(\mathbf{a}\times\mathbf{b}) = -a^2\mathbf{b}$ for perpendicular vectors $\mathbf{a}$ and $\mathbf{b}$ result in the effective field

$$\mathbf{H}_{\text{eff}} = \frac{\mathbf{M}}{\gamma M_s^2}\times\frac{d\mathbf{M}}{dt} + \frac{\alpha}{\gamma M_s}\frac{d\mathbf{M}}{dt} - \frac{b_j}{\gamma M_s^2}\mathbf{M}\times(\mathbf{j}\cdot\nabla)\mathbf{M} - \frac{\xi b_j}{\gamma M_s}(\mathbf{j}\cdot\nabla)\mathbf{M} - h\mathbf{M}. \tag{4.3}$$

The summands on the right-hand side can be interpreted in terms of equivalent fields [36]. The equivalent field $\mathbf{H}^m = h\mathbf{M}$ with the proportionality factor h can be neglected, because it does not interact with the magnetization.
The gyroscopic equivalent field and the dissipative equivalent field read

$$\mathbf{H}^g = -\frac{1}{\gamma M_s^2}\mathbf{M}\times\frac{d\mathbf{M}}{dt} \tag{4.4}$$

and

$$\mathbf{H}^\alpha = -\frac{\alpha}{\gamma M_s}\frac{d\mathbf{M}}{dt}, \tag{4.5}$$

the adiabatic and the nonadiabatic spin-torque equivalent fields [37]

$$\mathbf{H}^{adiabatic} = \frac{b_j}{\gamma M_s^2}\mathbf{M} \times (\mathbf{j} \cdot \nabla)\mathbf{M} \tag{4.6}$$

and

$$\mathbf{H}^{nonadiabatic} = \frac{b_j \xi}{\gamma M_s}(\mathbf{j} \cdot \nabla)\mathbf{M}. \tag{4.7}$$

The steady-state motion of a vortex core can be described as the motion of a quasiparticle with the velocity $\mathbf{v}$ [36, 38], [P1]

$$\frac{d\mathbf{M}}{dt} = -\big(\frac{d\mathbf{r}}{dt} \cdot \frac{d}{dr}\big)\mathbf{M} = -(\mathbf{v} \cdot \nabla)\mathbf{M}. \tag{4.8}$$

In the following terms with repeated indices are assumed to be summed. The components of the force density [36]

$$f_i = -\mu_0 H_k \partial M_k / \partial x_i \tag{4.9}$$

are products between the components of the corresponding equivalent fields H_i and the spatial derivatives of the magnetization $\partial M_j/\partial x_i$. They can be used to derive the forces of vortex dynamics [38], [P1].
Inserting the component of the gyroscopic equivalent field $H_k^g = -\frac{1}{M_s^2\gamma}\varepsilon_{kmn}M_m\frac{dM_n}{dt}$ and the component $\frac{dM_i}{dt} = -v_j\frac{\partial M_i}{\partial x_j}$ into Eqn. 4.9 yields the gyroscopic force density

$$\begin{aligned} f_i^g &= -\mu_0 H_k^g \frac{\partial M_k}{\partial x_i} = \mu_0 \frac{1}{M_s^2\gamma}\varepsilon_{kmn}M_m\frac{dM_n}{dt}\frac{\partial M_k}{\partial x_i} \\ &= -\mu_0 \frac{1}{M_s^2\gamma}\varepsilon_{kmn}M_k\frac{\partial M_m}{\partial x_j}\frac{\partial M_n}{\partial x_i}v_j = G_{ij}v_j. \end{aligned} \tag{4.10}$$

The gyrotensor G_{ij} can be expressed by a gyrovector $\mathbf{g}$ using the relation $g_i = -\frac{1}{2}\varepsilon_{ijk}G_{jk}$. In vector notation the gyroscopic force density reads $\mathbf{f}^g = -\mathbf{g} \times \mathbf{v}$. The force density due to the dissipation is

$$f_i^\alpha = -\mu_0 H_k^\alpha \frac{\partial M_k}{\partial x_i} = \frac{\alpha\mu_0}{M_s\gamma}\frac{dM_k}{dt}\frac{\partial M_k}{\partial x_i} = -\frac{\alpha\mu_0}{M_s\gamma}\frac{\partial M_k}{\partial x_j}\frac{\partial M_k}{\partial x_i}v_j = -\alpha d_{ij}v_j. \tag{4.11}$$

In vector notation $\mathbf{f}^\alpha = -\alpha\mathbf{d} \cdot \mathbf{v}$. The force densities due to the adiabatic and the nonadiabatic spin-torques are

$$\mathbf{f}^{adiabatic} = \mu_0 \mathbf{g} \times b_j \mathbf{j} \tag{4.12}$$

and

$$\mathbf{f}^{nonadiabatic} = -\mu_0 \xi b_j \mathbf{d} \cdot \mathbf{j}. \tag{4.13}$$

The force density of the energy density ρ_{eff} of the effective field is [36]

$$\mathbf{f}^{\mathsf{eff}} = (\delta\rho_{\mathsf{eff}}/\delta\theta)\nabla\theta + (\delta\rho_{\mathsf{eff}}/\delta\phi)\nabla\phi. \tag{4.14}$$

This force density $\mathbf{f}^{\mathsf{eff}} = \mathbf{f}^{in} + \mathbf{f}^{ex}$ can be devided into an internal force density $\mathbf{f}^{in}$ compris-

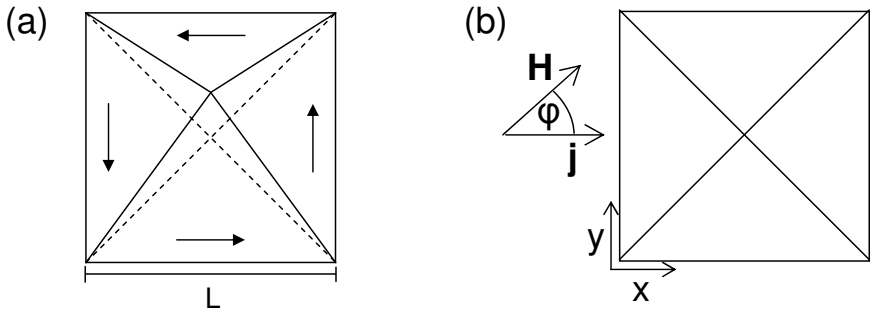

Fig. 4.3: (a) Scheme of a vortex in a square. The core is displaced into the y-direction if the component M_x of the magnetization increases. The arrows depict the direction of the magnetization in the domains, the dashed lines indicate the equilibrium magnetization. (b) Angle φ between the exciting field and the current density.

ing the force density due to the demagnetization energy and an external force density $\mathbf{f}^{ex}$ comprising the force density due to the Zeeman field [36].
Integration of all force densities over the volume leads to the total force

$$\mathbf{F} = -\mathbf{G} \times (\mathbf{v} + b_j \mathbf{j}) - \mathbf{D}(\alpha \mathbf{v} + \xi b_j \mathbf{j}), \tag{4.15}$$

where the total gyroscopic vector is $\mathbf{G} = \int \mathbf{g} dV$ and the total dissipation tensor $\mathbf{D} = \int \mathbf{d} dV$. For small core displacements the vortex can be treated as a quasiparticle in an isotropic parabolic potential

$$E_d = \tfrac{1}{2} m \omega_r^2 r^2, \tag{4.16}$$

see Fig. 4.2 (c). Here m is the effective mass of the quasiparticle, ω_r the resonance frequency, and r the amplitude of gyration.
The energy due to the Zeeman field can be obtained approximating the domains of the vortex of chirality c in a Landau pattern by saturated triangles of length L and height $L/2$. This approximation assumes undistorted domain walls [38], [P1]. If an external field $\mathbf{H}$ is applied in the x-direction, only the x-component of the magnetization

$$M_x = \frac{cM_s}{2L}\left[\left(\frac{L}{2}+y\right) - \left(\frac{L}{2}-y\right)\right] = cM_s L^{-1} y \tag{4.17}$$

increases and the vortex core is displaced in the y-direction, see Fig. 4.3 (a) and Figure 1 in Ref. [38], [P1]. The Zeeman energy reads

$$E_{Zeeman} = -\frac{\mu_0 cM_s LtH}{2}\left[\left(\frac{L}{2}+y\right) - \left(\frac{L}{2}-y\right)\right] = -\mu_0 cM_s LtHy \tag{4.18}$$

with the thickness t. For the general case of a vortex of an arbitrary chirality or c-value [39], [P2] and an arbitrary direction of the external field the resulting force due to the

Zeeman and the demagnetization field is

$$\begin{aligned}\mathbf{F} &= -\nabla(E_{Zeeman}+E_D)\\ &= \mu_0 M_s H l t \begin{pmatrix}\cos(\varphi) & -\sin(\varphi)\\ \sin(\varphi) & \cos(\varphi)\end{pmatrix}\begin{pmatrix}-n\cos\left(\frac{\pi c}{2}\right)\\ \sin\left(\frac{\pi c}{2}\right)\end{pmatrix} - m\omega_r^2\begin{pmatrix}x\\ y\end{pmatrix}.\end{aligned} \tag{4.19}$$

The angle φ between the x-axis and the Zeeman field is illustrated in Fig. 4.3 (b). A cross product of Eqn. 4.15 with the total gyrovector $\mathbf{G}$ from the left-hand side using the identity $\mathbf{a}\times(\mathbf{a}\times\mathbf{b}) = -a^2\mathbf{b}$ for perpendicular vectors $\mathbf{a}$ and $\mathbf{b}$ leads to the equation of motion of vortices as found by Benjamin Krüger [38], [P1]

$$\begin{pmatrix}\dot{x}\\ \dot{y}\end{pmatrix} = \frac{\mathbf{G}\times\mathbf{F} - D_0\alpha\mathbf{F} - (G_0^2 + D_0^2\alpha\xi)b_j\mathbf{j} + D_0\mathbf{G}\times b_j\mathbf{j}(\xi-\alpha)}{G_0^2+D_0^2\alpha^2}. \tag{4.20}$$

The gyrovector is given by $\mathbf{G} = G_0\mathbf{e}_z$ with $G_0 = -\frac{2\pi M_s\mu_0 tnp}{\gamma}$. The diagonal element of the dissipation tensor is $D_0 = -\frac{\pi M_s\mu_0 t\ln(l/a)}{\gamma}$.
Inserting Eqn. 4.19 into Eqn. 4.20 leads to the explicit equation of motion of vortices ($n=1$) and antivortices ($n=-1$) of arbitrary chiralities or c-values excited by a current in the x-direction and a magnetic field of an arbitrary direction:

$$\begin{aligned}\begin{pmatrix}\dot{x}\\ \dot{y}\end{pmatrix} = &\begin{pmatrix}-\Gamma & -pn\omega_f\\ np\omega_f & -\Gamma\end{pmatrix}\begin{pmatrix}x\\ y\end{pmatrix} + \begin{pmatrix}-v_j - \frac{\Gamma^2}{\omega_f^2+\Gamma^2}\frac{\xi-\alpha}{\alpha}v_j\\ \frac{np\omega_f\Gamma}{\omega_f^2+\Gamma^2}\frac{\xi-\alpha}{\alpha}v_j\end{pmatrix}\\ &- \frac{\omega_f^2 v_H}{\omega_f^2+\Gamma^2}\begin{pmatrix}\cos(\varphi) & -\sin(\varphi)\\ \sin(\varphi) & \cos(\varphi)\end{pmatrix}\begin{pmatrix}-np\sin(\frac{\pi c}{2}) + \frac{\Gamma}{\omega_f}n\cos(\frac{\pi c}{2})\\ -p\cos(\frac{\pi c}{2}) - \frac{\Gamma}{\omega_f}\sin(\frac{\pi c}{2})\end{pmatrix}.\end{aligned} \tag{4.21}$$

In this equation $\omega_f = \frac{-npG_0 m\omega_r^2}{G_0^2+D_0^2\alpha^2}$ is the free frequency and $\Gamma = \frac{-D_0\alpha m\omega_r^2}{G_0^2+D_0^2\alpha^2}$ the damping constant, $v_j = b_j j$ the velocity due to the electrical current, and $v_H = HL\gamma/2\pi$ the velocity due to the magnetic-field excitation [38], [P1].
In case of an alternating excitation of the form $\mathbf{v}_{ext} = (A\mathbf{e}_x + B\mathbf{e}_y)e^{i\Omega t}$ the analytical solution of Eqn. 4.21 can be obtained from the method of variation of constants [38], [P1]. The result is

$$\begin{aligned}\begin{pmatrix}x\\ y\end{pmatrix} = &K_1\begin{pmatrix}i\\ np\end{pmatrix}e^{(-\Gamma t + i\omega_f t)} + K_2\begin{pmatrix}-i\\ np\end{pmatrix}e^{(-\Gamma t - i\omega_f t)}\\ &+\chi\begin{pmatrix}A(i\Omega+\Gamma) - Bnp\omega_f\\ Anp\omega_f + B(i\Omega+\Gamma)\end{pmatrix}e^{i\Omega t}.\end{aligned} \tag{4.22}$$

The coefficients K_1 and K_2 include the initial conditions and $\chi = 1/[\omega_f^2 + (i\Omega+\Gamma)^2]$ is the dynamical susceptibility of a harmonic oscillator. The coefficients A and B of the velocity due to the excitation $\mathbf{v}_{ex}$ are given by the x- and the y-component of the inhomogeneous

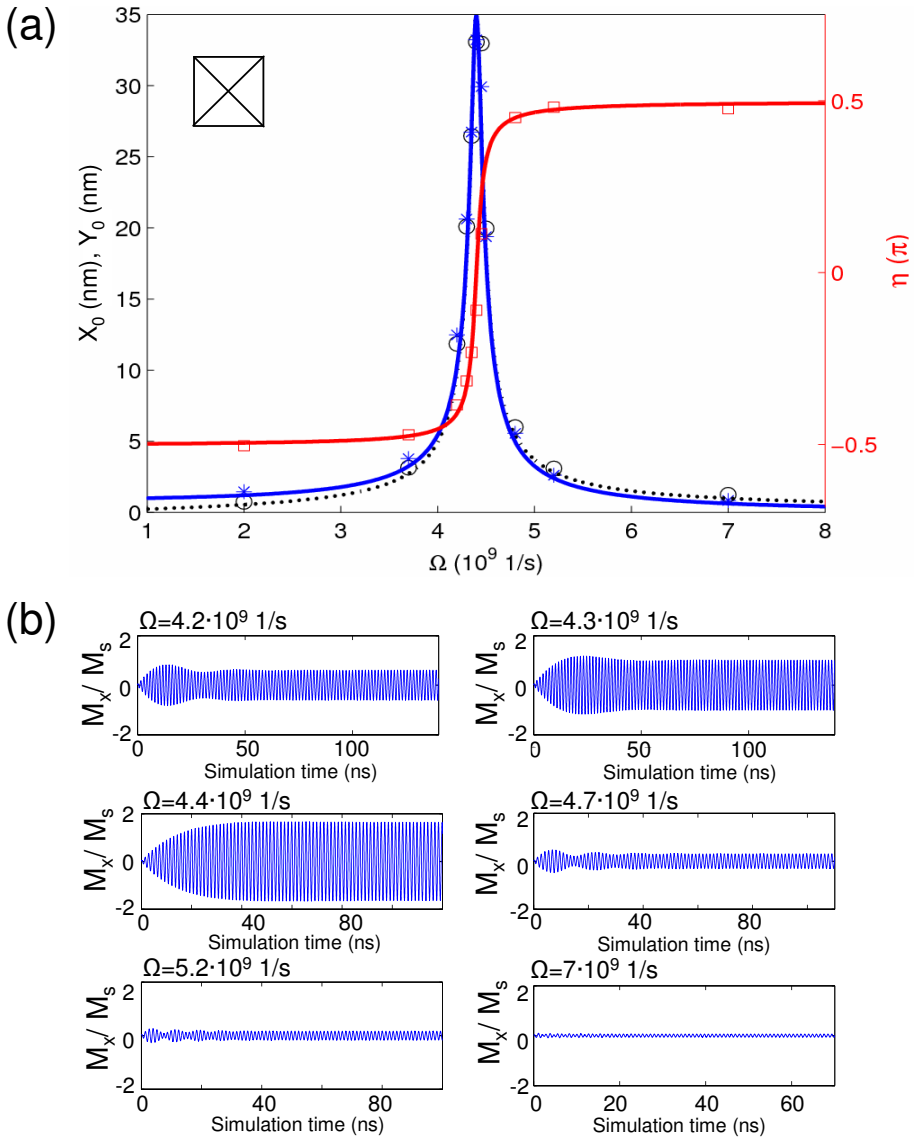

Fig. 4.4: (a) Resonant core gyration of a vortex in a permalloy square ($200 \times 200 \times 20$ nm^3). The black circles (blue asterisks) depict simulated results of the semiaxes X_0 and Y_0 of the core gyration in dependence on the exciting frequency Ω. The dashed black (solid blue) line denotes analytical results from the harmonic oscillator model. The red squares represent simulated phases η of the core gyration, the red line is the phase from the harmonic oscillator model. (b) Amplitude of vortex gyration represented by the x-component of the magnetization M_x in dependence on the simulation time for frequencies below ($\Omega < \omega_r$), at ($\Omega = \omega_r$), and above ($\Omega > \omega_r$) the resonance frequency.

part of Eqn. 4.21.

Usually vortex states in permalloy microstructures are weakly damped systems. For example for a vortex in a square of dimensions $200 \times 200 \times 20$ nm^3 micromagnetic simulations yield a ratio of $\Gamma/\omega \approx 0.01$. For permalloy the Gilbert damping α and the nonadiabaticity constant ξ are approximately equal ($\alpha \approx \xi$). Hence Eqn. 4.21 can be simplified by omitting terms that include the factors $\frac{\Gamma}{\omega} << 1$ and $\frac{\xi-\alpha}{\alpha} << 1$. Using these

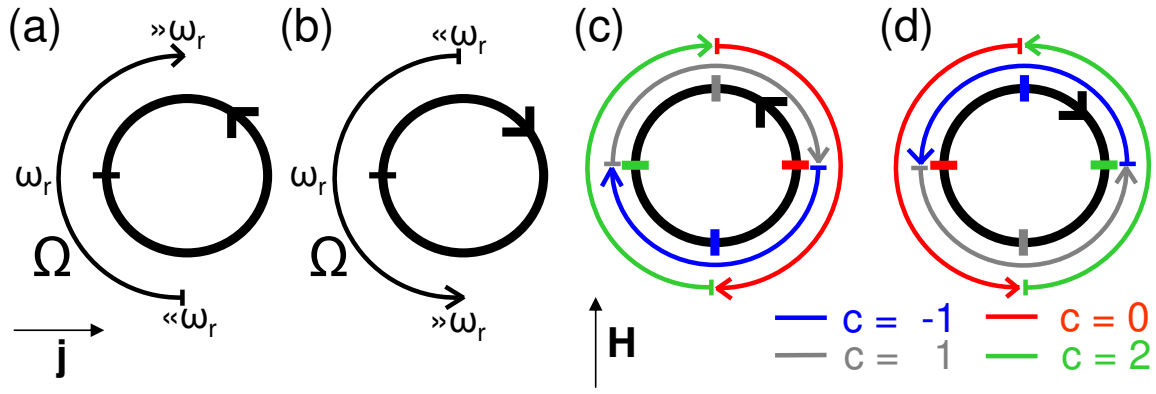

Fig. 4.5: Core position of a vortex in dependence on the exciting frequency Ω at the maximum amplitude of (a) and (b) an alternating current in x-direction, (c) and (d) a magnetic-field in y-direction. The circles represent the core gyration of a vortex of (a) and (c) $np = 1$, (b) and (d) $np = -1$. The arrow heads in the circles illustrate the sense of gyration, the lines the position of the core at the resonance frequency. (a) - (d) The thin half circles illustrate the core positions for frequencies from far below resonance $\omega_r >> \Omega > \Gamma$ to far above resonance $\omega_r^2/\Gamma > \Omega >> \omega_r$. In (c) and (d) different colors of the half circles show the chirality or c-value dependent core position for magnetic-field excitation. The different colors of the bars in the circles denote the position of the core at resonance.

approximations and assuming an alternating current $j(t) = j\cos(\Omega t)$ in x-direction and an alternating magnetic field $H = H\cos(\Omega t)$ in y-direction ($\varphi = \pi/2$), Eqn. 4.22 yields the steady-state motion of vortices [38, 32], [P1, P3]

$$\begin{pmatrix} x \\ y \end{pmatrix} = -\chi \begin{pmatrix} v_H \sin(\frac{\pi c}{2})\omega_f + i\Omega[v_H p\cos(\frac{\pi c}{2}) + v_j] \\ [v_H n\cos(\frac{\pi c}{2}) + v_j np]\omega_f - i\Omega v_H np\sin(\frac{\pi c}{2}) \end{pmatrix} e^{i\Omega t}. \tag{4.23}$$

For alternating excitations the semiaxes X_0 and Y_0 and the phase η of gyration depend on the exciting frequency as shown in Figs. 4.4 (a) and 4.4 (b). The core performs elliptical trajectories, which at resonance become circular with a maximum amplitude ($r = X_0 = Y_0$), see Fig 4.4 (a). The phase between excitation and gyration η is defined by the time shift between maximum amplitude of excitation and maximum displacement in x-direction. For varying frequencies the phase varies by π as illustrated in Fig. 4.4 (a). Only in case of magnetic-field excitation the phase depends on the chirality or the c-value [30, 32, 38], [P4, P1, P3]. This is evident in Eqn. 4.23 and illustrated in Fig. 4.5.

For an excitation with a constant current density j or magnetic field H the core is displaced and performs a damped gyration around a new equilibrium position as shown in Figs. 4.6 (b) and 4.6 (e). The displacement of a vortex excited by a constant current is

$$\begin{pmatrix} x \\ y \end{pmatrix} = \frac{1}{\omega_f^2 + \Gamma^2} \begin{pmatrix} -v_j\Gamma \\ -v_j np\omega_f \end{pmatrix} \tag{4.24}$$

as obtained from Eqns. (4.21) and (4.22). Only for field excitation the direction of the

core displacement depends on the chirality or the c-value.

For an excitation by a current pulse of density $\Theta(t_1 - t_2)\,j$ or a magnetic field $\Theta(t_1 - t_2)H$ with the step function $\Theta(t_1 - t_2)$, the vortex is displaced during the duration of the pulse. After that it performs a free relaxation around the equilibrium position as illustrated in Fig. 4.6 (c) and 4.6 (f). The equation of motion can be derived by inserting the velocities $v_j = b_j j\Theta(t_2 - t_1)$ or $v_H = \frac{Hl\gamma}{2\pi}H\Theta(t_2 - t_1)$ into Eqn. 4.21. For arbitrary shapes of the pulse the equation of motion can only be solved numerically. For example the pulses in Figs. 4.6 (c) and 4.6 (f) are mixtures of a step function and a triangular function.

A spatially rotating magnetic field $\mathbf{H} = H(e^{i\Omega t}\mathbf{e}_x \pm ie^{i\Omega t}\mathbf{e}_y)$ or current $\mathbf{j} = j(e^{i\Omega t}\mathbf{e}_x \pm ie^{i\Omega t}\mathbf{e}_y)$ can be realized by superimposing two alternating excitations in perpendicular directions with a phase of $\pm\pi/2$. The sign of the phase determines the sense of rotation of the excitation. It rotates clockwise for $+\pi/2$ and anticlockwise for $-\pi/2$ [40, 41].

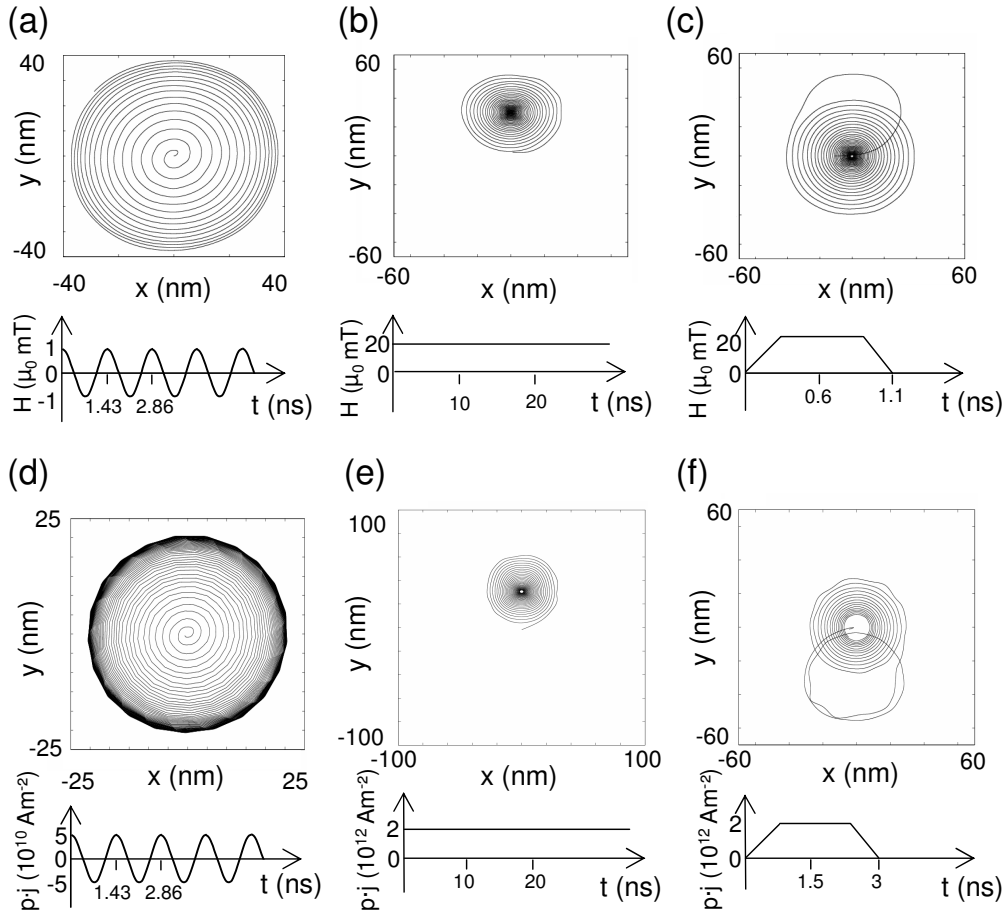

Fig. 4.6: Vortex trajectories for magnetic-field [(a), (b), (c)] and current [(d), (e), (f)] excitation. (a) and (d) depict the core trajectories for an alternating excitation, (b) and (e) for a constant excitation, (c) and (f) for a pulsed excitation. The sketches below the trajectories show the amplitude and the time dependence of the exciting fields and current densities.

The motion of a vortex for a rotating current reads

$$\begin{pmatrix} x \\ y \end{pmatrix} = \chi \begin{pmatrix} v_j i(\Omega \pm np\omega_f) \\ v_j(np\omega_f \pm \Omega) \end{pmatrix} e^{i\Omega t}, \tag{4.25}$$

see Eqns. (4.21) and (4.22). For rotating excitations the trajectory always has a circular shape. This is evident in Eqn. 4.25.

4.1.2 Vortices as harmonic oscillators

To get the values for the free frequency ω_f and for the damping constant Γ the vortex core can be displaced first and then the free relaxation can be fitted to the solution

$$x(t) = Ae^{-\Gamma t}\cos(\omega_f t) \tag{4.26}$$

of a damped harmonic oscillator, see Fig. 4.7. The damping Γ and the frequency ω_f determine the resonance frequency $\omega_r = \sqrt{\omega_f^2 + \Gamma^2}$. Figure 4.7 (b) shows a fit of the x-component of the magnetization of a vortex in a square.
The potential due to the demagnetization field depends on the geometry of the sample. Simulations of the gyration in squares of different sizes yield the correlations between the free frequency ω_f, the width L and the thickness t of the square, as illustrated in Fig. 4.7 (a). The fitted resonance frequency

$$\omega_r(L,t) = a_1(t + a_2)/L \cdot 10^9 \text{ 1/s} \tag{4.27}$$

is similar to the analytical resonance frequency in disks [42]. A useful ansatz to fit the damping constant is

$$\Gamma(L) = b_1 \frac{\ln(L/b_2)}{L} \cdot 10^9 \text{ 1/s}. \tag{4.28}$$

The constants a_1, a_2, b_1 and b_2 are fit parameters.

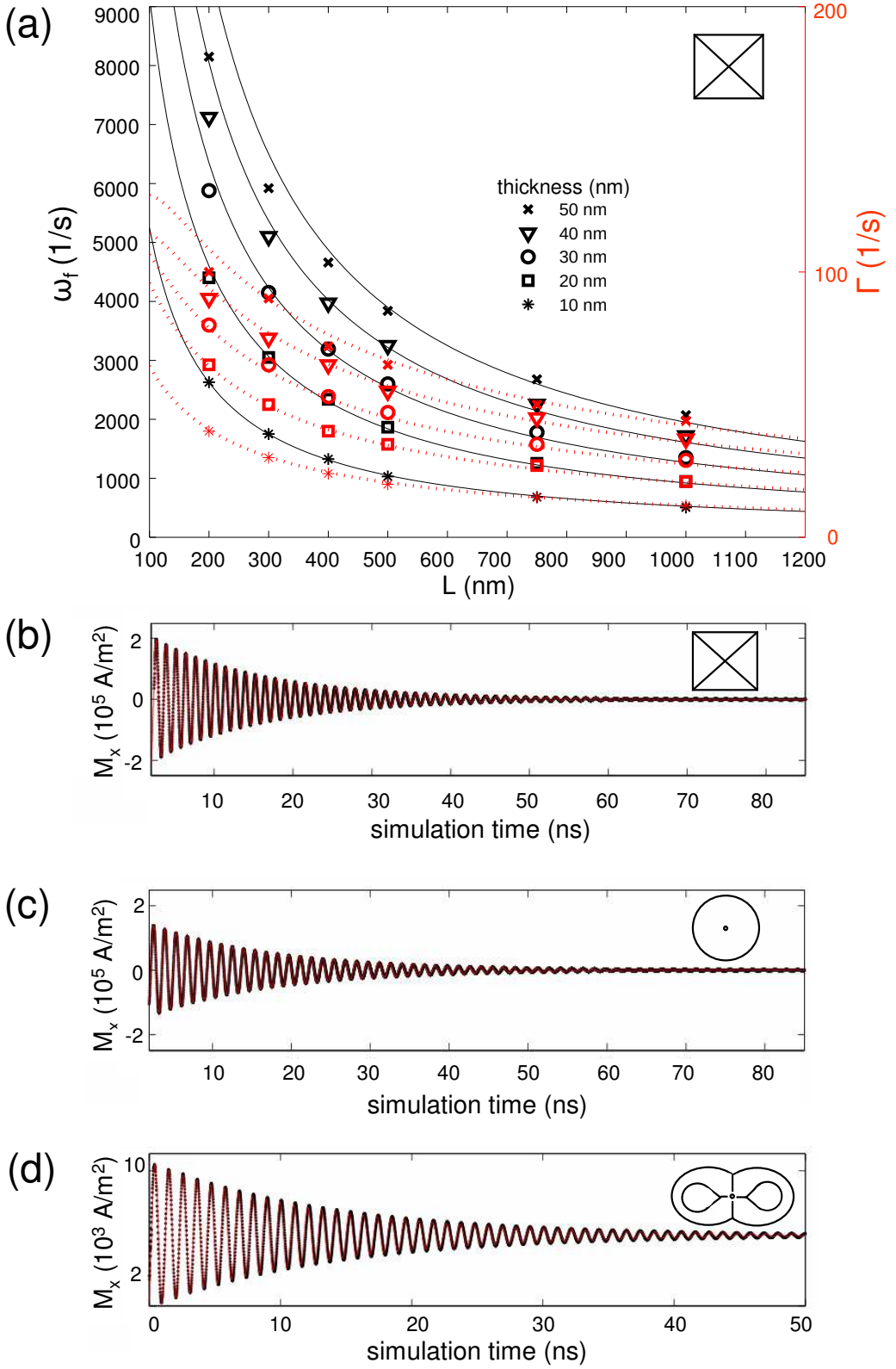

Fig. 4.7: (a) Free frequency ω_f (black lines and black symbols) and damping constant Γ (red lines and red symbols) of the vortex gyration in squares of different lengths and thicknesses. Free gyration (b) in a square ($200 \times 200 \times 20$ nm^3), (c) in a disk of radius $r = 100$ nm and thickness $t = 20$ nm and (d) in an infinity-shaped sample ($840 \times 400 \times 50$ nm^3) illustrated by the M_x-component. (b) - (d) The black lines are simulated results, the red lines are fits with a harmonic oscillator model with the free frequency and the damping constant as fitting parameters. (d) Note that the equilibrium magnetization $M_x \neq 0$ is caused by a slightly asymmetry of the infinity-shaped sample.

Publication 1

Reprinted with permission from B. Krüger, A. Drews, M. Bolte, U. Merkt, D. Pfannkuche, and G. Meier,

Harmonic oscillator model for current- and field-driven magnetic vortices,

Phys. Rev. B **76**, 224426-1-224426-5, 2007

Harmonic oscillator model for current- and field-driven magnetic vortices

Benjamin Krüger,[1] André Drews,[2] Markus Bolte,[2] Ulrich Merkt,[2] Daniela Pfannkuche,[1] and Guido Meier[2]

[1] *I. Institut für Theoretische Physik, Universität Hamburg, Jungiusstr. 9, 20355 Hamburg, Germany*
[2] *Institut für Angewandte Physik und Zentrum für Mikrostrukturforschung, Universität Hamburg, Jungiusstr. 11, 20355 Hamburg, Germany*

(Dated: October 17, 2007)

In experiments the distinction between spin-torque and Oersted-field driven magnetization dynamics is still an open problem. Here, the gyroscopic motion of current- and field-driven magnetic vortices in small thin-film elements is investigated by analytical calculations and by numerical simulations. It is found that for small harmonic excitations the vortex core performs an elliptical rotation around its equilibrium position. The global phase of the rotation and the ratio between the semi-axes are determined by the frequency and the amplitude of the Oersted field and the spin torque.

PACS numbers: 75.60.Ch, 72.25.Ba

I. INTRODUCTION

Recently it has been found that a spin-polarized current flowing through a magnetic sample interacts with the magnetization and exerts a torque on the local magnetization.[1,2] A promising system for the investigation of the spin-torque effect is a vortex in a micro- or nanostructured magnetic thin-film element. Vortices are formed when the in-plane magnetization curls around a center region. In this few nanometer large center region[3], called the vortex core, the magnetization turns out-of-plane to minimize the exchange energy.[4] It is known that these vortices precess around their equilibrium position when excited by magnetic field pulses[5,6] and it was shown that spin-polarized electric currents can cause the same precession.[7–10] The spacial restriction of the vortex core as well as its periodic motion around its ground state yield an especially accessible system for space- and time-resolved measurements with scanning probe and time-integrative techniques such as soft X-ray microscopy or X-ray photoemission electron microscopy.[5,6,11–13] Magnetic vortices also occur in vortex domain walls. The motion of such walls has recently been investigated intensively.[14,15] Understanding the dynamics of confined vortices can give deeper insight in the mechanism of vortex-wall motion.[16] An in-plane Oersted field accompanying the current flow also influences the motion of the vortex core. For the interpretation of experimental data it is crucial to distinguish between the influence of the spin torque and of the Oersted field.[17]

In this paper we investigate the current- and field-driven gyroscopic motion of magnetic vortices in square thin-film elements of size l and thickness t as shown in Fig. 1 and present a method to distinguish between spin torque and Oersted field driven magnetization dynamics.

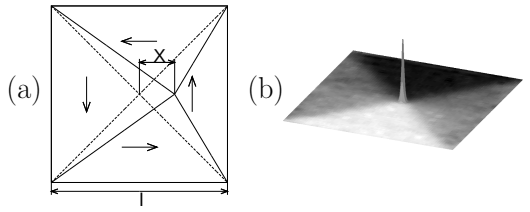

FIG. 1: (a) Scheme of the magnetization in a square magnetic thin-film element with a vortex that is deflected to the right. (b) Magnetization of a vortex in its static ground state. The height denotes the z-component while the gray scale corresponds to the direction of the in-plane magnetization.

II. ANALYTICAL CALCULATIONS

In the presence of a spin-polarized current the time evolution of the magnetization is given by the extended Landau-Lifshitz-Gilbert equation

$$\begin{aligned}\frac{d\vec{M}}{dt} =& -\gamma\vec{M}\times\vec{H}_{\text{eff}} + \frac{\alpha}{M_s}\vec{M}\times\frac{d\vec{M}}{dt} \\ &- \frac{b_j}{M_s^2}\vec{M}\times\left(\vec{M}\times(\vec{j}\cdot\vec{\nabla})\vec{M}\right) \\ &- \xi\frac{b_j}{M_s}\vec{M}\times(\vec{j}\cdot\vec{\nabla})\vec{M}\end{aligned} \tag{1}$$

with the coupling constant $b_j = P\mu_B/[eM_s(1+\xi^2)]$ between the current and the magnetization where P is the spin polarization, M_S the saturation magnetization, and ξ the degree of non-adiabaticity.[18] If the vortex keeps its static structure, its motion with the velocity $\vec{v}$ can be described using the Thiele equation.[19] This equation was expanded by Nakatani et al.[20] to include the action of a spin-polarized current flowing in the sample,

$$\vec{F} + \vec{G}\times(\vec{v} + b_j\vec{j}) + D(\alpha\vec{v} + \xi b_j\vec{j}) = 0. \tag{2}$$

Denoting the out-of-plane angle of the magnetization with θ and the angle of the in-plane magnetization with

ϕ, the force due to the external and the stray field is

$$\vec{F} = -\mu_0 \int dV \left[(\vec{\nabla}\theta)\frac{\partial}{\partial\theta} + (\vec{\nabla}\phi)\frac{\partial}{\partial\phi} \right] (\vec{H}_{sz} \cdot \vec{M}). \quad (3)$$

The gyrovector

$$\begin{aligned} \vec{G} &= -\frac{M_s\mu_0}{\gamma} \int dV \, \sin(\theta)(\vec{\nabla}\theta \times \vec{\nabla}\phi) \\ &= -\frac{2\pi M_s\mu_0 tp}{\gamma}\vec{e}_z = G_0\vec{e}_z, \end{aligned} \quad (4)$$

indicates the axis of precession and points out-of-plane. The dissipation tensor is given by

$$D = -\frac{M_s\mu_0}{\gamma} \int dV \, (\vec{\nabla}\theta\vec{\nabla}\theta + \sin^2(\theta)\vec{\nabla}\phi\vec{\nabla}\phi). \quad (5)$$

It is diagonal with

$$D_{xx} = D_{yy} = D_0 \approx -\frac{\pi M_s\mu_0 t \ln(l/a)}{\gamma}, \qquad D_{zz} = 0. \quad (6)$$

The constant a is the lower bound of the integration. It is in the order of magnitude of the radius of the vortex core.[3,16,21,22] A polarization p of $+1$ (-1) denotes that the magnetization in the vortex core is parallel (antiparallel) to the z-axis. The velocity of the vortex core is in-plane and hence perpendicular to the gyrovector. Thus Eq. (2) can be rewritten as

$$\vec{G} \times \vec{F} - G_0^2(\vec{v} + b_j\vec{j}) + D_0\vec{G} \times (\alpha\vec{v} + \xi b_j\vec{j}) = 0. \quad (7)$$

By calculating $\vec{G}\times\vec{v}$ from Eq. (7) and inserting the result in Eq. (2)

$$\begin{aligned} (G_0^2 + D_0^2\alpha^2)\vec{v} = \vec{G} \times \vec{F} - D_0\alpha\vec{F} - (G_0^2 + D_0^2\alpha\xi)b_j\vec{j} \\ + b_j D_0\vec{G} \times \vec{j}(\xi - \alpha) \end{aligned} \quad (8)$$

we can derive the velocity of the vortex core. As for any square-symmetric confining potential, the stray-field energy for small deflections can be modeled as a parabolic potential

$$E_s = \frac{1}{2}m\omega_r^2(X^2 + Y^2) \quad (9)$$

with the coordinates X and Y of the vortex core (see Fig. 1a).

In the following a spacially homogeneous current in x-direction is investigated. Due to possible inhomogeneities in real samples the current flow may vary in the out-of-plane direction. This results in an in-plane Oersted field which is perpendicular to the direction of the current flow. In the following this Oersted field is accounted for by a homogeneous magnetic field in y-direction. Both driving forces may depend on time. To estimate the Zeeman energy due to the Oersted field H, the magnetization pattern is divided into four triangles (see Fig. 1a). Assuming that the magnetization is uniform in each of these triangles the total Zeeman energy is given by

$$E_z = \frac{\mu_0 M_s H l t c}{2}\left[\left(\frac{l}{2} + X\right) - \left(\frac{l}{2} - X\right)\right], \quad (10)$$

with the chirality c of the vortex. A chirality of $+1$ (-1) denotes a counterclockwise (clockwise) curling of the magnetization around the vortex core. We will see that this simple approximation describes the field-induced vortex motion sufficiently well. In this case the force is given by

$$\vec{F} = -\vec{\nabla}(E_s + E_z) = -\mu_0 M_s H l t c\vec{e}_x - m\omega_r^2 X\vec{e}_x - m\omega_r^2 Y\vec{e}_y. \quad (11)$$

Inserting Eq. (11) in Eq. (8) yields the equation of motion for the vortex. In the absence of current and field the excited vortex performs an exponentially damped spiral rotation around its equilibrium position with its free frequency

$$\omega = -\frac{pG_0 m\omega_r^2}{G_0^2 + D_0^2\alpha^2} \quad (12)$$

and the damping constant

$$\Gamma = -\frac{D_0\alpha m\omega_r^2}{G_0^2 + D_0^2\alpha^2}. \quad (13)$$

From Eqs. (12) and (13) one easily obtains that

$$D_0\alpha = \frac{\Gamma p G_0}{\omega}. \quad (14)$$

For thin-film systems ($t/l \lesssim 0.1$) the resonance frequency of a vortex is proportional to the inverse lateral dimension $1/l$.[23] Here, we obtain from Eq. (14) that the damping constant Γ also has a characteristic length dependence, $\Gamma \propto \ln(l/a)/l$. Substituting $D_0\alpha$ using Eq. (14) the equation of motion of the vortex can be written as

$$\begin{aligned} \begin{pmatrix} \dot{X} \\ \dot{Y} \end{pmatrix} &= \begin{pmatrix} -\Gamma & -p\omega \\ p\omega & -\Gamma \end{pmatrix} \begin{pmatrix} X \\ Y \end{pmatrix} \\ &+ \begin{pmatrix} \frac{p\omega\Gamma}{\omega^2+\Gamma^2}\frac{\mu_0 M_s H l t c}{G_0} - b_j j - \frac{\Gamma^2}{\omega^2+\Gamma^2}\frac{\xi-\alpha}{\alpha}b_j j \\ -\frac{\omega^2}{\omega^2+\Gamma^2}\frac{\mu_0 M_s H l t c}{G_0} + \frac{p\omega\Gamma}{\omega^2+\Gamma^2}\frac{\xi-\alpha}{\alpha}b_j j \end{pmatrix}. \end{aligned} \quad (15)$$

In the following we assume harmonic excitations, i.e., the magnetic field and the electrical current are of the form $H(t) = H_0 e^{i\Omega t}$ and $j(t) = j_0 e^{i\Omega t}$. The magnetic (Oersted) field and the electrical current are in phase. Assuming that the squared Gilbert damping is small ($\alpha^2 \ll 1$), the damping constant of the vortex is small compared to its frequency ($\Gamma^2 \ll \omega^2$). Then Eq. (15) has the solution

$$\begin{aligned} \begin{pmatrix} X \\ Y \end{pmatrix} &= A\begin{pmatrix} i \\ p \end{pmatrix} e^{-\Gamma t + i\omega t} + B\begin{pmatrix} -i \\ p \end{pmatrix} e^{-\Gamma t - i\omega t} \\ &- \frac{e^{i\Omega t}}{\omega^2 + (i\Omega + \Gamma)^2} \\ &\times \begin{pmatrix} \left(\tilde{H} + \frac{\Gamma}{\omega}\frac{\xi}{\alpha}\tilde{j}\right)\omega + & \left(\frac{\Gamma}{\omega}\tilde{H} + \tilde{j}\right) i\Omega \\ \tilde{j}\omega p & - \left(\tilde{H} + \frac{\Gamma}{\omega}\frac{\xi-\alpha}{\alpha}\tilde{j}\right) i\Omega p \end{pmatrix}, \end{aligned} \quad (16)$$

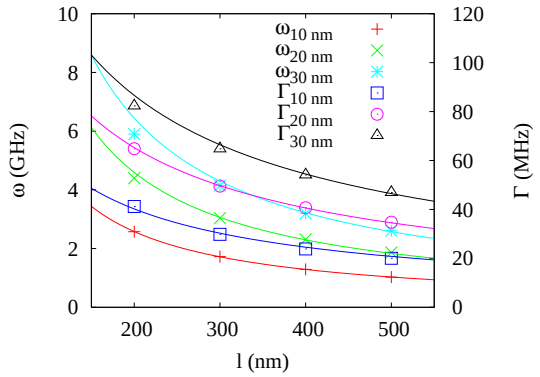

FIG. 2: (Color Online) Dependence of the free frequency ω and the damping constant Γ on the length l for various thicknesses t of the system. The symbols denote numerical results while the lines are fits with the analytical results.

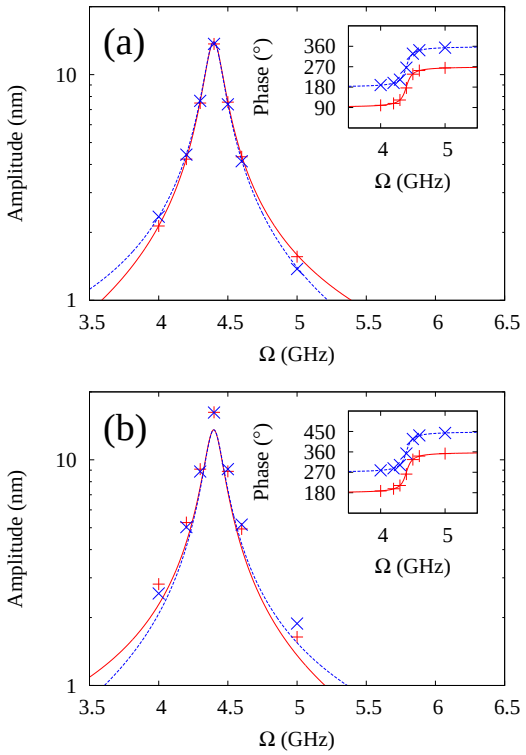

FIG. 3: (Color Online) Amplitude of the (a) current-driven and (b) field-driven vortex oscillation in x-direction (solid red line, pluses) and y-direction (dashed blue line, crosses) for a spin-polarized current density of $jP = 2.5 \cdot 10^{10}$ A/m^2 and a field of $H = 250$ A/m. The insets show the phases between the maximum of the applied current or field and the core displacement in x-direction (solid red line, pluses) and y-direction (dashed blue line, crosses). The symbols denote numerical results while the lines are derived from the analytical expression in Eq. (16).

with $\tilde{H} = \gamma H_0 lc/(2\pi)$ and $\tilde{j} = b_j j_0$. The first two terms with prefactors A and B are exponentially damped and depend on the starting configuration. Independent of the source of excitation, i.e., field or current, the sense of rotation of the vortex is given by its polarization, i.e., $p = +1$ ($p = -1$) denotes a counterclockwise (clockwise) rotation of the vortex core. Changing the sign of the chirality has the same effect as turning the magnetic field by 180°.[10] Similar to the motion of magnetic domain walls in thin nanowires[24] the vortex is driven by the current and the magnetic field as well as by their time derivatives.

At resonance the amplitude of the vortex core displacement in x- and y-direction is the same and the vortex performs a circular rotation. A vortex which is excited with a non-resonant frequency has an elliptic trajectory. The ratio between the semi-axes is given by the ratio between the frequency of the excitation and the resonance frequency.[25]

III. NUMERICAL CALCULATIONS

To test the applicability of the approximations leading to the analytical result in Eq. (16) we performed micromagnetic simulations for magnetic thin-film elements with different lengths, thicknesses, polarizations, and chiralities. The material parameters of permalloy are used, i.e., an exchange constant of $A = 13 \cdot 10^{-12}$ J/m and a saturation magnetization of $M_s = 8 \cdot 10^5$ A/m. For the Gilbert damping we use a value of $\alpha = 0.01$ which is in the regime as found by recent experiments.[26–28] The degree of non-adiabaticity ξ is chosen to be equal to α.[14,29]

For the micromagnetic simulations we extended the implementation of the Landau-Lifshitz-Gilbert equation in the Object Oriented Micro Magnetic Framework (OOMMF) by the additional current-dependent terms of Eq. (1).[24,30] The simulation cells are 2 nm in x- and y-direction which is well below the exchange length of permalloy. One cell of thickness t was used in z-direction. As in the analytical model we substitute the Oersted field by a homogeneous magnetic field.

At first the four ground states with $c = \pm 1$ and $p = \pm 1$ are calculated for each l and t. The ground states are then excited by a short current pulse. The free frequency ω and the damping constant Γ are obtained by fitting the subsequent free oscillation with the first two terms in Eq. (16). Results are presented in Fig. 2 and exhibit a good agreement between the analytical model and the micromagnetic simulations.[31]

For the driven oscillation we choose a magnetic film element with length $l = 200$ nm and thickness $t = 20$ nm. This system size allows for reasonable computing time. The magnetization is excited with har-

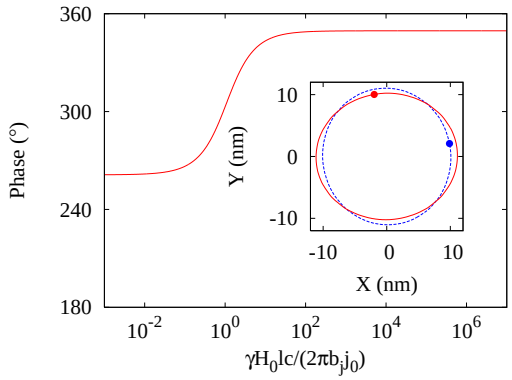

FIG. 4: (Color Online) Analytically calculated phase between the maximum current or magnetic field and the x-deflection of the vortex core for a 200 nm x 200 nm x 20 nm permalloy square excited with a frequency of $\Omega = 4.8$ GHz (above the resonance frequency of $\omega = 4.4$ GHz). The inset shows a section of the sample with the simulated trajectories of the vortex core excited with i) (solid red line) a spin-polarized current density with an amplitude of $jP = 1.2 \cdot 10^{11}$ A/m^2 and ii) (dashed blue line) a magnetic field with an amplitude of $H = 1000$ A/m. Points denote the position of the vortex at maximum current (i) and magnetic field (ii), respectively.

monic currents with a spin-polarized current density $jP = 2.5 \cdot 10^{10}$ A/m^2 in x-direction. The field excitation was performed with a harmonic field of $H = 250$ A/m in y-direction. The amplitudes and the phases of the oscillation in x- and y-direction of a vortex with positive polarization and chirality are depicted in Fig. 3. In the numerical calculations the position of the vortex is defined by the maximum amplitude of the out-of-plane magnetization. To determine this maximum, the simulation cell with maximum out-of-plane magnetization and its next neighbors are interpolated with a polynomial of second order. In the current-driven oscillation an excellent accordance between analytical calculations and numerical simulations is found. In the field-driven case the amplitudes of the analytical solution are smaller than the amplitudes obtained from the micromagnetic simulations. These deviations are caused by the differences between the approximate magnetization depicted in Fig. 1 and the exact state. The phases between the maximum of the exciting magnetic field and the maximum deflection in x- and y-direction agree very well. Vortices with other polarization and chirality (not shown) yield the same accordance.[9]

IV. DISCRIMINATION BETWEEN OERSTED FIELD AND SPIN TORQUE

From Eq. (16) one can see that the current and field induced forces on the vortex are of the same form. For experiments it is important to separate the Oersted-field and the spin-torque driven case. We describe the ratio between the field and current-induced forces on the vortex by $\tan\zeta = F_{\mathrm{Oe}}/F_{\mathrm{st}}$, i.e., a mixing angle of $\zeta = 0$ and $\zeta = \pm\pi/2$ denote the fully spin-torque driven and the fully field-driven case, respectively. There are two possibilities to determine the ratio of both forces. On the one hand for non-resonant excitations the trajectory of the vortex core is elliptical as illustrated in Fig. 4. According to Eq. (16) the direction of the major axis of the ellipse is determined by ζ. The amplitude of the vortex motion decreases very fast when the excitation frequency deviates from resonance, i.e., for experimental observation very high current densities with frequencies close to resonance are needed. On the other hand the excitation mechanisms can be distinguished using the phase of the vortex deflection.[17] As indicated by the dots in Fig. 4 the position of the vortex at maximum current depends on ζ, which can be determined from Eq. (16). The latter method is also applicable with excitations at resonance frequency.

V. CONCLUSION

In conclusion we derived an analytical expression for the current- and field-driven trajectory of a vortex in thin-film elements. The analytical result is compared to micromagnetic simulations. The accordance between both approaches is very good. The analytical expression enables us to determine the ratio between spin torque and Oersted field driven motion.

Acknowledgments

Financial support by the Deutsche Forschungsgemeinschaft via SFB 668 "Magnetismus vom Einzelatom zur Nanostruktur" and via Graduiertenkolleg 1286 "Functional metal-semiconductor hybrid systems" is gratefully acknowledged.

[1] L. Berger, Phys. Rev. B **54**, 9353 (1996).
[2] J. Slonczewski, J. Magn. Magn. Mater. **159**, L1 (1996).
[3] A. Wachowiak, J. Wiebe, M. Bode, O. Pietzsch, M. Morgenstern, and R. Wiesendanger, Science **298**, 577 (2002).
[4] T. Shinjo, T. Okuno, R. Hassdorf, K. Shigeto, and T. Ono, Science **289**, 930 (2000).
[5] S.-B. Choe, Y. Acremann, A. Scholl, A. Bauer, A. Doran, J. Stöhr, and H. A. Padmore, Science **304**, 420 (2004).
[6] B. Van Waeyenberge, A. Puzic, H. Stoll, K. W. Chou, T. Tyliszczak, R. Hertel, M. Fähnle, H. Brückl, K. Rott,

G. Reiss, et al., Nature **444**, 461 (2006).
[7] J. Shibata, Y. Nakatani, G. Tatara, H. Kohno, and Y. Otani, Phys. Rev. B **73**, 020403(R) (2006).
[8] S. Kasai, Y. Nakatani, K. Kobayashi, H. Kohno, and T. Ono, Phys. Rev. Lett. **97**, 107204 (2006).
[9] K. Yamada, S. Kasai, Y. Nakatani, K. Kobayashi, H. Kohno, A. Thiaville, and T. Ono, Nature Materials **6**, 270 (2007).
[10] S.-K. Kim, Y.-S. Choi, K.-S. Lee, K. Y. Guslienko, and D.-E. Jeong, Appl. Phys. Lett. **91**, 082506 (2007).
[11] H. Stoll, A. Puzic, B. Van Waeyenberge, P. Fischer, J. Raabe, M. Buess, T. Haug, R. Höllinger, C. Back, D. Weiss, et al., Appl. Phys. Lett. **84**, 3328 (2004).
[12] K. Y. Guslienko, X. F. Han, D. J. Keavney, R. Divan, and S. D. Bader, Phys. Rev. Lett. **96**, 067205 (2006).
[13] J. Raabe, C. Quitmann, C. H. Back, F. Nolting, S. Johnson, and C. Buehler, Phys. Rev. Lett. **94**, 217204 (2005).
[14] G. Meier, M. Bolte, R. Eiselt, B. Krüger, D. H. Kim, and P. Fischer, Phys. Rev. Lett. **98**, 187202 (2007).
[15] M. Kläui, C. A. F. Vaz, J. A. C. Bland, W. Wernsdorfer, G. Faini, E. Cambril, L. J. Heyderman, F. Nolting, and U. Rüdiger, Phys. Rev. Lett. **94**, 106601 (2005).
[16] J. He, Z. Li, and S. Zhang, Phys. Rev. B **73**, 184408 (2006).
[17] M. Bolte, G. Meier, R. Eiselt, L. Bocklage, A. Drews, B. Krüger, B. Van Waeyenberge, K. W. Chou, H. Stoll, and G. Schütz, submitted.
[18] S. Zhang and Z. Li, Phys. Rev. Lett. **93**, 127204 (2004).
[19] A. A. Thiele, J. Appl. Phys. **45**, 377 (1974).
[20] Y. Nakatani, A. Thiaville, and J. Miltat, Nature Materials **2**, 521 (2003).
[21] D. L. Huber, Phys. Rev. B **26**, 3758 (1982).
[22] K. Y. Guslienko, W. Scholz, R. W. Chantrell, and V. Novosad, Phys. Rev. B **71**, 144407 (2005).
[23] K. Y. Guslienko, B. Ivanov, V. Novosad, Y. Otani, H. Shima, and K. Fukamichi, J. Appl. Phys. **91**, 8037 (2002).
[24] B. Krüger, D. Pfannkuche, M. Bolte, G. Meier, and U. Merkt, Phys. Rev. B **75**, 054421 (2007).
[25] K.-S. Lee and S.-K. Kim, Appl. Phys. Lett. **91**, 132511 (2007).
[26] J. Nibarger, R. Lopusnik, and T. Silva, Appl. Phys. Lett. **82**, 2112 (2003).
[27] M. Schneider, T. Gerrits, A. Kos, and T. Silva, Appl. Phys. Lett. **87**, 072509 (2005).
[28] Z. Liu, F. Giesen, X. Zhu, R. D. Sydora, and M. R. Freeman, Phys. Rev. Lett. **98**, 087201 (2007).
[29] M. Hayashi, L. Thomas, Y. B. Bazaliy, C. Rettner, R. Moriya, X. Jiang, and S. S. P. Parkin, Phys. Rev. Lett. **96**, 197207 (2006).
[30] **OOMMF User's Guide, Version 1.0** M.J. Donahue and D.G. Porter Interagency Report **NISTIR 6376**, National Institute of Standards and Technology, Gaithersburg, MD (Sept 1999) (http://math.nist.gov/oommf/).
[31] Note: a is a fit parameter. The values used are 8.85 nm, 11.66 nm, and 13.59 nm for film thicknesses of 10 nm, 20 nm, and 30 nm, respectively.

Publication 2

Reprinted with permission from B. Krüger, A. Drews, M. Bolte, U. Merkt, D. Pfannkuche, and G. Meier,

Vortices and antivortices as harmonic oscillators,

J. Appl. Phys. **103**, 07A501-1-07A501-3, 2008

Vortices and antivortices as harmonic oscillators

Benjamin Krüger,[1] André Drews,[2] Markus Bolte,[2] Ulrich Merkt,[2] Daniela Pfannkuche,[1] and Guido Meier[2]

[1] *I. Institut für Theoretische Physik, Universität Hamburg, Jungiusstr. 9, 20355 Hamburg, Germany*
[2] *Institut für Angewandte Physik und Zentrum für Mikrostrukturforschung, Universität Hamburg, Jungiusstr. 11, 20355 Hamburg, Germany*

(Dated: September 11, 2007)

It is shown that the current- and field-induced gyration of magnetic vortices and antivortices follows the analytical model of a two-dimensional harmonic oscillator. Quantities of the harmonic oscillator, i.e., resonance frequency, damping constant, gyration amplitude, and the phase can be linked to material parameters and sample dimensions. This description is useful for the investigation of vortex-switching and vortex-antivortex annihilation processes.

PACS numbers: 75.60.Ch, 72.25.Ba

The study of magnetic singularities such as magnetic vortices and antivortices is appealing as they have been suggested as data storage units[1]. Due to their rotational symmetry they are also attractive objects for studying the interaction between the local magnetization and alternating magnetic fields or spin-polarized currents.[2–12] Isolated magnetic vortices form in laterally confined ferromagnetic thin film elements when it is energetically favorable for the magnetization to point in-plane and parallel to the edges. In the center the magnetization is then forced out-of-plane to avoid large angles between magnetic moments as this would drastically increase the exchange energy.[13] Antivortices, also called cross Bloch lines,[13] form either in cross-tie walls or when magnetic thin films are artificially patterned in such a way that the magnetization of four domains meet radially in one point.[14] In both cases, the region with a strong out-of-plane magnetization component, called the vortex or antivortex core, is only a few nanometers in diameter.[15,16] The direction of the magnetization in the core, called the core polarization, can only assume two values $p = +1$ or $p = -1$, indicating the direction out of or into the plane, respectively. The direction of the in-plane magnetization direction with respect to the polarization is called chirality. Vortices have chiralities $c = +1(-1)$ for counterclockwise (clockwise) in-plane curling of the magnetization, while antivortex chirality is defined by the angle of the magnetization to the current- or field-excitation and can assume values in the interval $(-2, 2]$.[17] Thus antivortices also with non-integer chiralities can be stable, e.g., in a clover-shaped sample.[14,17] Chirality and polarization unambiguously define the (anti-)vortex configuration.

It has been found that magnetic vortices can be brought to gyration by magnetic fields[2–4] or spin-polarized currents.[5,6,18] Excitation of magnetic vortices induced by oscillating spin-polarized currents or magnetic fields can be described by a harmonic oscillator model.[19] In this paper we show that vortices and antivortices can be analytically described by the same formalism by introducing a third quantity, the skyrmion number $q = np/2$, where $n = +1$ and $n = -1$ is the winding number of vortices and antivortices, respectively.[10,17] We extend the harmonic oscillator model description of current- and field-induced motion of magnetic vortices to antivortices.

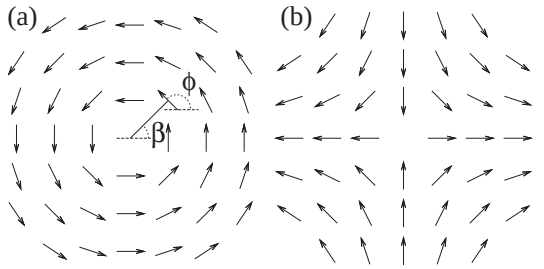

FIG. 1: Scheme of the in-plane magnetization of (a) a vortex ($n = 1$) with chirality $c = 1$ and (b) an antivortex ($n = -1$) with chirality $c = 0$ determined from Eq. (1).

For magnetic vortices and antivortices the angle of the in-plane magnetization ϕ at a given position generally obeys the relation[20,21]

$$\phi = n\beta + \pi c/2, \tag{1}$$

where β is the angular coordinate with respect to the (anti)vortex core (see Figs. 1 and 2). The winding number n can assume every integer number except zero while the chirality c is a real number with $-2 < c \leq 2$. Furthermore the core can point in positive or negative z-direction which is denoted by the polarization $p = +1$ and $p = -1$, respectively. The variables X and Y denote the position of the vortex relative to its equilibrium position without applied current or field. In a film of thickness t the Thiele equation[22,23]

$$\vec{F} + \vec{G} \times (\vec{v} + b_j\vec{j}) + D(\alpha\vec{v} + \xi b_j\vec{j}) = 0 \tag{2}$$

yields the velocity $\vec{v}$ of the vortex[19]

$$(G_0^2 + D_0^2\alpha^2)\vec{v} = \vec{G} \times \vec{F} - D_0\alpha\vec{F} - (G_0^2 + D_0^2\alpha\xi)b_j\vec{j} + b_j D_0\vec{G} \times \vec{j}(\xi - \alpha). \tag{3}$$

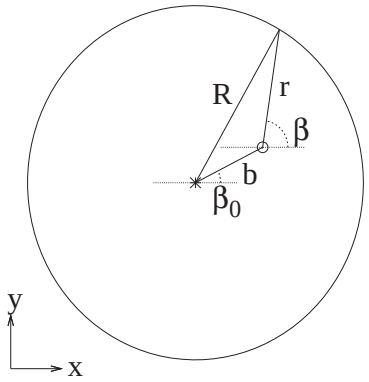

FIG. 2: Scheme of a skyrmion core (circle) in a disc with radius R. The vortex core is displaced from its equilibrium position (asterisk) by a distance $b = \sqrt{X^2 + Y^2}$.

Here

$$\vec{G} = -\frac{2\pi M_s \mu_0 tpn}{\gamma}\vec{e}_z = G_0\vec{e}_z, \tag{4}$$

is the gyrovector, $\vec{F}$ is the force due to the magnetic fields, and D is the diagonal dissipation tensor with $D_{xx} = D_{yy} = D_0$, and $D_{zz} = 0$. The value of D_0 depends on the geometry of the sample.[19,20] b_j is the coupling constant between the current density $\vec{j}$ and the magnetization $\vec{M}$. The saturation magnetization, the Gilbert damping, and the ratio between exchange relaxation time and spin-flip relaxation time are denoted by M_s, α, and ξ, respectively. In the rest of this paper we assume a current density that flows in x-direction and a magnetic field in y-direction.

For small excitation the stray-field energy of the skyrmion is modeled by a harmonic potential

$$E_s = \frac{1}{2}m\omega_r^2(X^2 + Y^2). \tag{5}$$

For the calculation of the Zeeman energy of a skyrmion in a magnetic field $\vec{H}$ that is applied in y-direction we start with a skyrmion that is located in a disc with radius R as shown in Fig. 2. The position of the skyrmion is given by $X = b\cos(\beta_0)$ in x-direction and $Y = b\sin(\beta_0)$ in y-direction. According to Guslienko et al.[21] the magnetization is given by Eq. (1). For the integration we use cylindrical coordinates with the origin at the skyrmion core. From Fig. 2 the relation $R^2 = b^2 + r^2 - 2rb\,\cos(180° - \beta + \beta_0)$ can be obtained using the law of cosine. Thus the Zeeman energy is given by

$$\begin{aligned} E_z &= -\mu_0 M_s H t \int_0^{2\pi} d\beta\ \sin(\phi) \int_0^r dr' r' \\ &= -\mu_0 M_s H t \int_0^{2\pi} d\beta\ \sin(\phi)\frac{r^2}{2} \end{aligned} \tag{6}$$

with $r = -b\cos(\beta - \beta_0) + \sqrt{b^2\cos^2(\beta - \beta_0) - b^2 + R^2}$. For small displacements b, i.e., $b^2 \ll R^2$, $r^2 \approx R^2 - 2Rb\cos(\beta - \beta_0)$ and the Zeeman energy can be written as

$$\begin{aligned} E_z =& \mu_0 M_s H b R t \int_0^{2\pi} d\beta\ \sin\left(n\beta + \frac{\pi c}{2}\right)\cos(\beta - \beta_0) \\ =& \mu_0 M_s H b R t \int_0^{2\pi} d\beta \\ &\times \left[\sin(n\beta)\cos\left(\frac{\pi c}{2}\right) + \cos(n\beta)\sin\left(\frac{\pi c}{2}\right)\right] \\ &\times \left[\cos(\beta)\cos(\beta_0) + \sin(\beta)\sin(\beta_0)\right]. \end{aligned} \tag{7}$$

Here we neglected the term proportional to R^2 which does not depend on the position of the skyrmion.

Due to the orthogonality of the $sin(nx)$ and $cos(nx)$ functions the integral is non-zero only if $|n| = 1$. Thus in first order only skyrmions with winding numbers $n = \pm 1$ move in an external Zeeman field. Therefore, in the following we focus on the winding numbers $n = 1$ and $n = -1$ which denote a vortex and an antivortex, respectively. The Zeeman energy is then given by

$$E_z = \mu_0 M_s H R\pi t \left[\sin\left(\frac{\pi c}{2}\right) X + n\cos\left(\frac{\pi c}{2}\right) Y\right]. \tag{8}$$

Accordingly, the Zeeman energy for a skyrmion in a quadratic sample is[19]

$$E_z = \mu_0 M_s H L t \left[\sin\left(\frac{\pi c}{2}\right) X + n\cos\left(\frac{\pi c}{2}\right) Y\right], \tag{9}$$

with the length L of the square. Both expressions have the same form. Thus we can write

$$E_z = \mu_0 M_s H l t \left[\sin\left(\frac{\pi c}{2}\right) X + n\cos\left(\frac{\pi c}{2}\right) Y\right], \tag{10}$$

with the characteristic length l, i.e., $l = R\pi$ for the circular and $l = L$ for the quadratic sample. The total force on the vortex is then given by

$$\begin{aligned} \vec{F} =& -\vec{\nabla}(E_s + E_z) \\ =& -\mu_0 M_s H l t \left[\sin\left(\frac{\pi c}{2}\right)\vec{e}_x + n\cos\left(\frac{\pi c}{2}\right)\vec{e}_y\right] \\ &- m\omega_r^2 X\vec{e}_x - m\omega_r^2 Y\vec{e}_y. \end{aligned} \tag{11}$$

Inserting this result in Eq. (3) we obtain the equation of motion of the skyrmion

$$\begin{aligned} \begin{pmatrix}\dot{X}\\ \dot{Y}\end{pmatrix} =& \begin{pmatrix}-\Gamma & -np\omega\\ np\omega & -\Gamma\end{pmatrix}\begin{pmatrix}X\\ Y\end{pmatrix} \\ &+ \begin{pmatrix}-b_j j - \frac{\Gamma^2}{\omega^2+\Gamma^2}\frac{\xi-\alpha}{\alpha}b_j j\\ \frac{np\omega\Gamma}{\omega^2+\Gamma^2}\frac{\xi-\alpha}{\alpha}b_j j\end{pmatrix} \\ &+ \begin{pmatrix}\frac{np\omega\Gamma\sin\left(\frac{\pi c}{2}\right)+\omega^2 n\cos\left(\frac{\pi c}{2}\right)}{\omega^2+\Gamma^2}\frac{\mu_0 M_s H l t}{G_0}\\ \frac{p\omega\Gamma\cos\left(\frac{\pi c}{2}\right)-\omega^2\sin\left(\frac{\pi c}{2}\right)}{\omega^2+\Gamma^2}\frac{\mu_0 M_s H l t}{G_0}\end{pmatrix}, \end{aligned} \tag{12}$$

with its free frequency

$$\omega = -\frac{npG_0 m\omega_r^2}{G_0^2 + D_0^2\alpha^2} \tag{13}$$

and damping constant

$$\Gamma = -\frac{D_0 \alpha m\omega_r^2}{G_0^2 + D_0^2\alpha^2}. \tag{14}$$

In the following we assume harmonic excitations, i.e., the magnetic field and the electrical current are of the form $H(t) = H_0 e^{i\Omega t}$ and $j(t) = j_0 e^{i\Omega t}$. The magnetic (Oersted) field and the electrical current are in phase. For weakly damped systems, i.e., $\Gamma \ll \omega$, the solution is

$$\begin{aligned}\begin{pmatrix} X \\ Y \end{pmatrix} = &- \frac{e^{i\Omega t}\omega}{\omega^2 + (i\Omega + \Gamma)^2} \begin{pmatrix} \tilde{H}\sin\left(\frac{\pi c}{2}\right) \\ \tilde{H} n \cos\left(\frac{\pi c}{2}\right) + \tilde{j} np \end{pmatrix} \\ &- \frac{e^{i\Omega t} i\Omega}{\omega^2 + (i\Omega + \Gamma)^2} \begin{pmatrix} \tilde{H} p \cos\left(\frac{\pi c}{2}\right) + \tilde{j} \\ -\tilde{H} np \sin\left(\frac{\pi c}{2}\right) \end{pmatrix},\end{aligned} \tag{15}$$

with $\tilde{H} = \gamma H_0 l/(2\pi)$ and $\tilde{j} = b_j j_0$. For a vortex $n = 1$ and $c = \pm 1$ hold. Therefore, $\sin(\pi c/2) = c$ and $\cos(\pi c/2) = 0$. Thus the above result reveals the known expression for the vortex.[19]

In conclusion we have shown that the harmonic oscillator model for the current- and field-driven trajectory of a vortex can be extended to antivortices. An analytical expression for the current- and field-driven motion of skyrmions for harmonic excitations is given.

Acknowledgments

Financial support by the Deutsche Forschungsgemeinschaft via SFB 668 "Magnetismus vom Einzelatom zur Nanostruktur" and via Graduiertenkolleg 1286 "Functional metal-semiconductor hybrid systems" is gratefully acknowledged.

[1] R. Höllinger, A. Killinger, and U. Krey, J. Magn. Magn. Mat. **261**, 178 (2003).
[2] B. E. Argyle, E. Terrenzio, and J. C. Slonczewski, Phys. Rev. Lett. **53**, 190 (1984).
[3] K. Y. Guslienko, B. Ivanov, V. Novosad, Y. Otani, H. Shima, and K. Fukamichi, J. Appl. Phys **91**, 8037 (2002).
[4] S.-B. Choe, Y. Acremann, A. Scholl, A. Bauer, A. Doran, J. Stöhr, and H. A. Padmore, Science **304**, 420 (2004).
[5] J. Shibata, Y. Nakatani, G. Tatara, H. Kohno, and Y. Otani, Phys. Rev. B **73**, 020403(R) (2006).
[6] S. Kasai, Y. Nakatani, K. Kobayashi, H. Kohno, and T. Ono, Phys. Rev. Lett. **97**, 107204 (2006).
[7] R. Hertel and C. M. Schneider, Phys. Rev. Lett. **97**, 177202 (2006).
[8] R. Hertel, S. Gliga, M. Fähnle, and C. M. Schneider, Phys. Rev. Lett. **98**, 117201 (2007).
[9] J.-G. Caputo, Y. Gaididei, F. G. Mertens, and D. D. Sheka, Phys. Rev. Lett. **98**, 056604 (2007).
[10] O. A. Tretiakov and O. Tchernyshyov, Phys. Rev. B **75**, 012408 (2007).
[11] K. Yamada, S. Kasai, Y. Nakatani, K. Kobayashi, H. Kohno, A. Thiaville, and T. Ono, Nature Materials **6**, 269 (2007).
[12] D. D. Sheka, J. P. Zagorodny, J.-G. Caputo, Y. Gaididei, and F. G. Mertens, Phys. Rev. B **71**, 134420 (2005).
[13] A. Hubert and R. Schäfer, *Magnetic Domains: The Analysis of Magnetic Microstructures* (Springer, Berlin, Germany, 1998).
[14] K. Shigeto, T. Okuno, K. Mibu, T. Shinjo, and T. Ono, Appl. Phys. Lett. **80**, 4190 (2002).
[15] T. Shinjo, T. Okuno, R. Hassdorf, K. Shigeto, and T. Ono, Science **289**, 930 (2000).
[16] A. Wachowiak, J. Wiebe, M. Bode, O. Pietzsch, M. Morgenstern, and R. Wiesendanger, Science **298**, 577 (2002).
[17] A. Drews, B. Krüger, M. Bolte, and G. Meier (2007), submitted.
[18] M. Bolte, G. Meier, R. Eiselt, L. Bocklage, A. Drews, B. Krüger, B. Van Waeyenberge, K. W. Chou, H. Stoll, and G. Schütz, unpublished.
[19] B. Krüger, A. Drews, M. Bolte, U. Merkt, D. Pfannkuche, and G. Meier (2007), submitted.
[20] J. He, Z. Li, and S. Zhang, Phys. Rev. B **73**, 184408 (2006).
[21] K. Y. Guslienko, V. Novosad, Y. Otani, H. Shima, and K. Fukamichi, Appl. Phys. Lett. **78**, 3848 (2001).
[22] A. A. Thiele, J. Appl. Phys. **45**, 377 (1974).
[23] Y. Nakatani, A. Thiaville, and J. Miltat, Nature Materials **2**, 521 (2003).

Publication 3

Reprinted with permission from M. Bolte, G. Meier, B. Krüger, A. Drews, R. Eiselt, L. Bocklage, S. Bohlens, T. Tyliszczak, A. Vansteenkiste, B. Van Waeyenberge, K. W. Chou, A. Puzic, and H. Stoll,

Time-Resolved X-Ray Microscopy of Spin-Torque-Induced Magnetic Vortex Gyration,

Phys. Rev. Lett. **100**, 176601-1-176601-4, 2008

Time-Resolved X-ray Microscopy of Spin-Torque-Induced Magnetic Vortex Gyration

Markus Bolte,[1,*] Guido Meier,[1] Benjamin Krüger,[2] André Drews,[1] René Eiselt,[1] Lars Bocklage,[1] Stellan Bohlens,[2] Tolek Tyliszczak,[3] Arne Vansteenkiste,[4] Bartel Van Waeyenberge,[4,5] Kang Wei Chou,[5] Aleksandar Puzic,[5] and Hermann Stoll[5]

[1]*Institut für Angewandte Physik und Zentrum für Mikrostrukturforschung, Universität Hamburg, Jungiusstrasse 11, 20355 Hamburg, Germany*
[2]*I. Institut für Theoretische Physik, Universität Hamburg, Jungiusstrasse 9, 20355 Hamburg, Germany*
[3]*Advanced Light Source, LBNL, 94720 Berkeley, California, USA*
[4]*Department of Subatomic and Radiation Physics, Ghent University, Proeftuinstraat 86, 9000 Ghent, Belgium*
[5]*Max Planck Institut für Metallforschung, Heisenbergstrasse 3, 70569 Stuttgart, Germany*

(Dated: 30 January 2008)

Time-resolved X-ray microscopy is used to image the influence of alternating high-density currents on the magnetization dynamics of ferromagnetic vortices. Spin-torque induced vortex gyration is observed in micrometer-sized permalloy squares. The phases of the gyration in structures with different chirality are compared to an analytical model and micromagnetic simulations, considering both alternating spin-polarized currents and the current's Oersted field. In our case the driving force due to spin-transfer torque is about 70% of the total excitation while the remainder originates from the current's Oersted field. This finding has implications to magnetic storage devices using spin-torque driven magnetization switching and domain-wall motion.

PACS numbers: 68.37.Yz, 72.25.Ba , 75.25.+z, 75.40.Mg, 85.75.-d

The discovery that spin-polarized electrons traveling through ferromagnets apply a torque on the local magnetization[1] opened up a new field of research in solid state physics that could potentially result in new magnetic storage media. It is now understood that the spin-transfer torque acts on inhomogeneities in the magnetization, e.g., on interfaces between magnetic layers,[2] on domain walls,[3,4] i.e., interfaces between regions of uniform magnetization, or on magnetic vortices.[5–8] Magnetic domain walls, usually vortex walls,[9] can be driven by spin-polarized currents to store information in bit registers.[10]

Vortices appear in laterally confined thin films when it is energetically favorable for the magnetization to point in-plane and parallel to the edges. In the center the magnetization is forced out-of-plane to avoid large angles between magnetic moments that would drastically increase the exchange energy. The region with a strong out-of-plane magnetization component is called the vortex core and is only a few nanometers in diameter.[11,12] The direction of the magnetization in the vortex core, also called the *core polarization* p, can only point out-of- or into-the-plane (p=$+1$ or p=-1, respectively). Hence ferromagnetic thin films containing vortex cores have been suggested as data storage elements. The *chirality* $c = +1(-1)$ denotes the counterclockwise (clockwise) in-plane curling direction of the magnetization. It is known that vortices can be excited to gyrate around their equilibrium position by magnetic fields.[13,14] Recently it has been shown that field excitation can also switch the core polarization.[15–20] Micromagnetic simulations predict that spin-polarized currents can cause vortices both to gyrate[5,7] and to switch their polarization.[8,21,22] Both for field- and spin-torque-driven excitation, the direction of gyration is governed by the vortex polarization according to the right-hand rule (see Fig. 2 of Ref.[14]). The phase of field-driven gyration depends also on the chirality, while spin-torque driven gyration is independent of the chirality as the spin-transfer torque is proportional to the spatial derivative of the magnetization.[7] Time- and spatially averaging experimental techniques indicate that spin-torque-driven vortex gyration and switching indeed occurs, but conclusive evidence by time-resolved domain imaging technique that resolves the phase of gyration is still elusive.

Here we show by time-resolved X-ray microscopy that magnetic vortices in confined structures can be excited to gyration by high-frequency currents of high density passing directly through the ferromagnetic element. By observing the phase of the gyration relative to the excitation, we can discriminate between the current's spin-torque and its Oersted field contributions to the vortex motion. Field strengths of 30 μT that are due to the current in the gold contacts and an inhomogeneous current distribution within the ferromagnetic element itself are calculated.

We investigated 2×2 μm^2 large and 20 nm thick permalloy ($Ni_{80}Fe_{20}$) squares in which Landau-domain patterns with a single vortex are energetically favorable at remanence. Microstructured permalloy squares were prepared on 200 nm thin Si_3N_4 membranes for minimal absorption of the X-rays. The squares were prepared onto the membranes by electron-beam lithography, electron-beam evaporation, and lift-off processing. To excite the structures with alternating currents, they were contacted by 40 nm thick gold strip lines with an overlap of 150 nm as shown in Fig. 1. Thus the current had to pass through the ferromagnetic material. Additional permalloy squares having the same dimensions were placed completely underneath the strip lines to compare the phases of the current-driven gyration to field-driven gyration within the same experiment.

The magnetization was excited by high density AC-currents, and the magnetization's response was imaged by time-resolved X-ray microscopy. For this the samples were placed in the scanning transmission X-ray microscope (STXM) of beam line 11.0.2 at the Advanced Light Source (ALS) in Berkeley. The monochromatic, circularly polarized X-ray beam from the undulator beam line was focused onto the sample with the help of a Fresnel zone plate. The reso-

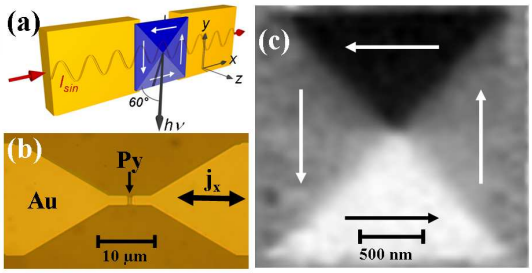

FIG. 1: (color online) (a) Scheme of the permalloy square contacted by two gold wires. The sample is tilted by 60° relative to the incident X-ray beam. (b) Optical micrograph of a permalloy square and its contacts on the Si_3N_4-membrane. (c) Magnetic contrast of the relaxed permalloy square with a thickness of 20 nm showing the x-component of the magnetization as black-to-white contrast.

lution of this X-ray microscope was about 30 nm. The sample was scanned in the xy-plane with a high resolution scanning stage under interferometric control and the transmitted intensity was recorded. The photon energy was set at the Ni L_3-absorption edge (852.7 eV), where X-ray circular dichroism (XMCD)[23] yields the magnetic contrast. With XMCD, the transmitted photon intensity is higher when the magnetic moments and polarization are antiparallel than in the parallel case. In our case, the sample plane was set at an angle of 60° with respect to the incident beam (see Fig. 1(a)) so that the microscope can detect the in-plane magnetization. We can thus unambiguously determine the chirality of the vortices.

The temporal resolution of the microscope, here about 70 ps, is given by the width of the electron bunches that produce the X-ray photon flashes. In the standard multi-bunch operation mode of the synchrotron used here, the flash repetition rate is 500 MHz. To resolve the individual flashes, a fast avalanche photo diode was used as a photon detector. With fast data acquisition electronics, the signals from individual bunches were recorded.[24] At the ALS, one of the 328 electron bunches has a much larger amplitude. It produces a brighter flash and is used as a reference marker to align the excitation signal with the data acquisition. The absolute phase relation between the recorded images and the excitation current is made by sending a short pulse through the detector electronics. By aligning its arrival to the pulse produced by the photons of the reference marker an accuracy of approximately 100 ps is achieved. A signal generator was synchronized with the X-ray flashes of the ALS, and an excitation frequency of $500\ \mathrm{MHz}/8 = 62.5$ MHz was selected since it is close to the expected resonance frequency of the vortex.[25] The alternating current was sent through the permalloy squares and the magnetic response was detected at different phases (see Fig. 2(a)). Figures 2(b) and 2(c) show the magnetic contrast of two different samples at eight different phases of the excitation.[26]

The permalloy square ($c = +1$) in Fig. 2(b) was excited with a current density amplitude of $j = 1.2 \cdot 10^{11}$ A/m^2. The vortex performs a counterclockwise gyration, it must therefore have a positive polarization ($p = +1$).[14] The amplitude

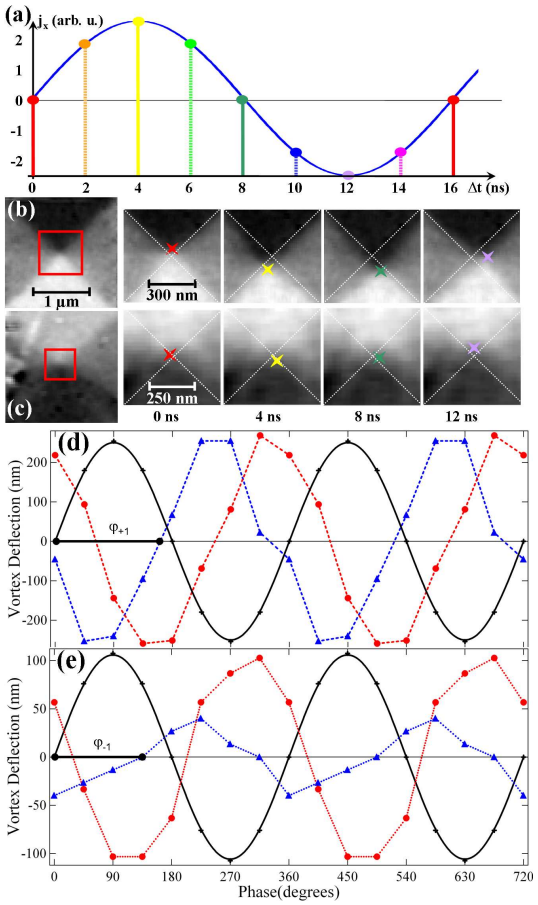

FIG. 2: (color online) (a) Sampling of the response to an 62.5 MHz AC-current excitation (j_x) at eight different phases in steps of 45°. Shown in (b) and (c) are X-ray images of complete Landau-domain pattern (left) and blow-ups of the center piece at four channels corresponding to phases 0°, 90°, 180°, and 270° (right). (d) and (e) show the vortex deflection in x direction (blue) and y direction (red) depicted in (b) and (c), respectively. The black solid curves represent the exciting current. Points represent the measured data, lines are guides to the eye.

of the gyration is 250 ± 20 nm, i.e., the vortex gyrates at a velocity of 100 ± 8 m/s. The vortex in Fig. 2(c) was excited with a lower excitation amplitude of $j = 4.7 \cdot 10^{10}$ A/m^2. It has a negative chirality ($c = -1$) and also gyrates counterclockwise, i.e., $p = +1$. As can be expected, the amplitude of gyration is much smaller. From the analysis of the vortex position at certain excitation phases and by using differential images,[27] the relative phase with respect to the excitation can be derived (see Fig. 2(d) and (e)). The phase difference $\Delta\varphi = \varphi_{+1} - \varphi_{-1}$ between the gyration of the vortices with different chiralities is about 45°. The permalloy squares underneath the strip lines were also imaged and

analyzed in like manner. They showed phase differences of $180°$ for vortices with opposite chirality as shown in Fig. 3. Because the Au strip line has a 20 times larger cross section and a 20 times higher conductivity than the permalloy square, the current flowing through the permalloy squares underneath the strip line exerts a negligible spin-transfer torque. Numerical simulations yield a torque that is a factor of $10^{-3} - 10^{-4}$ lower than the torque due to the magnetic field.

To better understand the dependence of the phases on current and field excitation, micromagnetic simulations were conducted. AC-excitations of a small permalloy square with either spin-polarized currents j_x or magnetic fields H_y were simulated at different frequencies, i.e., below resonance, at resonance, and above resonance, for all chiralities and polarizations. For the simulations the Object Oriented Micromagnetic Framework (*OOMMF*) was extended by additional spin-torque terms.[3,4] A Landau-domain pattern of $200 \times 200 \times 20$ nm^3 with a vortex was chosen.[28] We assumed a saturation magnetization of $M_\mathrm{s} = 8 \cdot 10^5$ A/m, an exchange constant of $A = 1.3 \cdot 10^{-11}$ J/m, a Gilbert damping of $\alpha = 0.01$, and a ratio $\xi = \alpha$ between spin-flip and spin-relaxation time.[29,30] The amplitude of the spin-polarized current was set to $P \cdot j = 2.5 \cdot 10^{10}$A/m, and the amplitude of the magnetic field was $H = 250$ A/m^2. The size of the simulation cells was $2 \times 2 \times 20$ nm^3. The resonance frequency ω_r of the vortex element was derived by fitting the motion of a vortex relaxed from an initially excited state to the equation of motion of a damped harmonic oscillator.[7] The simulations show that the phase with respect to the AC-excitation differs between spin-transfer-torque- and field-excitation, because the latter depends on the chirality, in agreement with previous micromagnetic simulations.[5,6]

Following the 'rigid model' for magnetic vortices in thin films,[31,32] the vortex gyration due to alternating fields can be described by a two-dimensional harmonic oscillator.[33] This model can be generalized to include torques due to spin-polarized currents.[7,34] In this model, the alternating magnetic field or current forces the vortex to oscillate along the direction of the field or current. The magnetostatic field created by the deviation of the vortex from its equilibrium position drives the oscillator perpendicular to the excitation. For a current passing through the permalloy square in x direction (see Fig. 1), the resulting Oersted field is in y direction. Thus the solution of the equation of motion of the vortex core in the oscillator model can be written as[7]

$$\begin{pmatrix} X \\ Y \end{pmatrix} = \frac{e^{i\Omega t}}{\omega^2 + (i\Omega + \Gamma)^2} \times \left(\frac{\gamma l}{2\pi} c H_y \begin{pmatrix} -\omega \\ i\Omega p \end{pmatrix} - b_j j_x \begin{pmatrix} i\Omega \\ p\omega \end{pmatrix} \right). \quad (1)$$

Here, Ω is the excitation frequency, ω the gyration frequency of the free vortex, Γ the damping constant of the vortex harmonic oscillator which is proportional to the Gilbert damping α, and $\gamma = 2.21 \cdot 10^5$ m/As the gyromagnetic ratio for permalloy. The constant $b_j = P\mu_\mathrm{B}/(eM_\mathrm{s})$ with the saturation magnetization M_s and the spin polarization P describes the coupling between the electrical current and the magnetization.

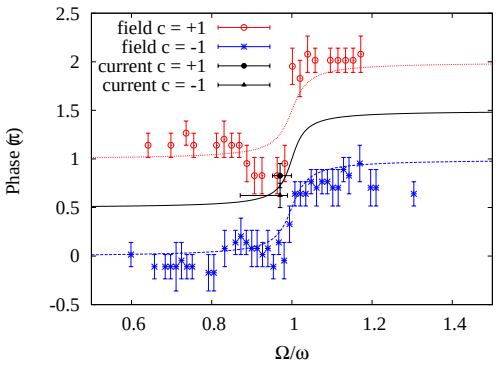

FIG. 3: (color online) Phase response of magnetic vortex oscillators as detected by time-resolved X-ray microscopy normalized to the respective resonance frequency. The red circles and the blue stars represent the phase responses of two permalloy squares excited purely by an AC-magnetic field. The black circle and triangle represent the phases of the current-fluxed samples shown in Fig. 2(b) and (c), respectively.

The model is used to extract the contributions of Oersted field and spin-torque to the phases observed in the experimental data. The blue crosses shown in Fig.3 represent the phases of field-driven vortex-core gyration ($c = -1$) with respect to the excitation at different excitation frequencies, while the dashed blue line is a fit from Eq. 1. The red circles and the corresponding fit (dotted red line) are from a vortex having $c = +1$.[35] The good agreement between the experimental data and the fit shows the validity of the harmonic oscillator model. The X-ray microscopy data from the current-fluxed samples is plotted as a black circle and a black triangle, and the corresponding fit is shown by a solid black line. The error bars in y direction are derived by error propagation from the measurements. The error bars in x direction follow from an uncertainty in the resonance frequency when assuming the resonance frequencies of the vortices are not the same. By estimating the Oersted field due to the current using Eq. 1 and $\Delta\varphi = 45°$, values of up to 30 μT for a current density of $1.2 \cdot 10^{11}$A/m^2 are derived. The driving force on the vortex due to an Oersted field of this magnitude corresponds to about 30% of the total driving force. Micromagnetic simulations using *both* spin-torque and field excitation with current and field values as calculated above yielded $40°$ phase difference between vortices having $c = +1$ and $c = -1$. This is almost the same phase difference as observed by X-ray microscopy.

Three-dimensional current-path and Oersted-field calculations were also performed for our sample geometry, taking an inhomogeneous current density in the gold contacts and in the permalloy into account. The calculations showed fields of very similar magnitude (20 μT) as deduced from the experiments. The fields originate from the perpendicular currents leading from the contacts into the permalloy as well as from an inhomogeneous current density in the permalloy, because the current enters and exits the permalloy on the upper side of

the ferromagnet. For smaller and thicker vortex geometries, the influence of the current leads and the inhomogeneous current density is much larger. For example, permalloy layers of 1 μm length and 50 nm thickness with 40 nm thick gold contacts and higher current densities than in our cases lead to Oersted-field strengths of up to several Millitesla, more than sufficient for field-induced switching.

The presence of Oersted fields due to an asymmetric setup can be seen as a general challenge to spin-torque experiments, but so far have not been taken into account. One must be careful to rule out field-driven or field-assisted magnetization dynamics in spin-torque experiments. In our case the observations of the phase of magnetic vortex gyration were possible due to its periodic motion in a confined structure. The dynamics of other magnetic objects, e.g., vortex-domain walls, are more difficult to record, but are also subject to Oersted fields from spin-polarized currents. As seen from our observations, one cannot safely assume that the change of a magnetic structure is due to a traversing spin-polarized current alone.

With time-resolved X-ray microscopy we have observed magnetic vortex gyration driven by spin-polarized currents that can be described by a harmonic oscillator model. We identified the spin torque as the main driving force, however, we have also recognized a non-negligible contribution of the current's Oersted field. In experiments, one needs to resolve the phase and the sense of gyration to separate the contribution of the current's spin-torque to magnetic vortex gyrations from the current's Oersted field. These observations are relevant to technological applications since spin-polarized currents that switch the polarization of vortices have been suggested for data storage devices[8].

Acknowledgments

We thank Ulrich Merkt for valuable discussions. Financial support from the Deutsche Forschungsgemeinschaft via the SFB 668 "Magnetismus vom Einzelatom zur Nanostruktur" as well as the GK 1286 "Functional Metal-Semiconductor Hybrid Systems" is gratefully acknowledged.

* Electronic address: mbolte@physik.uni-hamburg.de

[1] L. Berger, J. Appl. Phys. **55**, 1954 (1984).
[2] J. Slonczewski, J. Magn. Magn. Mater. **159**, L1 (1996).
[3] S. Zhang and Z. Li, Phys. Rev. Lett. **93**, 127204 (2004).
[4] B. Krüger, D. Pfannkuche, M. Bolte, G. Meier, and U. Merkt, Phys. Rev. B **75**, 054421 (2007).
[5] J. Shibata, Y. Nakatani, G. Tatara, H. Kohno, and Y. Otani, Phys. Rev. B **73**, 020403(R) (2006).
[6] S. Kasai, Y. Nakatani, K. Kobayashi, H. Kohno, and T. Ono, Phys. Rev. Lett. **97**, 107204 (2006).
[7] B. Krüger, A. Drews, M. Bolte, U. Merkt, D. Pfannkuche, and G. Meier, Phys. Rev. B **76**, 224426 (2007).
[8] K. Yamada, S. Kasai, Y. Nakatani, K. Kobayashi, H. Kohno, A. Thiaville, and T. Ono, Nature Materials **6**, 270 (2007).
[9] Y. Nakatani, A. Thiaville, and J. Miltat, J. Magn. Magn. Mater. **290**, 750 (2005).
[10] S. S. P. Parkin, US Patents 6,834,005, 6,898,132, 6,920,062, 7,031,178, and 7,236,386 (2004-2007).
[11] T. Shinjo, T. Okuno, R. Hassdorf, K. Shigeto, and T. Ono, Science **289**, 930 (2000).
[12] A. Wachowiak, J. Wiebe, M. Bode, O. Pietzsch, M. Morgenstern, and R. Wiesendanger, Science **298**, 577 (2002).
[13] B. E. Argyle, E. Terrenzio, and J. C. Slonczewski, Phys. Rev. Lett. **53**, 190 (1984).
[14] S.-B. Choe, Y. Acremann, A. Scholl, A. Bauer, A. Doran, J. Stöhr, and H. A. Padmore, Science **304**, 420 (2004).
[15] B. Van Waeyenberge, A. Puzic, H. Stoll, K. W. Chou, T. Tyliszczak, R. Hertel, M. Fähnle, H. Brückl, K. Rott, G. Reiss, et al., Nature **444**, 461 (2006).
[16] R. Hertel, S. Gliga, C. M. Schneider, and M. Fähnle, Phys. Rev. Lett. **98**, 117201 (2007).
[17] D. Sheka, Y. Gaididei, and F. Mertens, Appl. Phys. Lett. **91**, 082509 (2007).
[18] S.-K. Kim, Y.-S. Choi, K.-S. Lee, K. Y. Guslienko, and D.-E. Jeong, Appl. Phys. Lett. **91**, 082506 (2007).
[19] K.-S. Lee, K. Y. Guslienko, J.-Y. Lee, and S.-K. Kim, Phys. Rev. B **76**, 174410 (2007).
[20] Q. F. Xiao, J. Rudge, E. Girgis, J. Kolthammer, B. C. Choi, Y. K. Hong, and G. W. Donohoe, J. Appl. Phys. **102**, 103904 (2007).
[21] J.G. Caputo, Y. Gaididei, F.G. Mertens, and D.D. Sheka, Phys. Rev. Lett. **98**, 056604 (2007).
[22] Y. Liu, S. Gliga, R. Hertel, and C. Schneider, Appl. Phys. Lett. **91**, 112501 (2007).
[23] G. Schütz, W. Wagner, W. Wilhelm, P. Kienle, R. Zeller, R. Frahm, and G. Materlik, Phys. Rev. Lett. **58**, 737 (1987).
[24] Y. Acremann, V. Chembrolu, J. P. Strachan, T. Tyliszczak, and J. Stöhr, Rev. Sci. Instr. **78**, 014702 (2007).
[25] V. Novosad, F. Y. Fradin, P. E. Roy, K. S. Buchanan, K. Y. Guslienko, and S. D. Bader, Phys. Rev. B **72**, 024455 (2005).
[26] See also *movie1.avi* and *movie2.avi* in the online supporting material.
[27] A. Puzic, B. Van Waeyenberge, K. W. Chou, P. Fischer, H. Stoll, G. Schütz, T. Tyliszczak, K. Rott, H. Brückl, G. Reiss, et al., J. Appl. Phys. **97**, 10E704 (2005).
[28] The smaller element size allowed for an adequate simulation cell size while drastically decreasing the computation time. This approach is justified because only the gyration frequency (see Ref.[25]) and amplitude (see Ref.[7]) changes with the sample dimensions, but not the phase relative to the excitation.
[29] M. Hayashi, L. Thomas, C. Rettner, R. Moriya, Y. B. Bazaliy, and S. S. P. Parkin, Phys. Rev. Lett. **98**, 037204 (2007).
[30] G. Meier, M. Bolte, R. Eiselt, B. Krüger, D.-H. Kim, and P. Fischer, Phys. Rev. Lett. **98**, 187202 (2007).
[31] A. A. Thiele, Phys. Rev. Lett. **30**, 230 (1973).
[32] D. L. Huber, Phys. Rev. B **26**, 3758 (1982).
[33] K.-S. Lee, S.-K. Kim, D.-E. Jung, Y.-S. Yu, and Y.-S. Choi, cond-mat **0712**, 0758 (2007).
[34] K.-S. Lee and S.-K. Kim, Appl. Phys. Lett. **91**, 132511 (2007).
[35] The blue and red data points in Fig. 3 originate from 1.5×1.5 μm^2 $\times$ 50 nm and 1×1 μm^2 $\times$ 50 nm permalloy squares ($p = +1$) fitted by the phase response of an harmonic oscillator having $\omega = 222.6$ MHz, $\Gamma = 6.8$ MHz and $\omega = 316.9$ MHz, $\Gamma = 9.7$ MHz, respectively.

4.1.3 Amplitude of core gyration

At simultaneous current and magnetic-field excitations the resulting forces are superimposed constructively or destructively depending on their relative orientation and on the magnetization pattern. Both forces are of equal strengths for a ratio $j/H = L\gamma/(2\pi b_j)$ between current and magnetic field, see Eqn. 4.21. For this ratio the core displacement is doubled or completely quenched when the forces are directed into the same direction or into the opposite direction.
For an alternating magnetic field perpendicular to an alternating current, the x-component of the trajectory of an antivortex at resonance reads

$$x = \frac{1}{2\Gamma}\left(-\left[v_H p \cos\left(\frac{\pi c}{2}\right) + v_j \right] + i v_H \sin\left(\frac{\pi c}{2}\right)\right) e^{i\Omega t}. \tag{4.29}$$

The amplitude $r = \sqrt{Re(x)^2 + Im(x)^2}$ is [32], [P3]

$$r = r_0 \sqrt{\cos^2\left(\frac{\pi c}{4}\right)\left(\frac{v_H}{vj} + p\right)^2 + \sin^2\left(\frac{\pi c}{4}\right)\left(\frac{v_H}{v_j} - p\right)^2}, \tag{4.30}$$

where $r_0 = v_j/2\Gamma$ is the amplitude of gyration for an excitation with only a current. The factor v_H/v_j describes the ratio between the velocities v_H due to field and v_j due to current excitation ($v_j \neq 0$). From Eqn 4.30 follows that antivortices with the c-values $c = 0$ ($c = 2$) show a maximum amplitude of gyration for the polarizations $p = 1$ ($p = -1$) and a minimum amplitude for the same c-values but for opposite polarizations $p = -1$ ($p = 1$).

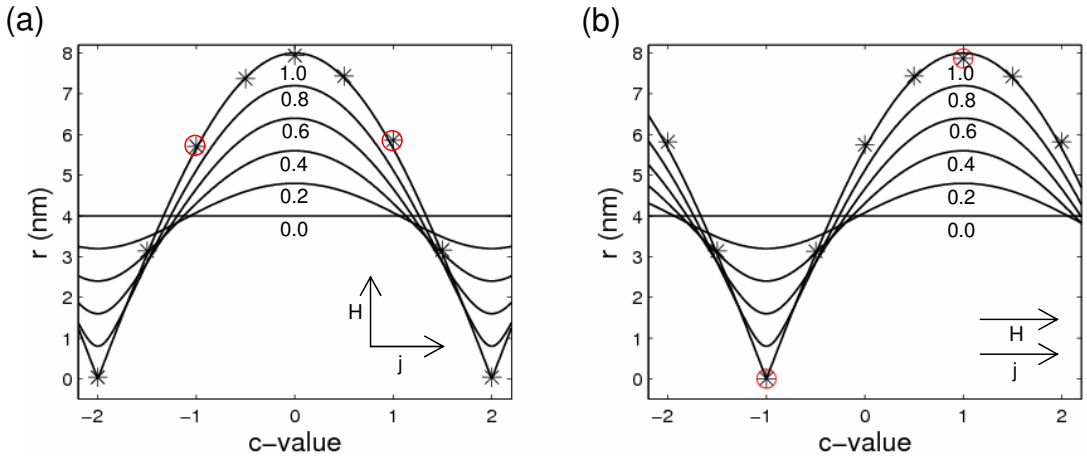

Fig. 4.8: Amplitude of the gyration of an antivortex ($p = 1$) in a clover-shaped permalloy sample ($500 \times 500 \times 40$ nm^3) excited at resonance by an alternating magnetic field (a) perpendicular to the alternating current and (b) parallel to the alternating current. The magnetic field has an amplitude of 122 A/m, the current density has an amplitude of $j \cdot P = 0.7 \cdot 10^{10}$ Am^{-2}. The asterisks are simulated results for $v_H/v_j = 1.0$. The black lines are analytical results for different ratios v_H/v_j as indicated on the lines. The red circles denote amplitudes of vortices with the chiralities $c = -1$ and $c = 1$.

For parallel alternating magnetic field and current the x-component of the deflection

$$x = \frac{1}{2\Gamma}\Big(- \Big[v_H p \sin\Big(\frac{\pi c}{2}\Big) - v_j \Big] + i v_H \cos\Big(\frac{\pi c}{2}\Big)\Big) e^{i\Omega t} \tag{4.31}$$

and the amplitude is

$$r = r_0 \sqrt{\cos^2\Big(\frac{\pi(1-c)}{4}\Big)\Big(\frac{v_h}{vj} + p\Big)^2 + \sin^2\Big(\frac{\pi(1-c)}{4}\Big)\Big(\frac{v_h}{v_j} - p\Big)^2}. \tag{4.32}$$

A maximum amplitude can be observed at chiralities or c-values $c = 1$ ($c = -1$) and polarizations $p = 1$ ($p = -1$), a minimum amplitude for the same chiralities or c-values but for opposite polarizations $p = -1$ ($p = 1$). Analytical and simulated results of the amplitude of antivortex core gyration for fields perpendicular and parallel to the current are shown in Fig. 4.8 for different ratios v_H/v_j.

For a rotating magnetic field or a rotating current the forces due to the excitation and the gyroscopic force point into the same direction or into the opposite direction. This leads to a maximum enhancement or suppression of the core gyration. The sense of gyration of the gyroscopic force [43] is given by the product np of winding number and polarization. An excitation that rotates in the mathematical positive or negative direction determines the sense of gyration of the external force. At resonance the amplitude of gyration of a vortex excited by a rotating current reads

$$r = r_0 \sqrt{2 v_j^2 \Omega^2 (1 \pm np)}, \tag{4.33}$$

see Eqn. 4.25. Thus for a product $np = 1$ ($np = -1$) and a mathematic positive (negative) sense of rotation of the excitation the amplitude of gyration is enhanced and for a mathematic negative (positive) sense of rotation of the excitation the amplitude is suppressed.

Publication 4

Reprinted with permission from A. Drews, B. Krüger, M. Bolte, and G. Meier,

Current- and field-driven magnetic antivortices,

Phys. Rev. B **77**, 094413-1-094413-5, 2008

Current- and field-driven magnetic antivortices

André Drews,[1] Benjamin Krüger,[2] Markus Bolte,[1] and Guido Meier[1]

[1] *Institut für Angewandte Physik und Zentrum für Mikrostrukturforschung, Universität Hamburg, Jungiusstr. 11, 20355 Hamburg, Germany*

[2] *I. Institut für Theoretische Physik, Universität Hamburg, Jungiusstr. 9, 20355 Hamburg, Germany*

(Dated: May 18, 2009)

Antivortices in ferromagnetic thin-film elements are in-plane magnetization configurations with a core pointing perpendicular to the plane. By using micromagnetic simulations, we find that magnetic antivortices gyrate on elliptical orbits similar to magnetic vortices when they are excited by alternating magnetic fields or by spin-polarized currents. The phase between high-frequency excitation and antivortex gyration is investigated. In case of excitation by spin-polarized currents the phase is determined by the polarization of the antivortex, while for excitation by magnetic fields the phase depends on the polarization as well as on the in-plane magnetization. Simultaneous excitation by a current and a magnetic field can lead to a maximum enhancement or to an entire suppression of the amplitude of the core gyration, depending on the angle between excitation and in-plane magnetization. This variation of the amplitude can be used to experimentally distinguish between spin-torque and Oersted-field driven motion of an antivortex core.

PACS numbers: 75.60.Ch, 72.25.Ba, 76.50.+g

I. INTRODUCTION

Magnetic vortices and antivortices exist in ferromagnetic thin-film elements, where the interplay of demagnetization and exchange energy forces the magnetization out of plane to form a core in the centers.[1,2] The orientation of the vortex or antivortex core, denoted as the polarization p, is highly interesting for technical applications, e.g. magnetic memory devices, as it can be binary-coded.[3,4] Magnetic vortices have been studied intensively in the last years. It has been shown that a vortex core is deflected from its equilibrium position when excited by magnetic fields or spin-polarized currents.[5,6] The deflection causes a magnetic stray field which in turn exerts a force on the core.[7,8] The resulting gyroscopic motion can be described by a damped two-dimensional harmonic oscillator.[9]

The dynamics of magnetic antivortices has hitherto-fore not been studied as intensively as magnetic vortex dynamics. Antivortices appear, e.g., in cross-tie domain walls and individual antivortices have been found in clover-shaped samples.[3,10,11] As illustrated in Fig. 1, their in-plane magnetization shows a twofold rotational symmetry that is different from the continuous rotational symmetry of a vortex state. Due to their different in-plane magnetizations, antivortex dynamics differs from vortex dynamics as is shown in this paper. An understanding of the dynamics of both, antivortices and vortices, is crucial for the description of vortex-antivortex creation and annihilation. These processes have recently received a lot of attention as they are predominant features in the motion of cross-tie walls and in the switching of vortex cores.[3,13–16]

Here we investigate the dynamics of antivortex cores, i.e. sense, phase, and amplitude of gyration, and compare them to the dynamics of magnetic vortices. We show that the direction of the in-plane magnetization around the (anti)vortex core determines the phase between the exciting alternating magnetic field and the deflection of the (anti)vortex core. For spin-polarized alternating currents the direction of the in-plane magnetization has no effect on the phase. Both micromagnetic simulations and an analytical model show that simultaneous excitation by magnetic fields and spin-polarized currents can lead to an enhancement or to an entire suppression of the antivortex core displacement.

To classify vortices and antivortices the in-plane magnetization can be described by the relation[17]

$$\phi = n\beta + \phi_0 \tag{1}$$

between the angular coordinate of the local in-plane magnetization ϕ and the angle β in real space with respect to the center of the (anti)vortex core, as shown in Fig. 1. The angles ϕ and β follow the mathematical sense of rotation. For a vortex, $n = 1$, so that the in-plane magnetization turns in the same direction as the angle in real space with a constant difference ϕ_0 between ϕ and β. For vortices, the angle ϕ_0 is independent of the choice of the axis to which β and ϕ are measured. Thus for vortices ϕ_0 is an intrinsic quantity which can be expressed by the chirality c as $\phi_0 = c\pi/2$. In standard geometries and fer-

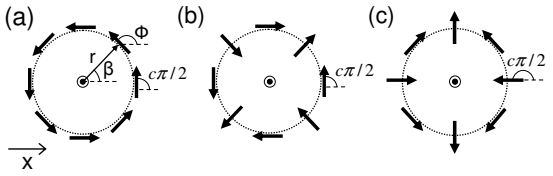

Figure 1: Definition of $c = 2/\pi \cdot (\phi - n\beta)$ for vortices and antivortices by Eq. (1). (a) Magnetic vortex ($n = 1$) with $c = 1$. (b) Antivortex ($n = -1$) with $c = 1$. (c) Antivortex ($n = -1$) with $c = 2$.

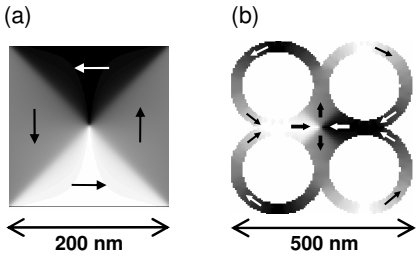

Figure 2: Size and shape of (a) the vortex and (b) the antivortex sample.

romagnetic materials stable vortices can only possess the chiralities $c = 1$ or $c = -1$. They can be mapped onto each other by mirroring the sample. In case of an antivortex $n = -1$. This means that the in-plane magnetization turns opposite to the angle in real space. Though for antivortices the angle ϕ_0 is generally not conserved, because rotations of the sample lead to different values, we define a quantity $c = 2\phi_0/\pi$ for antivortices with respect to a distinct axis.[28] Antivortices exhibit values c in the interval $(-2, 2]$. A rotation of the antivortex by an anlge of Θ leads to a change of the c-value of $c = 2\Theta$. This is due to the two-fold symmetry of the in-plane magnetization of an antivortex.

II. MICROMAGNETIC SIMULATIONS

To simulate magnetic-field induced antivortex dynamics the OOMMF[18] code sped up by higher order Runge-Kutta algorithms is used. The extended code includes the spin-torque terms in the Landau-Lifshitz-Gilbert equation as given by Zhang and Li[19,20],

$$\begin{aligned}\frac{d\boldsymbol{M}}{dt} =& -\gamma'\boldsymbol{M}\times\left(\boldsymbol{H}_{\text{eff}}+\frac{\alpha}{M_S}\boldsymbol{M}\times\boldsymbol{H}_{\text{eff}}\right)\\ &-(1+\alpha\xi)\frac{b'_j}{M_s^2}\boldsymbol{M}\times(\boldsymbol{M}\times(\boldsymbol{j}\cdot\nabla)\boldsymbol{M})\\ &-(\xi-\alpha)\frac{b'_j}{M_s}\boldsymbol{M}\times(\boldsymbol{j}\cdot\nabla)\boldsymbol{M}.\end{aligned}\qquad(2)$$

In this equation $\gamma' = \gamma/(1+\alpha^2)$, where γ is the gyromagnetic ratio, α the Gilbert damping, and ξ the ratio between exchange and spin-flip relaxation time. The coupling between local current $\mathbf{j}$ and magnetization $\mathbf{M}$ is represented by $b'_j = \mu_B P/[eM_s(1+\alpha^2)]$, where P is the spin polarization. We simulate the excitation of a vortex in a $200\times200\times20$ nm^3 permalloy square and an antivortex in a $500\times500\times40$ nm^3 clover-shaped sample. The two geometries are shown in Fig. 2. Different thicknesses of $t = 20$ nm for the vortex and $t = 40$ nm for the antivortex sample are chosen in order to obtain similar eigenfrequencies for the two geometries. We assume a saturation magnetization $M_s = 8.6\cdot10^5$ A/m, an exchange constant $A = 1.3\cdot10^{-11}$ J/m, a Gilbert damping parameter

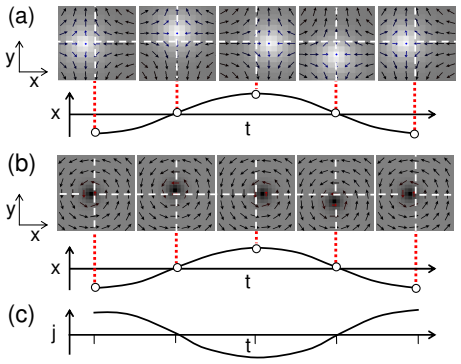

Figure 3: Simulation of one gyration period of (a) an antivortex and (b) a vortex. Both have the topological charge $q = -1/2$ and are excited at the resonance frequency (727 MHz for the antivortex and 700 MHz for the vortex) by a current of amplitude $j\cdot P = 1.5\cdot10^{10}$ A/m^2. The graphs below the magnetization images show the deflection in x-direction. (c) Exciting alternating current.

$\alpha = 0.01$, and a ratio $\xi = 0.9\alpha$ between exchange and spin-flip relaxation time.[21,22] A lateral cell size of 4 nm is used. Thus the cell size is below the exchange length of permalloy of $l_{ex} = \sqrt{2A/\mu_0 M_s^2} \approx 5.3$ nm. The position of the core is defined as the position of the maximum out-of-plane magnetization. To increase the spatial resolution, the magnetization of adjacent cells is matched by a polynomial of second order.[9]

III. EXCITATION BY MAGNETIC FIELD AND SPIN-POLARIZED CURRENT

The eigenfrequencies of vortex and antivortex are determined by exciting the core with a current. The free relaxation of the magnetization yields the free frequency ω_f and damping Γ of the vortex or antivortex. Because the damping is small compared to the free frequency ($\Gamma \ll \omega_f$), antivortex and vortex are weakly damped systems. Thus the frequency of the free oscillation ω_f and the resonance frequency ω_r are approximately the same. The simulated gyration of an antivortex core [$p = 1$, see Fig. 3(a)] and a vortex core [$p = -1$, see Fig. 3(b)] both driven by an ac current of amplitude $j\cdot P = 1.5\cdot10^{10}$ A/m^2 are shown in Fig. 3. They both possess the same sense of gyration as defined by the topological charge[23–25] $q = np/2 = -1/2$. It is known that vortices gyrate counterclockwise with positive and clockwise with negative polarization.[5] Antivortices, on the other hand, gyrate clockwise with positive and counterclockwise with negative polarization. This is directly observed in the simulations. For small current or small magnetic field amplitudes, the simulated displacement of the antivortex is found to increase linearly with increasing excitation amplitude. This is due to the harmonic po-

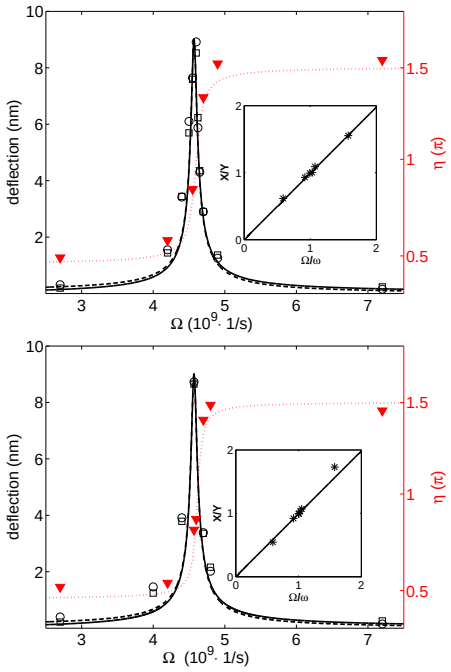

Figure 4: (Color online) Exemplary resonance curves for the semiaxes of the elliptical trajectories and the phase η of an antivortex core gyration excited by (a) a current of amplitude $j \cdot P = 1.5 \times 10^{10}$ A/m^2 ($c = 2$) and (b) a magnetic field of amplitude $H = 300$ A/m ($c = 0$). The symbols are results from micromagnetic simulations. The open squares illustrate the semiaxes in x-direction, the open circles the semiaxes in y-direction. The triangles show the phase η. The asterisks illustrate the ratio between the semiaxes x and y. The solid line is the x-component and the dashed line is the y-component of the amplitude of a fitted resonance curve of a harmonic oscillator. The dotted red line is a fit of the phase η. The insets show fits of the ratio between the semiaxes x and y as a function of the frequency.

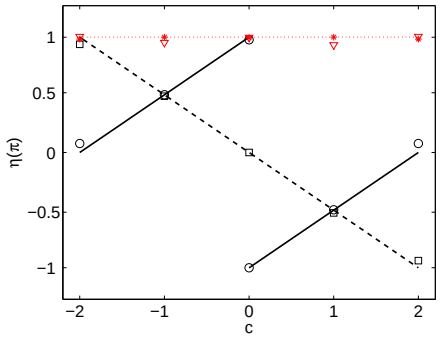

Figure 5: (Color online) Phase η between excitation and displacement for an antivortex core gyration at resonance. The dotted red line illustrates the phase when the antivortex core is excited by a spin-polarized current. The asterisks represent corresponding results from micromagnetic simulations for positive core polarization ($p = 1$) and the triangles for negative polarization ($p = -1$). For excitation with a magnetic field the solid line illustrates the phase for positive core polarization ($p = 1$), the dashed black line for negative polarization ($p = -1$). The numerical results are depicted by open circles and squares.

tential of the domains' stray field for small displacements of the antivortex core. Thus there is a linear restoring force on the antivortex, which has also been found for a vortex.[9]

To obtain the resonance curve for the amplitude and the phase η of the antivortex core, either sinusoidal currents or magnetic fields of frequencies at, above, and below the resonance frequency ω_r are applied. Throughout this paper, the current is applied in x-direction while the magnetic field is applied in y-direction. The resonance curve of a harmonic oscillator[26] with a resonance frequency $\omega_r/2\pi = 727$ MHz and a damping $\Gamma/2\pi = 6.4$ MHz matches very well the numerical data, as shown in Fig. 4 (a,b). In general the antivortex gyrates on elliptical orbits. The semi-major (semi-minor) axis of the ellipses at frequencies below resonance changes into the semi-minor (semi-major) axis at frequencies above resonance. At resonance the trajectories are circular. This is illustrated in Fig. 4 (a) for a current-driven antivortex with $c = 2$ and in Fig. 4 (b) for a magnetic-field driven antivortex with $c = 0$. For both the semi-major axes point in y-direction at frequencies below and in x-direction at frequencies above resonance.

The phase η is defined by the temporal delay between the maximum of the applied current or field and the maximum core displacement in x-direction. Like for a harmonic oscillator the phase η changes by π when the exciting frequency Ω is increased from values well below to values well above the resonance frequency ω_r. This is illustrated in Fig. 4 (a) for current and in Fig. 4 (b) for magnetic-field excitation.

We numerically simulate the dependence of the phase on the direction of the in-plane magnetization by exciting at resonance antivortices of all possible integer c-values and of both polarizations $p = -1$ and $p = 1$. For current excitation for all c-values the antivortex cores are deflected into the physical current direction ($\eta = \pi$). For magnetic field excitation, the phase is found to depend on the direction of the in-plane magnetization as shown in Fig. 5. For a constant frequency the phase varies by 2π when c is changed from -2 to 2, i.e. when rotating the sample by π with respect to the magnetic field. At resonance the phase changes from 0 to 2π for $p = 1$ and from π to $-\pi$ for $p = -1$ as illustrated in Fig. 5.

The phase η and its dependence on the direction of the in-plane magnetization is studied analytically by using the equation of motion for vortices and antivortices[26] assuming low damping ($\omega_r \gg \Gamma$). The equation for the

deflection

$$\begin{pmatrix} x \\ y \end{pmatrix} = -\chi \cdot \begin{pmatrix} v_H \sin(\frac{\pi c}{2})\omega + \left(v_H p \cos(\frac{\pi c}{2}) + v_j\right) i\Omega \\ \left(v_H n \cos(\frac{\pi c}{2}) + v_j np\right) \omega - v_H np \sin(\frac{\pi c}{2}) i\Omega \end{pmatrix} \cdot e^{i\Omega t} \tag{3}$$

is derived from the Thiele equation[8] for excitation with magnetic fields and the extension by Thiaville[7] for spin-polarized currents. A harmonic potential due to the demagnetizing field is assumed.[26] The velocity due to the adiabatic spin-torque term is $v_j = b_j j_0$, the velocity due to the magnetic field $v_H = \gamma H_0 l/(2\pi)$, and the susceptibility of a harmonic oscillator is $\chi = 1/[\omega^2 + (i\Omega + \Gamma)^2]$. Equation (3) states that a change of the c-value leads to a rotation of the magnetic force. This in turn causes a dependence of the phase on the in-plane magnetization. For example, a change from $c = -1$ to $c = 1$ is equivalent to a rotation of the magnetic force by an angle of π. At resonance Eqn. (3) yields the deflection

$$x(c, p, t) = \frac{v_H}{2\Gamma} e^{i\Omega t} e^{i\pi(\frac{1+p-pc}{2})}. \tag{4}$$

The maximum excitation is reached for $i\Omega t = -i\pi(\frac{1+p-pc}{2})$, so that the phase of the antivortex motion that is induced by a magnetic field at resonance reads

$$\eta_H = -\pi\left(\frac{1+p-pc}{2}\right). \tag{5}$$

For purely current-driven excitation Eqn. (3) gives

$$x(c, p, t) = -\frac{v_j}{2\Gamma} e^{i\Omega t}. \tag{6}$$

Hence the phase induced by a current is $\eta_j = \pi$ at resonance. This means that for current excitation the phase is independent of the direction of the in-plane magnetization as well as of the polarization. Figure 5 demonstrates that the analytical results agree well with the simulations.

IV. AMPLITUDE VARIATION OF GYRATION

In the following we simulate antivortices that are excited simultaneously by a magnetic field and a spin-polarized current. First the antivortex is excited by a current in x-direction in the absence of a magnetic field. Then the amplitude of a magnetic field in y-direction is tuned until the antivortex core gyration possesses the same amplitude as under current excitation. In our case the core is excited by a spin-polarized current of amplitude $j \cdot P = 0.7 \cdot 10^{10}$ A/m^2 that corresponds to a magnetic field of amplitude H = 122 A/m. Then the current and the magnetic field are applied simultaneously. Different directions of the in-plane magnetization (see Fig. 6)

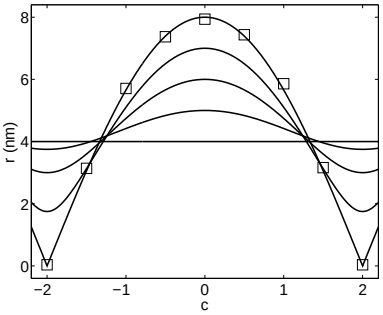

Figure 6: Amplitude of displacement of an antivortex core with polarization $p = 1$ at resonance. The antivortex is excited simultaneously by a magnetic field in y-direction and a current in x-direction. The symbols denote simulated results for $v_H = v_j$, the lines are fits for different ratios v_H/v_j according to Eqn. (7) .

are chosen to investigate the c-dependent variation of the core amplitude for a positive polarization. The simulation shows a doubling of the amplitude at $c = 0$ and a complete suppression at $c = 2$. Thus a superposition of the deflection by current and a perpendicular field leads to an amplitude variation in dependence on the direction of the in-plane magnetization of the sample. This is due to the c-dependent phase between antivortex core displacement and magnetic field, see Eqn. (5). The forces due to current and magnetic field are proportional to the deflections. If they are parallel or antiparallel, an enhancement or suppression of the core displacement is found, respectively. When both deflections have the same amplitude, the amplitde of gyration can be doubled or completely quenched, as shown in Fig. IV.
Using the addition theorem one can derive from Eqn. (3) the c-dependent amplitude variation

$$r = r_0 \sqrt{\left(\frac{v_H}{v_j} - p\right)^2 \sin^2\left(\frac{\pi c}{4}\right) + \left(\frac{v_H}{v_j} + p\right)^2 \cos^2\left(\frac{\pi c}{4}\right)}. \tag{7}$$

of the antivortex core gyration at resonance. This is a general expression for arbitrary ratios v_H/v_j between the antivortex core velocities due to current and to magnetic field, for both polarizations and all c-values. The amplitude is plotted in Fig. 6.

An inhomogeneous current distribution in the direc-

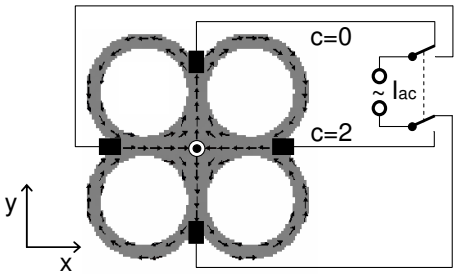

Figure 7: Proposed setup with electrical contacts to excite a single antivortex, here with polarization $p = 1$. The quantity c depends on the direction of the exciting ac current. For current in x- or y-direction the deflection is suppressed or amplified, respectively.

tion of the film normal generates a non-zero Oersted field perpendicular to the current.[27] For the experimental proof of a dependence of the amplitude on the direction of the in-plane magnetization, we propose a setup with a clover-shaped sample that is illustrated in Fig. 7. A similar sample was investigated by Shigeto et al.[10] with magnetic-force microscopy. Excitation by a spin current in x-direction or y-direction through electrical contacts corresponds to a direction of the in-plane magnetization for $c = 2$ and $c = 0$, respectively. For the polarization $p = 1$ we expect a suppressed motion when the current is applied in x-direction and an enhanced amplitude when it is applied in y-direction. The variation of the amplitude for $c = 0$ and $c = 2$ could be used to determine the ratio between the forces on the antivortex core due to an Oersted field and a current.

V. CONCLUSION

In conclusion, we have demonstrated by micromagnetic simulations that antivortices excited by spin-polarized ac currents or magnetic fields gyrate on elliptical orbits. These orbits can be well described by the analytical model of a two-dimensional harmonic oscillator. The sense of gyration of antivortices depends solely on the topological charge $q = np/2$. The phase of the antivortex motion excited by an alternating magnetic field depends also on the direction of the in-plane magnetization. Antivortices that are excited simultaneously by a spin-polarized current and a magnetic field show an enhancement or a suppression of the deflections amplitude in dependence on the direction of the in-plane magnetization. The effect of the amplitude variation in dependence on the in-plane magnetization can be used to experimentally investigate the influence of Oersted fields in current-induced antivortex dynamics.

Acknowledgments

We thank Ulrich Merkt and Daniela Pfannkuche for valuable discussions and encouragement. Financial support by the Deutsche Forschungsgemeinschaft via the Graduiertenkolleg 1286 "Functional metal-semiconductor hybrid systems" and via Sonderforschungsbereich 668 "Magnetismus vom Einzelatom zur Nanostruktur" is gratefully acknowledged.

[1] T. Shinjo, T. Okuno, R. Hassdorf, K. Shigeto, and T. Ono, Science **289**, 930 (2000).
[2] A. Wachowiak, J. Wiebe, M. Bode, O. Pietzsch, M. Morgenstern, and R. Wiesendanger, Science **298**, 577 (2002).
[3] Y. Liu, S. Gliga, R. Hertel, and C. M. Schneider, Appl. Phys. Lett. **91**, 112501 (2007).
[4] B. Van Waeyenberge, A. Puzic, H. Stoll, K. W. Chou, T. Tylisczak, R. Hertel, M. Fähnle, H. Brückl, K. Rott, G. Reiss, et al., Nature **444**, 461 (2006).
[5] S. B. Choe, Y. Acremann, A. Scholl, A. Bauer, A. Doran, J. Stöhr, and H. A. Padmore, Science **304**, 420 (2004).
[6] J. Shibata, Y. Nakatani, G. Tatara, H. Kohno, and Y. Otani, Phys. Rev. B **73**, 020403(R) (2006).
[7] A. A. Thiele, Phys. Rev. Lett. **30**, 230 (1973).
[8] A. Thiaville, Y. Nakatani, J. Miltat, and Y. Suzuki, Europhys. Lett. **69**, 990 (2005).
[9] B. Krüger, A. Drews, M. Bolte, U. Merkt, D. Pfannkuche, and G. Meier, Phys. Rev. B **76**, 224426 (2007).
[10] K. Shigeto, T. Okuno, K. Mibu, T. Shinjo, and T. Ono, Appl. Phys. Lett. **80**, 4190 (2002).
[11] Y. C. Chang, C. C. Chang, W. Z. Hsieh, H. M. Lee, and J. C. Wu, IEEE Trans. Mag. **41**, 959 (2005).
[12] H. Wang and C. E. Campbell, Phy. Rev. B **76**, 220407(R) (2007).
[13] R. Hertel and C. M. Schneider, Phys. Rev. Lett. **97**, 177202 (2006).
[14] A. Neudert, J. McCord, R. Schäfer, and L. Schultz, Phys. Rev. B **75**, 172404 (2007).
[15] S. K. Kim, Y. S. Choi, K. S. Lee, K. Y. Guslienko, and D. E. Jeong, Appl. Phys. Lett. **91**, 082506 (2007).
[16] K. Kuepper, M. Buess, J. Raabe, C. Quitmann, and J. Fassbender, Phy. Rev. Lett. **99**, 167202 (2007).
[17] J. He, Z. Li, and S. Zhang, Phys. Rev. B **73**, 184408 (2006).
[18] **OOMMF User's Guide, Version 1.0** M.J. Donahue and D.G. Porter Interagency Report **NISTIR 6376**, National Institute of Standards and Technology, Gaithersburg, MD (Sept 1999) (http://math.nist.gov/oommf/).
[19] S. Zhang and Z. Li, Phys. Rev. Lett. **93**, 127204 (2004).
[20] B. Krüger, D. Pfannkuche, M. Bolte, G. Meier, and U. Merkt, Phys. Rev. B **75**, 054421 (2007).
[21] G. Meier, M. Bolte, R. Eiselt, B. Krüger, D. H. Kim, and P. Fischer, Phys. Rev. Lett **98**, 187202 (2007).
[22] M. Hayashi, L. Thomas, Y. B. Bazaliy, C. Rettner, R. Moriya, X. Jiang, and S. S. P. Parkin, Phys. Rev. Lett. **96**, 197207 (2006).
[23] A. Abanov and V. L. Pokrovsky, Phys. Rev. B **58**, R8889

(1998).
[24] V. L. Golo and A. M. Perelomov, Mathematical Physics **2**, 477 (1978).
[25] O. A. Tretiakov and O. Tchernyshyov, Phys. Rev. B **75**, 012408 (2007).
[26] B. Krüger, A. Drews, M. Bolte, U. Merkt, D. Pfannkuche, and G. Meier, J. Appl. Phys. **103**, 07A501 (2008).
[27] M. Bolte, G. Meier, B. Krüger, A. Drews, R. Eiselt, L. Bocklage, S. Bohlens, T. Tyliszczak, A. Vansteenkiste, B. Van Waeyenberge, et al., unpublished (2008).
[28] Here, we use the x-axis as distinct axis.

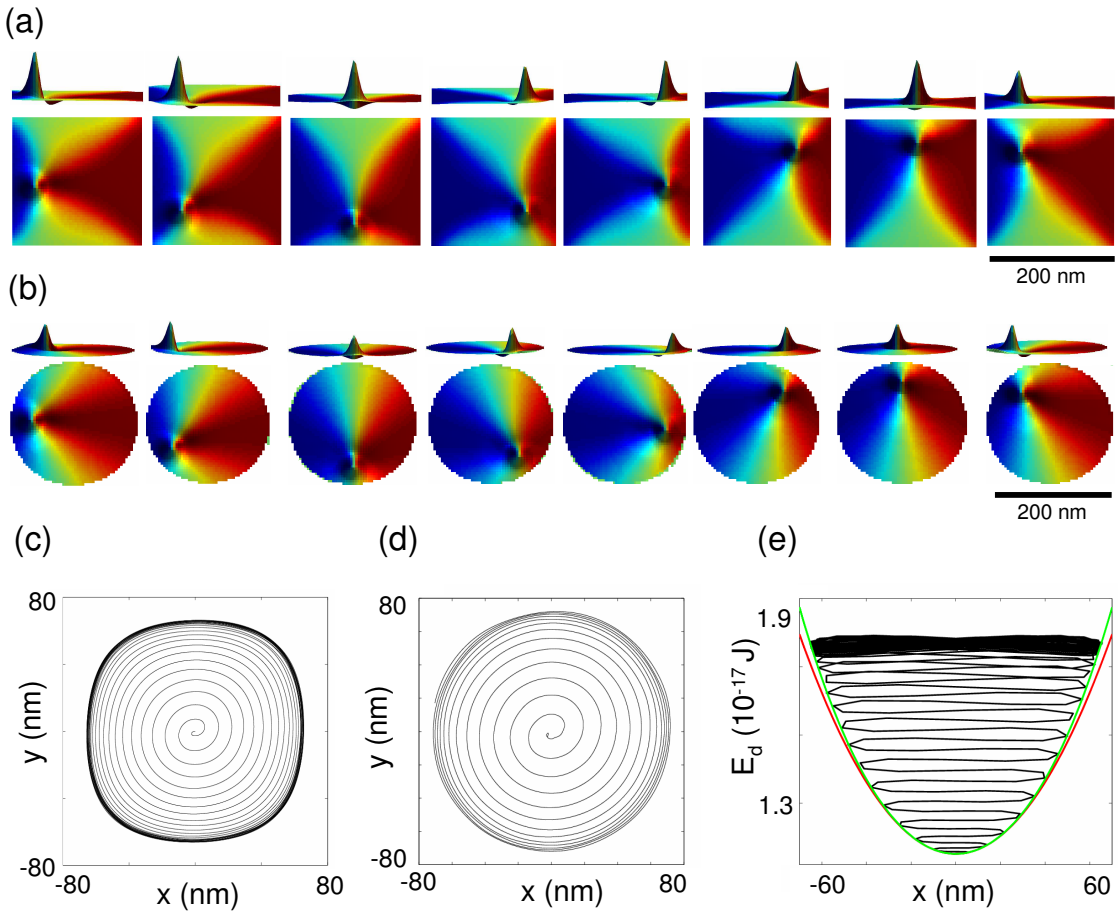

Fig. 4.9: Magnetization patterns during one gyration period of (a) a vortex (c=1, p=1) in a square excited by an alternating current density of amplitude $j \cdot P = 2 \cdot 10^{11}$ A/m^2 with a frequency $\Omega = 4.40 \cdot 10^9$ 1/s and (b) a vortex (c=1, p=1) in a disk excited by an alternating current density of amplitude $j \cdot P = 3 \cdot 10^{11}$ A/m^2 with a frequency of $\Omega = 4.95 \cdot 10^9$ 1/s. (c) Square-shaped trajectory of the vortex core in the square. (d) Circular trajectory in the disk. (e) Demagnetization energy of the vortex in the square. The red line denotes a parabolic fit, the green line shows a fit of fourth order.

4.2 Nonlinear dynamics of vortices and antivortices

The potential due to the demagnetization field is expanded with respect to the core's displacement from the equilibrium position up to higher-order terms. Inserting the resulting force into the Thiele equation gives a nonlinear equation of motion for the vortex gyration at large core displacements. The nonlinear dynamical characteristics like a gap in the resonance curve, a shift of the phase and a shift of the eigenfrequency are presented.

4.2.1 Origin of nonlinear vortex gyration

Only for small core displacements when the internal forces are proportional to the deflection of the core, vortices can be described as harmonic oscillators. For large displacements the internal forces increase nonlinearly resulting in a nonlinear vortex gyration [44, 45].

For example in a square the domain walls become distorted and the trajectory warps at the corners of the square which results in a square-shaped trajectory at the resonance frequency. Starting from the equilibrium position the nonlinear gyration of a vortex in a square induced by an alternating current reaches a steady state with a square-shaped trajectory, as illustrated in Fig. 4.9 (c). Magnetization patterns during one gyration period in the steady state are depicted in Fig. 4.9 (a). The closer the core is to the edges of the sample the smaller is the increase of the displacement of the vortex gyration. In case of a disk, which is excited at the resonance frequency, the nonlinear core trajectory retains a circular shape but again the amplitude of gyration is decreased near the edge of the sample. In Fig. 4.9 (d) the core in a disk that is excited by an alternating current performs a transient gyration starting from the equilibrium position. Figure 4.9 (b) shows magnetization patterns during one gyration period for large core displacements.
In soft magnetic materials the shape of the potential depends on the geometry of the sample. Generally, the potential is flat in the corners of the square. This is the reason why for large displacements the shape of the core trajectory approaches the shape of the sample.
The potential due to the demagnetization energy can be fitted by a polynomial of fourth order as demonstrated in Fig. 4.9 (e). In the simplest approximation the fourth order terms describe the potential of the nonlinear core gyration.

4.2.2 Nonlinear equation of motion of vortices

The potential

$$V(x,y) = V(x_0,y_0) + \frac{\partial^2}{\partial x^2}V|_{x_0,y_0}\frac{x^2}{2!} + \frac{\partial^4}{\partial x^4}V|_{x_0,y_0}\frac{x^4}{4!} + \frac{\partial^4}{\partial x^2\partial y^2}V|_{x_0,y_0}\frac{x^2y^2}{2!2!} + \frac{\partial^4}{\partial y^4}V|_{x_0,y_0}\frac{y^4}{4!} + \frac{\partial^6}{\partial x^6}V|_{x_0,y_0}\frac{x^6}{6!}\cdots . \tag{4.34}$$

due to the demagnetization energy can be expanded up to higher orders in a Taylor series. The term of zero order is an offset and can be set $V(x_0,y_0) = 0$. Linear terms are absent because x_0 and y_0 are the coordinates of the equilibrium position. All other odd terms vanish because of the symmetry of the potential. With such terms the equilibrium position would become unstable for small core displacements, because the potential would possess a saddlepoint at the equilibrium position. The potential of a vortex in a square

$$V(x,y) = \frac{m\omega_r^2}{2}\left(x^2+y^2+a(x^2+y^2)^2 - bx^2y^2\right) \tag{4.35}$$

exhibits the symmetry of the sample. A square exhibits mirror symmetries. The potential in its corners has tailing edges. The tailing edges are caused by the term proportional to the product x^2y^2. In case of a disk this term vanishes because the potential is isotropic due to the rotational symmetry of the sample and only the term that is proportional to (x^2+y^2)

remains.
The nonlinear force is

$$\mathbf{F} = -m\omega_r^2 \begin{pmatrix} x+4a(x^3+xy^2)-2bxy^2 \\ y+4a(y^3+x^2y)-2bx^2y \end{pmatrix}. \tag{4.36}$$

The nonlinear equation of motion

$$\begin{aligned} \begin{pmatrix} \dot{x} \\ \dot{y} \end{pmatrix} = -np\omega_f \begin{pmatrix} y+4ay^3+4ax^2y-2bx^2y \\ -x-4ax^3-4axy^2+2bxy^2 \end{pmatrix} \\ -\Gamma \begin{pmatrix} x+4ax^3+4axy^2-2bxy^2 \\ y+4ay^3+4ax^2y-2bx^2y \end{pmatrix} + v_j \end{aligned} \tag{4.37}$$

follows when the nonlinear force is inserted into Eqn. 4.20. This nonlinear equation of motion can only be solved numerically. This has been done by a Runge-Kutta-method of

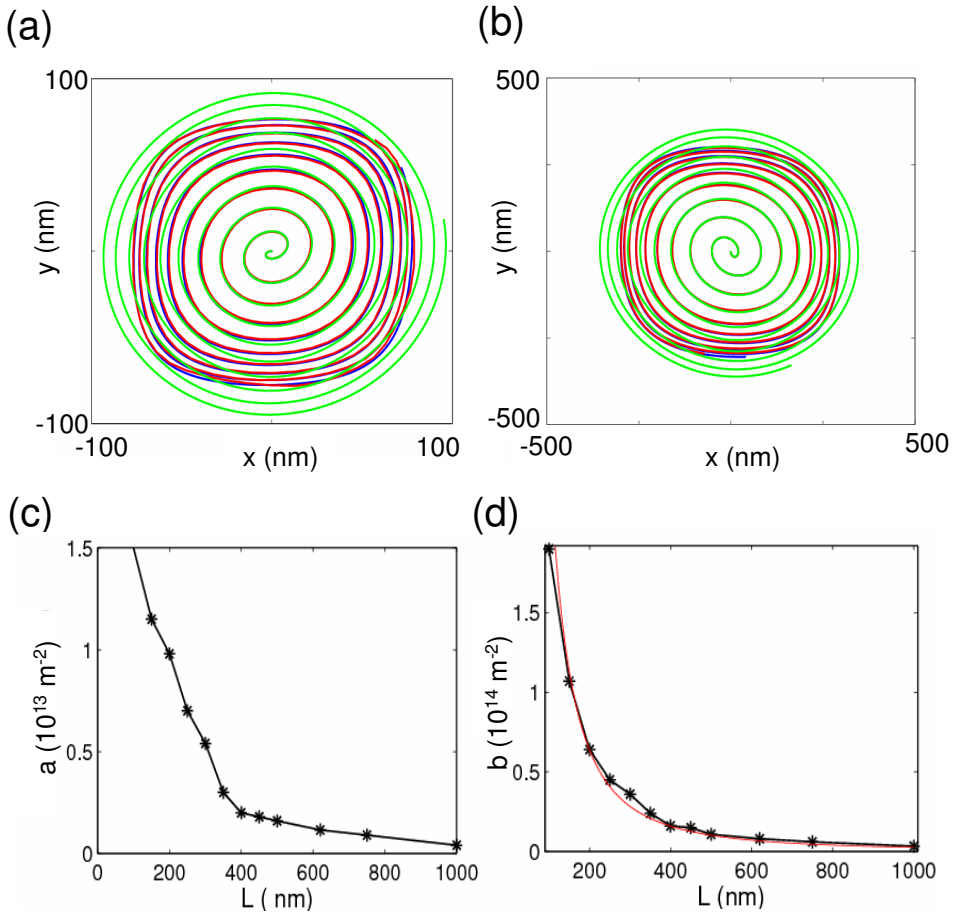

Fig. 4.10: Simulated transient trajectory of a vortex (a) in a $200 \times 200 \times 20$ nm^3 square and (b) in a $1000 \times 1000 \times 20$ nm^3 square. The blue lines are the trajectories obtained by a numerical solution of the analytical equation of motion. The green lines are the analytical trajectories without nonlinearities. (c) and (d) Dependence of the coefficients a and b on the sample length L. The red line is a fit $b \propto 1/L^2$.

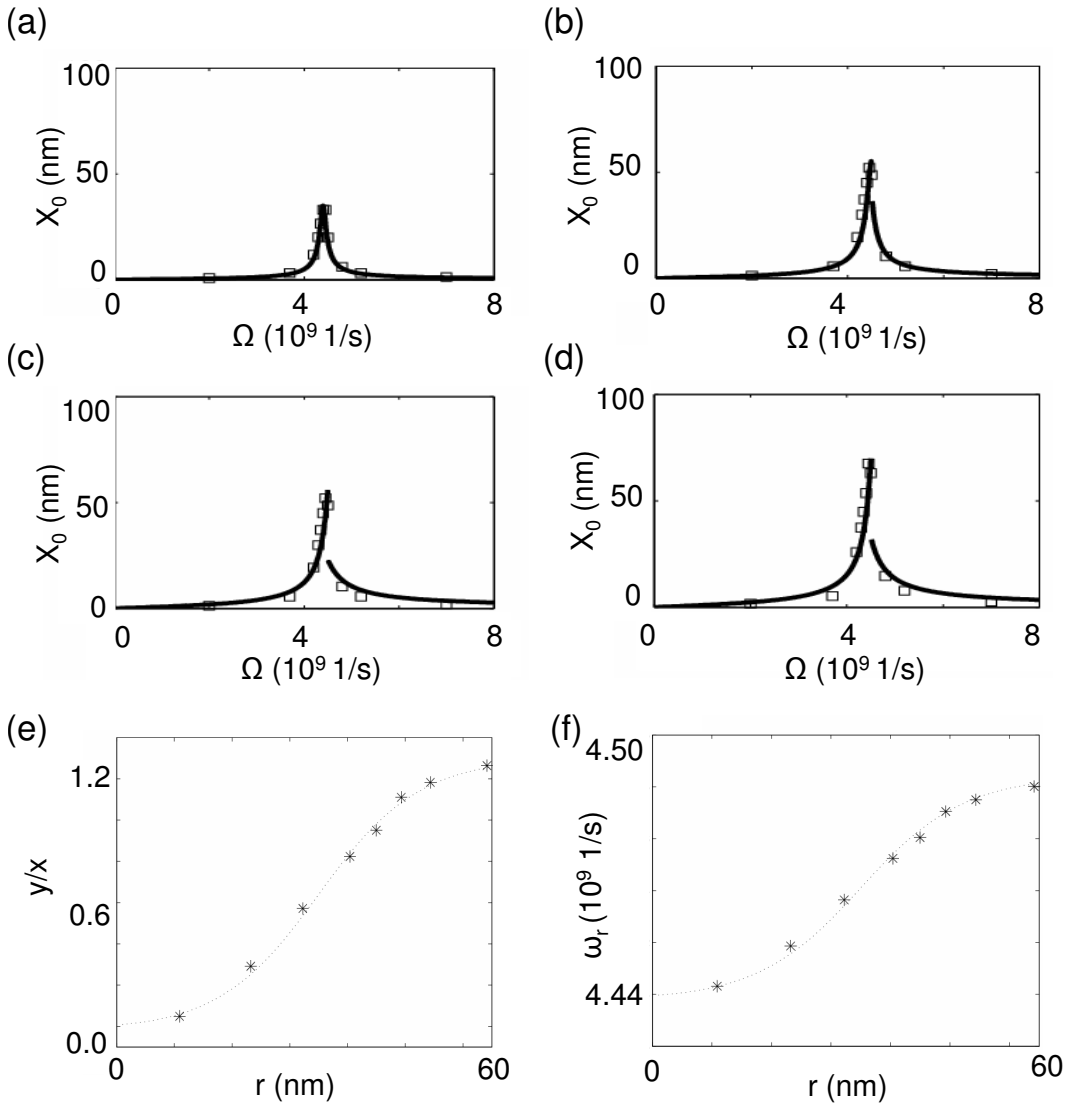

Fig. 4.11: Resonance curves of a vortex in a permalloy square ($200 \times 200 \times 20$ nm^3) excited by an alternating current density of amplitude (a) $j \cdot P = 7 \cdot 10^{11}$A/m^2, (b) $1.2 \cdot 10^{11}$m^2, (c) $j \cdot P = 1.7 \cdot 10^{11}$A/m^2, and (d) $j \cdot P = 2.2 \cdot 10^{11}$A/m^2. (e) Ratio between the y- and the x-coordinates of the vortex gyration versus the amplitude of gyration at resonance $\Omega = \Omega_r$. (f) Resonance frequency determined by Eqn. 4.40 from the phase $\pi/2$ between the force due to the excitation and the displacement of a harmonic oscillator.

fourth order. Figure 4.10 shows the simulated and the analytical trajectories for a vortex core in permalloy squares. Both vortices start from the equilibrium position and perform a transient gyration. The red line shows the simulated results, the blue line the analytical results with nonlinear terms and the green line the analytical results without nonlinear terms. The analytical and simulated nonlinear trajectories show good accordance. In the linear case the displacement of the core is larger compared to the displacement in the nonlinear case. Thus the harmonic potential is flatter compared to the nonlinear potential as was already evident in Fig 4.9 (e).

To reveal a correlation between the sample length and the nonlinear coefficients a and b of vortices in squares, simulations have been done for different sample sizes. The trajectories from analytical calculations have been fitted to the simulated trajectories by varying the nonlinear coefficients. The coefficient a, which is propotional to the term (x^2+y^2) in Eqn. 4.35, causes the decrease of the core displacements near the edges of the squares. This coefficient increases for decreasing size of the squares, as illustrated in Fig. 4.10 (c). The coefficient b that leads to the trailing edges of the potential in the corners of the square can be fitted by the relation $b \propto L^{-2}$, see Fig. 4.10 (d). The dependence of the coefficient b on the domain-wall length $L_{DW} = \frac{1}{\sqrt{2}}L$ [see Fig. 4.3 (a)] can be explained by the distortion of the domain walls. It can be concluded that the smaller the sample the steeper is the potential and the larger are the nonlinearities experienced by a vortex.

4.2.3 Vortices as nonlinear oscillators

The dynamical characteristics like the semiaxes, the amplitude in resonance, the phase, and the resonance frequency of the nonlinear gyration strongly differ from the linear case. The nonlinear resonance curves of the semiaxes become discontinuous. A gap of the semiaxes occurs near the resonance frequency. Figures 4.11 (a) - (d) depict the resonance curves of the semiaxis X_0 for alternating current excitations between $j \cdot P = 7 \cdot 10^{10}$ A/m^2 and $j \cdot P = 2.2 \cdot 10^{11}$ A/m^2. An increase of the excitation also leads to an increase of the gap. For a vortex that is excited at resonance the ratio of the coordinates y/x at the time of maximum excitation depends on the amplitude of gyration, as demonstrated in Fig. 4.11 (e). The ratios y/x are illustrated for amplitudes of alternating current densities between $j \cdot P = 2 \cdot 10^{10}$ A/m^2 and $j \cdot P = 2 \cdot 10^{11}$ A/m^2 which results in amplitudes of gyration between 10 nm and 60 nm at an exciting frequency of $\Omega = 4.4 \cdot 10^9$ 1/s. The simulated ratio y/x of nonlinear gyration can be compared to the ratio y/x of the linear gyration. For the linear case the phase is independent on the amplitude of excitation. The phase of current-induced vortex gyration in the linear case can be expressed by

$$\eta = \arctan\Big(-\frac{y}{x}\Big) + \pi. \tag{4.38}$$

From the susceptibility χ of a harmonic oscillator follows

$$\eta = \arctan\Big(\frac{\Omega^2 - \omega_r^2}{2\Omega\Gamma}\Big) + \pi. \tag{4.39}$$

The relation

$$\omega_r = \sqrt{\frac{y}{x}2\Omega\Gamma + \Omega^2} \tag{4.40}$$

yields the resonance frequency that a harmonic oscillator would have for the simulated ratio y/x of nonlinear vortex gyration. The resonance frequency is shifted to larger values for increasing amplitudes of gyration as demonstrated in Fig. 4.11 (f). This blue-shift is

due to the increase of the potential as already shown in Fig. 4.9 (e). H. Stoll et al. measured a red shift of the resonance frequency in the nonlinear regime [46]. K. Buchanan et al. discovered a mode splitting experimentally. Their numerical calculations yield a blue-shift and a mode splitting depending on the nonlinear parameters [44]. The parameters at mode splitting are larger than can be justified on simulations. It can be concluded that further investigations on nonlinear vortex gyration have to be done to clarify these discrepancies.

4.3 Switching of vortex and antivortex cores in the highly non-linear regime

In the highly nonlinear regime the vortex gyration culminates in the formation of a new vortex and a new antivortex and finally in a vortex with a core of opposite polarization. This process is called vortex-core switching [47, 48, 49, 50]. Only in very thin samples with small lateral sizes a highly excited core can leave the sample before it switches.

4.3.1 Intermediate states at core switching

When the gyroscopic motion of a vortex becomes nonlinear a so called dip particle forms in the vicinity of the core. Its out-of-plane magnetization points into the direction opposite to that of the core. The size of the dip particle increases when the velocity of the core increases. For higher amplitudes of excitation the dip particle splits into an antivortex and a vortex of opposite polarizations compared to the original vortex. The antivortex annihilates with the original vortex and a vortex of opposite polarization remains. At antivortex switching also a vortex-antivortex pair is formed and the vortex annihilates with the antivortex and an antivortex of opposite polarization remains. Figure 4.12 shows micromagnetic simulations of the switching process.

4.3.2 Topological considerations

The magnetization field is described by the nonlinear Landau-Lifshitz-Gilbert equation. As solutions of this equation topological objects like vortices and antivortices occur. They exhibit a sharp singularity in the center, when projecting the magnetization on the plane. These objects are characterized by the winding number n which does not change under symmetry operations like rotations and mirroring of the magnetization pattern. Other topological characteristics are the polarization p and the skyrmion number [51]

$$q = \int \mathbf{M} \cdot \left(\frac{\partial}{\partial x}\mathbf{M} \times \frac{\partial}{\partial y}\mathbf{M} \right) d^2\mathbf{r}. \tag{4.41}$$

The skyrmion number $q = \frac{np}{2}$ [51] of a vortex, which also includes the out-of-plane component of the magnetization by the polarization p, can be used to describe the switching

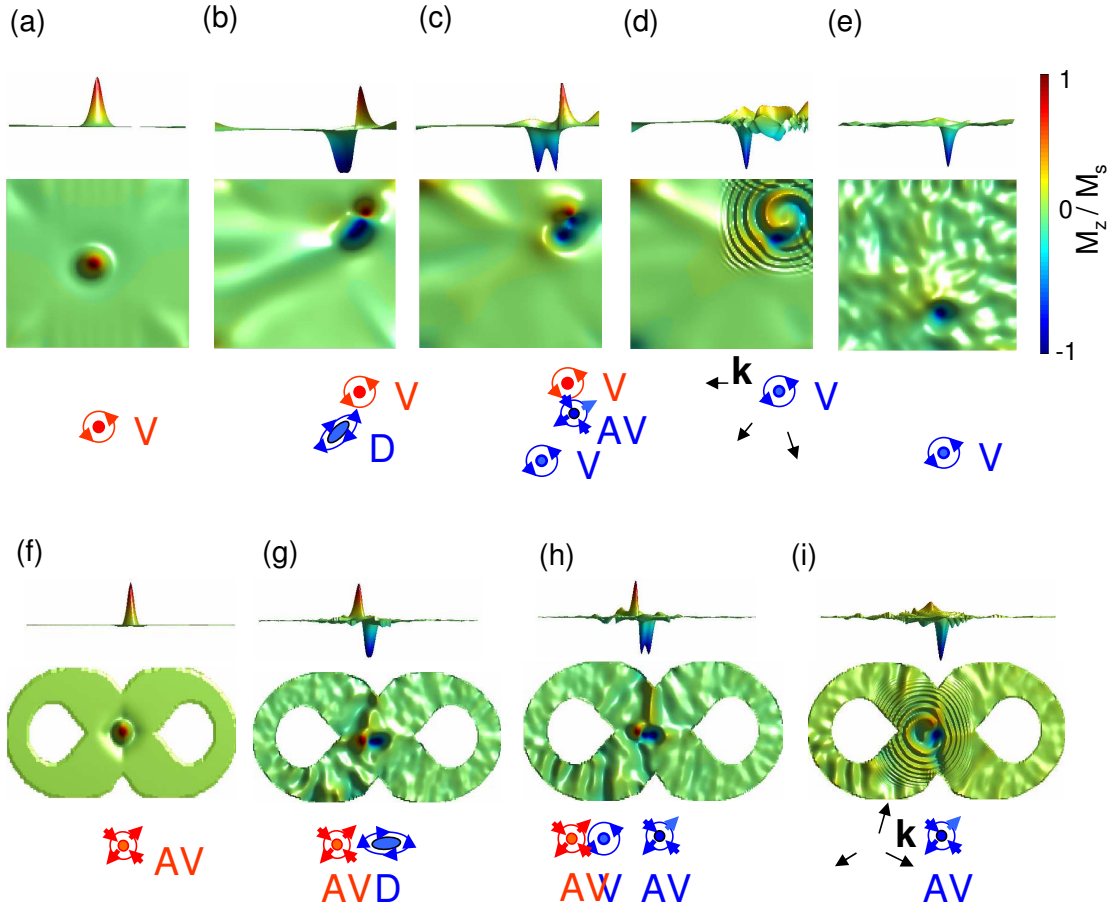

Fig. 4.12: Switching process of (a) - (e) a vortex in a square and (f) - (i) an antivortex in an infinity-shaped sample. The sketches show the corresponding intermediate states vortex core (V), antivortex core (AV), and dip particle (D). Red (blue) colors denote a positive (negative) z-component of the magnetization. (d) and (i) The wavevectors **k** depict the propagation direction of the spin waves at vortex-antivortex annihilation.

process of vortices and antivortices topologically. If the skyrmion number is not conserved, and thus the topology of the magnetization does not evolve continuously, discontinuities of the magnetization occur. At vortex-core switching this is the formation of a singularity that is called Bloch point [52]. If a vortex of positive polarization ($n = 1$, $p = 1$, $q = \frac{1}{2}$) gyrates, a dip particle ($n = 0$, $p = -1$, $q = 0$) can be formed continuously. A pair of an antivortex ($n = -1$, $p = -1$, $q = \frac{1}{2}$) and a vortex ($n = 1$, $p = -1$, $q = -\frac{1}{2}$) decouples continuously from the dip particle. The antivortex annihilates with the original vortex meaning an abrupt change of the skyrmion number from $q = 1$ to $q = 0$. This change violates the continuous topology of the magnetization field and leads to the formation of a Bloch point that decays into spin-waves. This is sometimes addressed as exchange explosion [53]. The energy of the spin waves released in the skyrmion decay including Bloch-point annihilation can be estimated by the skyrmion energy $E = 8\pi At$, where A is the exchange constant and t is the thickness of the sample [51].

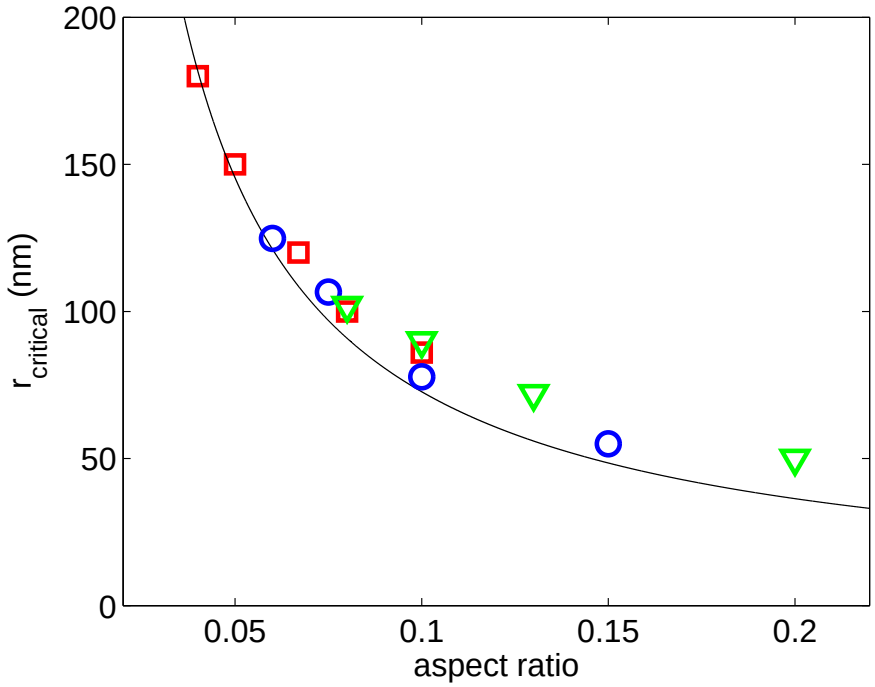

Fig. 4.13: (a) Critical amplitude versus the aspect ratio t/L of a square. At the critical amplitude the dip particle splits into a vortex and an antivortex. The black line is a plot of Eqn. 4.43. The symbols depict simulated results for thicknesses of $t = 20$ nm (red squares), $t = 30$ nm (blue circles), and $t = 40$ nm (green triangles).

4.3.3 Critical velocities at switching

The formation of a dip particle can be described micromagnetically. When assuming the origin of the coordinate system in the vortex core, similar to a Galilei transformation, the influence of the motion of the vortex core on the adjacent magnetization vectors is given by the gyration equivalent field in Eqn. 4.4, [54]. The z-component

$$(H_g)_z = \frac{1}{M_s^2\gamma}\left(\mathbf{M}\times\frac{\mathbf{M}}{dt}\right)_z = \frac{1}{M_s^2\gamma}\left(\mathbf{M}\times(\mathbf{v}\cdot\nabla)\mathbf{M}\right)_z \tag{4.42}$$

of the field leads to an orientation of the magnetization next to the vortex core into the negative z-direction and thus to the formation of the dip particle [50]. The gyrofield depends on the velocity of the vortex core and on the gradient of the magnetization near the core. The size and the shape of the dip particle increase when the core velocity increases. At the critical velocity the size of the dip particle is so large, that it is energetical favorable for the dip particle to decay into a vortex-antivortex pair. The critical velocity $v_{critical} = (340 \pm 20)$ m/s has been determined for disks by micromagnetic simulations [55]. The approximation $v_{critical} = \omega_f r$ for a circular core motion at resonance and the relations for disks $\omega_f \approx 49 \cdot 10^9 (t/L) 1/s$ and squares $\omega_f \approx 44 \cdot 10^9 (t/L) 1/s$ obtained from micromagnetic simulations can be used to approximate the amplitude

$$r = v_{critical}/\omega_f = a\frac{L}{t} \tag{4.43}$$

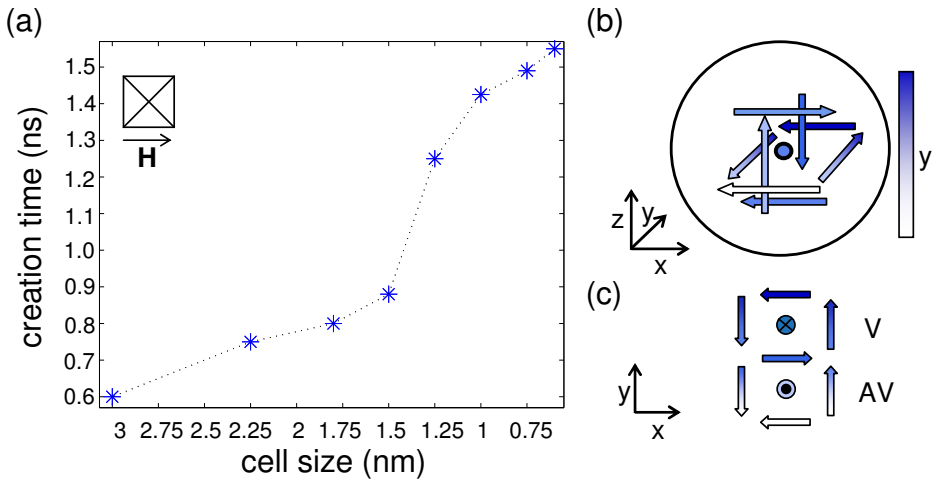

Fig. 4.14: (a) Creation time of a Bloch point at vortex-core switching in a permalloy square of dimensions $153 \times 153 \times 9$ nm^3 in dependence on the cell size. The vortex is excited by a magnetic field pulse of amplitude 80 mT. The asterisks are simulated results. The dashed line is a guide to the eyes. (b) Scheme of the magnetization vectors in the vicinity of the Bloch point. The Bloch point is indicated by the point in the center. (c) Top view of the scheme in (b) showing the magnetization of vortex-antivortex annihilation.

of the switching process with the constants $a = 7.7$ nm for a square and $a = 6.9$ nm for a disk. This amplitude is the upper border of the nonlinear vortex gyration.

4.3.4 Limits of the micromagnetic model

The micromagnetic model relies on a continuous theory. It cannot be used to describe a magnetic discontinuity like a Bloch point. A Bloch point is needed to annihilate a vortex-antivortex pair of opposite polarizations. Vortex-core switching including the formation of a Bloch point can only be observed by micromagnetic simulations because of the discretization of the magnetization. Then the Bloch point is located between adjacent simulation cells. The exchange energy density has the main influence on the formation and annihilation of the Bloch point because of the short range of the exchange interaction. The exchange energy density between two adjacent cells in a distance $|r_2 - r_1|$ reads

$$E_{ex} = \frac{A}{M_s^2}\left(\frac{\mathbf{M}_2 - \mathbf{M}_1}{|r_2 - r_1|}\right)^2. \tag{4.44}$$

If variations of both magnetization vectors $\mathbf{M}_1$ and $\mathbf{M}_2$ do not scale with the cell size $|r_2 - r_1|$, the exchange energy density depends on the cell size. The magnetization vectors in the vicinity of a Bloch point show strong variations on a short scale, as illustrated in Fig. 4.14 (b). Thus Bloch-point creation and annihilation depends on the cell size. Figure 4.13 (a) shows the creation time until a Bloch point is formed at vortex-core switching for different cell sizes. This dependence demonstrates that the switching can only be described in a quantitative way before the annihilation of the vortex-antivortex pair sets in

and again after the annihilation of the Bloch point. Although a quantitative description of Bloch-point dynamics by micromagnetic simulations is impossible, the annihilation of a vortex or an antivortex by the formation of a Bloch point is correct. This is known from topological considerations. A vortex ($n = 1$) can only be annihilated by its topological counterpart, an antivortex ($n = -1$).

5 Vortices in storage devices

Concepts to use ferromagnetic vortices in storage devices are presented. The vortex random access memory (VRAM) and the antivortex random access memory (AVRAM) work with a rotating current excitation or an excitation by a simultaneous current and magnetic field to read and write a bit. Rotating magnetic fields are impractical for dense storage devices due to their large range.

5.1 Logical states represented in vortices

Magnetization patterns can represent logical states. The magnetization is stable over a wide range of temperatures until the thermal energy $k_B T$ reaches the skyrmion energy $E_{skyrmion} = 8\pi At$ [51]. Of course, the maximum temperature is the Curie temperature that is $T_{Curie} \approx 869$ K for permalloy [8]. The upper limit of the stability due to parasitic magnetic fields, for example stray fields of adjacent vortices and Oersted fields, lies in the range of some Millitesla.

The chirality and the polarization of a vortex have been proposed to represent bits [56, 57, 58], but the realization of the read and the write processes is still a challenge. It takes a relatively long time to detect the chirality [59]. Large amplitudes of magnetic fields are required to change the chirality of a vortex. The polarization could be detected by the stray field of the vortex core, but this field has only a very small amplitude and it is superimposed by the fields of the magnetic domains. To switch the core polarization a constant out-of-plane magnetic field of large amplitude up to half a Tesla has to be applied to switch the core polarization.

The dynamics of vortex gyration could solve the problem of the read and the write process. The bits, represented by the chirality or the c-value and the polarization, are addressed by the vortex gyration. In case of rotating current excitations the amplitude of gyration depends on the polarization p, see Eqn. (4.25). In case of simultaneous current- and magnetic-field excitations the amplitude of gyration depends on the chirality c or the c-value and the polarization p [43], see Eqns. (4.30) and (4.32). In the following the polarization combined with the chirality or c-value leading to an enlarged (suppressed) gyration amplitude are interpreted as a logical one (zero). Note that for an unambiguous interpretation of the amplitude of gyration in case of simultaneous current- and magnetic-field excitation the field and the current always has to be applied in the same direction for the read process. In case of rotating excitations the sense of rotation always have to be

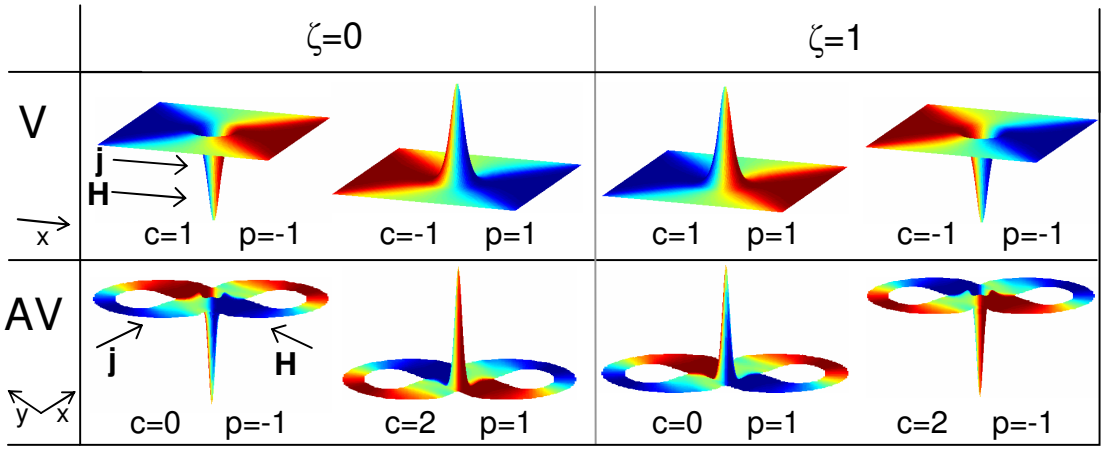

Fig. 5.1: Logical states $\zeta = 0$ and $\zeta = 1$ and the corresponding magnetization patterns of vortices (V) and antivortices (AV). The color code depicts the component M_y. The arrows below the vortex and the antivortex indicate the directions of the applied current and the applied magnetic field, the arrows on the left hand side show the space directions.

the same.

For rotating excitations the logical state $\zeta = 0$ or $\zeta = 1$ can be defined by

$$\zeta = (np+1)/2, \tag{5.1}$$

where the current has a mathematical positive sense of rotation. For simultaneous current- and magnetic-field excitations the logical state is

$$\zeta = (1+cp)/2, \tag{5.2}$$

in case of fields parallel to the current, where the chirality $c \in \{-1,1\}$. In case of magnetic fields perpendicular to the current

$$\zeta = (1+p-cp)/2, \tag{5.3}$$

where the c-value of the antivortex $c \in \{0,2\}$. Figure 5.1 illustrates the logical states $\zeta = 0$ or $\zeta = 1$ for simultaneous current- and magnetic-field excitations.

5.2 Read and write process

The amplitude of gyration could be detected by an inductive loop. This loop could be realized by a circular nanowire that is positioned asymmetrically on top of the sample. The asymmetry avoids a compensation of the magnetic flux of the symmetrical magnetization pattern. The magnetic flux density in the wire, that results from the stray field of the domains of the gyrating vortex, gives a sinusoidal magnetic flux $\Phi(t) = \int_{loop} B(t) d^2r$ and inductive voltage $U_{ind}(t) = -\frac{\partial}{\partial t}\Phi(t)$. Although the amplitude of the magnetic flux

$\Phi(t)$ is small due to the small area of the loop, the inductive voltage lies in the range of microvolt because of the high temporal variation of the magnetic flux.
Another possible read process can be realized by the integration of the vortex into a magnetic tunnel junction. The tunnel junction consists of a ferromagnetic layer with a vortex at the bottom, an insulator above the vortex and another ferromagnetic layer with a mono domain above the insulator. A current that is applied into the direction of the film normal experiences a different resistance in dependence on the amplitude of gyration due to the tunnel magneto resistance (TMR). This has been demonstrated experimentally by Kasai et al. [60].
To read the logical state the amplitude of excitation must be small enough to ensure that the vortex core does not switch. To write a logical $\zeta = 0$ or a logical $\zeta = 1$ the core can be excited by a rotating current or a simultaneous current and magnetic field of amplitudes that are sufficient to switch the polarization. If the vortex possesses the state $\zeta = 1$ the amplitude of gyration is enlarged until the core switches and the state $\zeta = 0$. Then the amplitude of gyration is suppressed and the core does not switch back. Hence, the switching serves as a stable write process. The current must be applied with the opposite sense of rotation for rotating excitations or it must be applied from the opposite direction at simultaneous current and magnetic field excitations to recover the state $\zeta = 1$.

5.3 Storage devices

Single storage cells containing vortices can be connected to a storage device. In the following, storage cells are presented that work with simultaneous current- and magnetic-field excitations. In a vortex random access memory (VRAM) a magnetic field parallel to the current for the read process and a magnetic field parallel or antiparallel to the current for the write process are required [61], [p5]. Figure 5.2 (a) illustrates two permalloy squares that are connected to current contacts. The current path splits and passes through the vortex and through a strip line. The strip line underneath the vortices generates an Oersted field that points parallel or antiparallel to the current in the permalloy square. Switches are needed to control which vortex is addressed and in which direction the current flows either parallel or antiparallel to the magnetic field. For the read process the magnetic field always points parallel to the current. In an antivortex random access memory (AVRAM), as shown in Fig. 5.2 (c), the magnetic field has to point perpendicular to the current [62], [P6]. This perpendicular field is realized by an Oersted field that is generated due to the inhomogeneity of the current density in the direction of the film normal. This gradient can be caused by the contact geometry or by vertical variations of the conductivity in the permalloy film due to the preparation process. The switches control which storage cells are addressed and if the direction of the current results in a c-value $c = 0$ or $c = 2$. For the read process the current is always applied into the direction illustrated in Fig. 5.2 (c).
The storage cells consist of a stack of layers. The ferromagnetic layer and the inductive loop are seperated by an insulating layer as shown in Figs. 5.2 (b) and 5.2 (d). The fer-

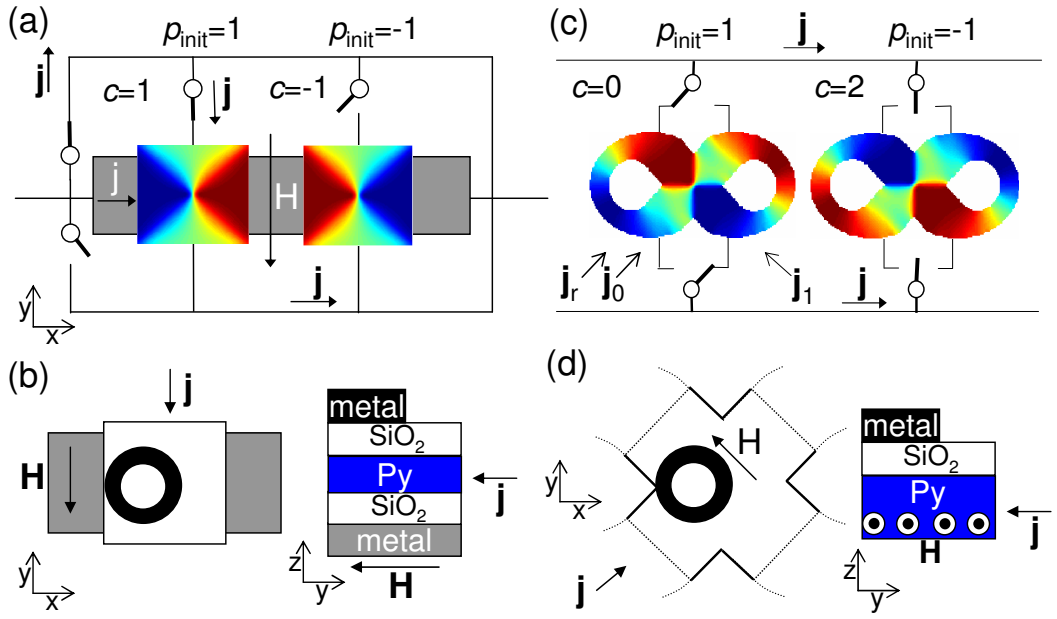

Fig. 5.2: Schemes of connected storage cells containing vortices and antivortices. The color code depicts the strength of the magnetization component M_y. The circles and bars symbolize switches. The lines denote electric lines. The symbols p_{init} depict the initial polarizations and the symbols c denote (a) the chiralities or (c) the c-values. The arrows indicate the directions of the current or the magnetic field. (a) The gray rectangle underneath the vortices illustrates the strip line. (b) and (d) The left sketches show the top view and the right sketches the side view of a single storage cell containing (b) a vortex and (d) an antivortex. In the top view the black rings illustrate inductive loops. The side view shows (b) a metallic layer of the strip line, (b) above this a layer of silicon dioxide as insulator, above this layers of permalloy containting (b) the vortex and (d) the antivortex, above this layers of silicon dioxide as insulator, and at the top, layers of metal of the inductive loops.

romagnetic layer is connected to electrical contacts. VRAM storage cells additionally consist of a strip line at the bottom and an insulating layer between the strip line and the ferromagnetic layer, see Fig. 5.2 (b).

The features of storage cells that operate with rotating current or simultaneous current and magnetic fields can be compared. For rotating excitations smaller amplitudes are required to displace the vortex core compared to unidirectional excitations [43]. Rotating excitations are realized by simultaneous currents from perpendicular directions that possess a phase shift of $\pi/2$. This demands a technically challenging phase synchronization. For fields parallel to the current only an external current has to be applied, but a phase synchronization between the current in the permalloy square and the current in the strip line is needed. For fields perpendicular to the current no phase synchronization is required but the generation of the Oersted field in the sample is difficult to control. In comparison with present nonvolatile storage devices like the flash memory or hard disks the VRAM and AVRAM have smaller access times and they can be written an infinite number of times.

Publication 5

Reprinted with permission from S. Bohlens, B. Krüger, A. Drews, M. Bolte, G. Meier, and D. Pfannkuche,

Current controlled random-access memory based on magnetic vortex handedness,

Appl. Phys. Lett. **93**, 142508-1-142508-3 (2008)

Current Controlled Random-Access Memory Based On Magnetic Vortex Handedness

Stellan Bohlens,[1] Benjamin Krüger,[1] André Drews,[2] Markus Bolte,[2] Guido Meier,[2] and Daniela Pfannkuche[1]

[1] *I. Institut für Theoretische Physik, Universität Hamburg, Jungiusstr. 9, 20355 Hamburg, Germany*
[2] *Institut für Angewandte Physik und Zentrum für Mikrostrukturforschung, Universität Hamburg, Jungiusstr. 11, 20355 Hamburg, Germany*

(Dated: September 22, 2008)

The theoretical foundation for a non-volatile memory device based on magnetic vortices is presented. We propose a realization of a Vortex Random-Access Memory (VRAM) containing vortex cells that are controlled by alternating currents only. The proposed scheme allows to transfer the vortex into an unambiguous binary state regardless of its initial state within a sub-nanosecond timescale. The vortex handedness defined as the product of chirality and polarization as a bit representation allows direct mechanisms for reading and writing the bit information. The VRAM is stable at room-temperature.

PACS numbers: 75.60.Ch, 72.25.Ba, 85.75.-d

The perception that magnetization dynamics is tunable by spin-polarized currents [1, 2] triggered an intensive investigation of applications within the last years. Compared to a magnetic field, an electrical current is much more appropriate to control a device since it can be handled with high precision and can be spatially restricted. Recently, it has been suggested to employ the polarization of a magnetic vortex core for data storage [3]. This is motivated by the experimental discovery [4, 5] and numerical investigation [6, 7] of vortex-core switching in various scenarios. In a ferromagnetic thin-film element a vortex state with a core of a few nanometers [8] is formed due to the interplay of exchange and demagnetization energy. The in-plane magnetization curls around a sharp singularity in the center, where the magnetization is forced out-of-plane to minimize exchange energy. Despite its complex structure the magnetic vortex in many ways behaves as a quasi-particle only characterized by the polarization p, the chirality c, and the coordinates X and Y of the vortex core in the sample plane as illustrated in Fig. 1. The vortex core pointing up (down) denoted by the polarization $p = +1$ ($p = -1$) provides a basis for a binary logic. The chirality characterizes the sense of rotation of the in-plane magnetization. For $c = +1$ ($c = -1$) the magnetization curls counter-clockwise (clockwise) around the core. In a ferromagnetic square or circular thin-film element with no crystalline anisotropy, e.g., made of permalloy, the vortex state constitutes the energetic ground state which is fourfold degenerate due to the combinations of chirality and polarization (cf. Fig. 1). To change its polarization, the vortex has to overcome an energy barrier which is of the order of ten electronvolts [9]. Hence, the vortex core is quite stable against thermal fluctuations at room temperature or magnetic stray fields in the millitesla regime. The benefit of using magnetic vortices in a memory device is their innate smallness and their generic existance. Therefore, the vortex is appropriate to serve as a non-volatile storage device.

We present a memory device based on the magnetic vortex handedness defined as the product cp of chirality and core polarization. The application of the handedness as a bit representation allows bit writing without the knowledge of the initial magnetization state as well as a direct reading of the bit information. Consequently, a main advantange is that the writing process requires no preceding reading operation.

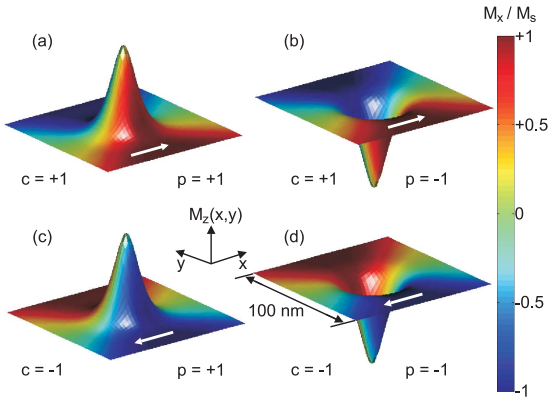

FIG. 1: (Color online) The fourfold degenerate ground state of a magnetic vortex in a thin-film element with chirality $c = \pm 1$ and core polarization $p = \pm 1$. The white arrows illustrate the sense of rotation of the in-plane magnetization. The magnetization in the center points out of plane. The height indicates the out-of-plane magnetization M_z while the colors visualize the x-component of the in-plane magnetization M_x normalized to the saturation magnetization M_s.

Recently, it has been shown that a vortex confined in a thin-film element performs elliptical rotations around its equilibrium position when excited by an alternating current [4, 10–15] or magnetic field [10, 11, 16]. We propose that a collinear arrangement of electrical current density and magnetic field as depicted in Fig. 2(a) yields a way to employ the magnetic vortex as a storage device. A possible technical realization of the VRAM is shown in Fig. 2(b), where the ferromagnetic cells are aligned on a strip-line. Each storage cell contains a vortex. The injected current splits up in two parts: one flowing in x-direction through a distinct cell and the other flowing in y-direction underneath the cell array. While the first part of the current flows straight through the ferromagnetic mate-

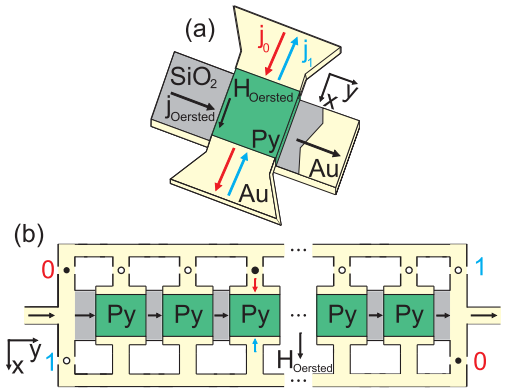

FIG. 2: (Color online) (a) A single Vortex Random-Access Memory (VRAM) cell with collinear current and Oersted field. (b) Possible technical realization of a VRAM. The cells are arranged in a two-dimensional array, from which one row is depicted. The high-ohmic permalloy squares constitute the memory cells while the gold striplines supply the read-write current. Open (filled) circles symbolize open (closed) switches that are used to store information in an individual cell. The numbers 0 and 1 denote the switches which have to be activated to write the according bit in the activated cell. The configuration shown here writes a binary "zero" into the third cell (red arrow).

rial of the selected VRAM cell, the second part of the current passes by the VRAM cells in a strip-line beneath the cells. The current in x-direction is the writing current which excites the vortex of a single cell due to the spin-torque effect [14, 17]. The role of the second current is to create an alternating, spatially homogeneous Oersted field in the cell above it, which results in a precession of the vortices in the cells. Thus, the scheme proposed in Fig. 2(a) provides a parallel arrangement of electrical current density and magnetic field. For a current density $\vec{j} = j\vec{e}_x$ and a magnetic field $\vec{H} = H\vec{e}_x$ the equation of motion for the quasi-particle vortex reads [10]

$$\begin{aligned}\begin{pmatrix}\dot{X}\\ \dot{Y}\end{pmatrix} &= \begin{pmatrix}-\Gamma & -p\omega\\ p\omega & -\Gamma\end{pmatrix}\begin{pmatrix}X\\ Y\end{pmatrix}\\ &+ \begin{pmatrix}-v_\mathrm{j} - \frac{\Gamma^2}{\omega^2+\Gamma^2}\frac{\xi-\alpha}{\alpha}v_\mathrm{j}\\ \frac{p\omega\Gamma}{\omega^2+\Gamma^2}\frac{\xi-\alpha}{\alpha}v_\mathrm{j}\end{pmatrix} + \frac{v_\mathrm{H}\omega c}{\omega^2+\Gamma^2}\begin{pmatrix}p\omega\\ \Gamma\end{pmatrix}.\end{aligned} \tag{1}$$

The free angular frequency $\omega = -pG_0 m\omega_r^2/(G_0^2 + D_0^2\alpha^2)$ and the damping constant $\Gamma = -D_0\alpha m\omega_r^2/(G_0^2 + D_0^2\alpha^2)$ are defined as in Ref. [10]. The driving velocity due to the magnetic field H is $v_\mathrm{H} = \gamma Hl/(2\pi)$ with the edge length l. The driving velocity of the current is $v_\mathrm{j} = b_j j$. The coupling constant between the current and the magnetization is $b_j = P\mu_B/[eM_s(1+\xi^2)]$, P is the spin polarization, M_s the saturation magnetization, ξ the degree of non-adiabaticity [17], and α the phenomenological Gilbert-damping parameter. The resonance frequency of the vortex due to the demagnetizing field [10] is ω_r and G_0, D_0 are constants of the gyrovector and dissipation-tensor [18], respectively. A special feature of Eq. 1 is that a parallel or antiparallel arrangement of current density and field leads to either an enhancement or a quenching of the gyration amplitude of vortex motion, in agreement with results for antivortices [19]. The steady-state solution of Eq. 1 with harmonic current excitation, for which the magnetic field and the electrical current density are of the form $H(t) = H_0 e^{i\Omega t}$ and $j(t) = j_0 e^{i\Omega t}$, yields [10]

$$\begin{aligned}\begin{pmatrix}X\\ Y\end{pmatrix} &= \frac{e^{i\Omega t}}{\omega^2 + (i\Omega+\Gamma)^2}\\ &\times \begin{pmatrix}-\frac{\Gamma}{\omega}\frac{\xi}{\alpha}v_\mathrm{j}\omega & + & (v_\mathrm{H}cp - v_\mathrm{j})\, i\Omega\\ (v_\mathrm{H}cp - v_\mathrm{j})\, p\omega & + & \frac{\Gamma}{\omega}\left(v_\mathrm{H}cp + \frac{\xi-\alpha}{\alpha}v_\mathrm{j}\right) ip\Omega\end{pmatrix}\end{aligned} \tag{2}$$

under the assumption that the squared Gilbert-damping parameter is small ($\alpha^2 \ll 1$) and thus the damping constant is small compared to the frequency ($\Gamma^2 \ll \omega^2$). At resonance ($\Omega = \omega$) and for weak damping ($\Gamma \ll \omega$) the steady-state vortex motion is a circle with radius

$$R(v_\mathrm{H}, v_\mathrm{j}, \Gamma, cp) = \sqrt{(\Re X)^2 + (\Re Y)^2} = \frac{|v_\mathrm{H}cp - v_\mathrm{j}|}{2\Gamma}, \tag{3}$$

which depends on the vortex handedness cp. When the driving velocities of field and current are equal ($|v_\mathrm{H}| = |v_\mathrm{j}|$), Eq. 3 yields a doubling or a quenching of the gyration amplitude dependent on the handedness.

The key mechanism of the VRAM is to employ that the gyration amplitude behaves oppositely for the cases $cp = 1$ and $cp = -1$ without the need to determine the absolute values of c or p separately. From the viewpoint of binary logic the proposed arrangement reduces the fourfold degenerate vortex ground state to two distinct cp states with two representations representing the single bit. In the following let us define the "zero" ("one") by cp-positive (cp-negative).

Recent numerical investigations of the vortex-core switching have shown that the switching depends only on the velocity of the vortex [20, 21] and thus on the radius of gyration. Furthermore, the critical velocity for switching was found to be an intrinsic parameter and hence does not depend on specific properties of the driving force [20]. There exist theories of Yamada et al. [4] and Guslienko et al. [21] about the critical velocity for switching. For permalloy Guslienko estimates $v_\mathrm{switch} \approx 320\frac{\mathrm{m}}{\mathrm{s}}$ while Yamada et al. found $v_\mathrm{switch} \approx 250\frac{\mathrm{m}}{\mathrm{s}}$, "regardless of the excitation current density" (cf. Ref. [4]). According to Guslienko et al. the critical velocity is proportional to the saturation magnetization or the square root of the exchange constant. Thus for permalloy structures (exchange constant of $A = 13 \cdot 10^{-12}\frac{\mathrm{J}}{\mathrm{m}}$, lateral sample size of 200 nm and a thickness of 20 nm), the critical current density is $1.3 \cdot 10^{11}\frac{\mathrm{A}}{\mathrm{m}^2}$ for pure current excitation and a critical velocity of $v_\mathrm{switch} \approx 320\frac{\mathrm{m}}{\mathrm{s}}$. This corresponds to a current of ≈ 0.5 mA and an absorbed power of 2.7 μW. Thus, if for $|v_\mathrm{H}| = |v_\mathrm{j}|$ the current amplitude is tuned to more than half of its critical value, that is defined as the current-amplitude needed for switching the vortex due to current alone, the vortex ends up with a distinct handedness: In the case of current parallel to

field, a quenching of the vortex motion occurs for positive cp (cf. Eq. 3) and the values of c and p remain the same. For negative cp, a doubling of the gyration amplitude and therefore a switching of the vortex occurs since the radius attains the critical value. While the polarization changes during the switching process the chirality is conserved. After the switching the vortex comes to rest being now in the opposite cp state which immediately leads to cancellation of the driving forces. The subsequent free damped oscillation results in a quenching of the vortex rotation. Irrespective of the starting configuration, the writing process leads to the defined property $cp = +1$ representing the binary value "zero". Accordingly to write the binary "one" $cp = -1$, the direction of the spin-torque has to be inverted. This can be achieved by reversing the direction of the current flowing in opposite x-direction through the cell ($v_\mathrm{j} \rightarrow -v_\mathrm{j}$) as shown in Fig. 2(b). The information is permanently stored in the magnetic-vortex configuration cp, even when the current is switched off.

Instead of using an alternating current it is possible to operate the VRAM with short current pulses v_H^p and v_j^p. Numerical investigations have shown that pulses offer the advantage of vortex switching that is up to one order of magnitude faster than switching by alternating currents [7, 22]. If we choose a collinear arrangement for current and field and consider that the damping constant is small compared to the frequency of the free vortex ($\Gamma \ll \omega$), Eq. 1 reduces to:

$$\begin{pmatrix} \dot{X} \\ \dot{Y} \end{pmatrix} = \begin{pmatrix} -\Gamma & -p\omega \\ p\omega & -\Gamma \end{pmatrix} \begin{pmatrix} X \\ Y \end{pmatrix} + \begin{pmatrix} v_\mathrm{H}^\mathrm{p} cp - v_\mathrm{j}^\mathrm{p} \\ 0 \end{pmatrix}. \qquad (4)$$

The last term is the driving force. Eq. 4 states that the action of short current and magnetic field pulses compensate or amplify each other depending on the handedness of the vortex.

In principle, a vortex excitation in a collinear alignment of current and field could be replaced by a rotating magnetic field making use of the polarization p instead of the combined quantity cp [23, 24]. However, a set-up with a rotating field requires two currents with a phase shift of $\frac{\pi}{2}$ (cf. Ref. [24]). We want to point out that a main advantage of our concept is to use one current only.

For the reading mechanism it is necessary to determine the product cp, as the bit information is encoded in the handedness. If current and field are aligned parallel, the binary value "zero" ("one") corresponds to a resting (rotating) vortex. In the absence of current and field precession or cessation of precession of the vortex holds no information about the actual memory state of the VRAM cell. Thus a small reading current together with the magnetic field in the collinear arrangement is needed to determine the cp-state. For parallel current and field reading collimates in the task of distinguishing a vortex at rest ($cp = +1$) from a rotating vortex ($cp = -1$). The proposed VRAM realization in Fig. 2 consists of a two-dimensional array of permalloy cells. The rotating vortex creates a time-varying magnetic flux which can be measured by placing a pickup coil (induction loops) above the storage cell or by detecting resistance changes [25, 26]. To read out the information a lower current density compared to the writing current density can be used. A current density less than half of the critical current density has neither an influence on the polarization nor on the chirality. Thus, the VRAM cell can be read an infinite number of times without affecting its binary state.

In conclusion we propose a magnetic Vortex Random-Access Memory (VRAM). In a collinear current and field arrangement, we established a one-to-one correspondence of the vortex handedness to the binary values "zero" and "one". The VRAM needs not be read or erased preceding the writing and, in general, allows an infinite number of read and write operations. This is an advantage compared to existing memory technologies, such as the FLASH memory, which requires a slow erasing procedure of the present memory state. The VRAM concept is non-volatile and fulfills the stability requirements for a memory device, since the vortex state is stable against temperature and magnetic fields as long as they remain in the millitesla regime. The VRAM shows a good scaling behavior, in general no material fatigue, and is foremost a fast memory concept.

We thank Ulrich Merkt, Dirk-Sören Lühmann, Bernd Güde, Massoud Najafi, Lars Bocklage, and Toru Matsuyama for valuable discussions. Financial support by the Deutsche Forschungsgemeinschaft via SFB 668, via SFB 508, and via Graduiertenkolleg 1286 is gratefully acknowledged.

[1] L. Berger, Phys. Rev. B **54**, 9353 (1996).
[2] J. Slonczewski, J. Magn. Magn. Mater. **159**, L1 (1996).
[3] K. Bussmann, G. A. Prinz, S.-F. Cheng, and D. Wang, Appl. Phys. Lett. **75**, 2476 (1999).
[4] K. Yamada, S. Kasai, Y. Nakatani, K. Kobayashi, H. Kohno, A. Thiaville, and T. Ono, Nature Materials **6**, 270 (2007).
[5] B. Van Waeyenberge, A. Puzic, H. Stoll, K. W. Chou, T. Tylisczak, R. Hertel, M. Fähnle, H. Brückl, K. Rott, G. Reiss, I. Neudecker, D. Weiss, C. H. Back, and G. Schütz, Nature **444**, 461 (2006).
[6] V. P. Kravchuk, D. D. Sheka, Y. Gaididei, and F. G. Mertens, J. Appl. Phys. **102**, 043908 (2007).
[7] R. Hertel, S. Gliga, M. Fähnle, and C. M. Schneider, Phys. Rev. Lett. **98**, 117201 (2007).
[8] A. Wachowiak, J. Wiebe, M. Bode, O. Pietzsch, M. Morgenstern, and R. Wiesendanger, Science **298**, 577 (2002).
[9] O. Tretiakov and O. Tchernyshyov, Phys. Rev. B **75**, 012408 (2007).
[10] B. Krüger, A. Drews, M. Bolte, U.Merkt, D. Pfannkuche, and G. Meier, Phys. Rev. B **76**, 224426 (2007).
[11] B. Krüger, A. Drews, M. Bolte, U.Merkt, D. Pfannkuche, and G. Meier, J. Appl. Phys. **103**, 07A501 (2008).
[12] J. Raabe, C. Quitmann, C. H. Back, F. Nolting, S. Johnson, and C. Buehler, Phys. Rev. Lett. **94**, 217204 (2005).
[13] K.-S. Lee and S.-K. Kim, Appl. Phys. Lett. **91**, 132511 (2007).
[14] M. Bolte, G. Meier, B. Krüger, A. Drews, R. Eiselt, L. Bocklage, S. Bohlens, T. Tyliszczak, A. Vansteenkiste, B. Van Waeyenberge, K. W. Chou, A. Puzic, and H. Stoll, Phys. Rev. Lett. **100**, 176601 (2008).
[15] S. Kasai, Y. Nakatani, K. Kobayashi, H. Kohno, and T. Ono, Phys. Rev. Lett. **97**, 107204 (2006).

[16] S.-B. Choe, Y. Acremann, A. Scholl, A. Bauer, A. Doran, J. Stöhr, and H. A. Padmore, Science **304**, 420 (2004).
[17] S. Zhang and Z. Li, Phys. Rev. Lett. **93**, 127204 (2004).
[18] A. A. Thiele, J. Appl. Phys. **45**, 377 (1974).
[19] A. Drews, B. Krüger, M. Bolte, U. Merkt, and G. Meier, Phys. Rev. B **77**, 094413 (2008).
[20] S. K. Kim, Y. S. Choi, K. S. Lee, K. Y. Guslienko, and D. E. Jeong, Appl. Phys. Lett. **91**, 082506 (2007).
[21] K. Y. Guslienko, K.-S. Lee, and S.-K. Kim, Phys. Rev. Lett. **100**, 027203 (2008).
[22] K.-S. Lee, K. Y. Guslienko, J.-Y. Lee, and S.-K. Kim, Phys. Rev. B **76**, 174410 (2007).
[23] S.-K. Kim, K.-S. Lee, Y.-S. Yu, and Y.-S. Choi, Appl. Phys. Lett. **92**, 0022509 (2008).
[24] M. Curcic, B. Van Waeyenberge, A. Vansteenkiste, M. Weigand, V. Sackmann, H.Stoll, M. Fähnle, T. Tyliszczak, G. Woltersdorf, C. H. Back, and G. Schütz, cond. mat. **arXiv:0804.2944v2 [cond-mat.other]** (2008).
[25] S. Kasai, K. Nakano, K. Kondou, N. Oshima, K. Kobayashi, and T. Ono, Appl. Phys. Express **1**, 091302 (2008).
[26] R. Moriya, L. Thomas, M. Hayashi, Y. B. Bazaliy, C. Rettner, and S. S. Parkin, Nature Materials **4**, 368 (2008).

Publication 6

Reprinted with permission from A. Drews, B. Krüger, G. Meier, S. Bohlens, L. Bocklage, T. Matsuyama, and M. Bolte,

Current- and field-driven magnetic antivortices for nonvolatile data storage,

Appl. Phys. Lett. **94**, 062504-1-062504-3 (2009)

Current- and Field-Driven Magnetic Antivortices for Nonvolatile Data Storage

André Drews,[1] Benjamin Krüger,[2] Guido Meier,[1] Stellan Bohlens,[2] Lars Bocklage,[1] Toru Matsuyama,[1] and Markus Bolte[1,3]

[1]*Institut für Angewandte Physik und Zentrum für Mikrostrukturforschung, Universität Hamburg, Jungiusstr. 11, 20355 Hamburg, Germany*
[2]*I. Institut für Theoretische Physik, Universität Hamburg, Jungiusstr. 9, 20355 Hamburg, Germany*
[3]*Arbeitsbereich Technische Informatiksysteme, Universität Hamburg, Vogt-Kölln-Str. 30, 20255 Hamburg, Germany*

(Dated: May 18, 2009)

We demonstrate by micromagnetic simulations that magnetic antivortices are potential candidates for fast non-volatile data-storage elements. These storage elements are excited simultaneously by alternating spin-polarized currents and their accompanying Oersted fields. Depending on the antivortex-core polarization p and the orientation of the in-plane magnetization c around the core, the superposition of current and field leads to either a suppression of gyration (logical 'zero') or an increased gyration amplitude (logical 'one'). Above an excitation treshold the gyration culminates in the switching of the antivortex core. The switching can be seen as a cp-dependent writing of binary data, allowing to bring the antivortex into a distinct state. Furthermore a read-out scheme using an inductive loop situated on top of the element is investigated.

PACS numbers: 75.60.Ch, 72.25.Ba

The dynamics of magnetic vortices has been intensely studied in recent years as they yield fundamentally interesting and often surprising properties. For example, it has been found that magnetic fields[1,2] or spin-polarized electric currents[3,4] can cause vortices to gyrate around their equilibrium position, but can also cause the small vortex core[5,6] to switch its out-of-plane component, the so-called vortex core polarization.[7–10] However, much less is known about the vortex' topological counterpart, the antivortex (AV), even though it commonly occurs in magnetic thin films, e.g., in cross-tie domain walls.[11–13] Micromagnetic simulations[14,15] and analytical theory[16] have predicted the existence and dynamics of magnetic antivortices.

Antivortices are formed in ferromagnetic thin-film elements of lateral dimensions of a few hundred nanometers, where the magnetization points in-plane and crosses at the out-of-plane AV core (see Fig. 1). The orientation of the core can point either up ($p = 1$) or down ($p = -1$), in analogy to the vortex core. The direction of the in-plane magnetization around the AV core can be characterized by the c-value.[15] In contrast to the vortex, whose chirality is conserved, the c-value varies continuously between $c = -2$ and $c = 2$ when rotating the AV around the core axis. Thus the c-value is not a conserved property of the AV. The c-value $c = \frac{2}{\pi}(\phi+\beta)$ is defined by the angle of the antivortex with respect to the coordinate system, where ϕ is the angle of the local magnetization and β is the angle of the position vector.[15] In the following the current is assumed to flow in the x-direction ($\beta = 0$). When exciting an AV by alternating magnetic fields or currents of moderate amplitudes, the core gyrates.[15,16] Larger field amplitudes can even switch the core polarization as has been shown by micromagnetic simulations.[14] For vortices it has been shown that core switching is due to a gyrotropic field at critical core velocities.[10] This switching phenomenon has been suggested to be utilized as a write process for a memory cell.[8,17,18] However, the problem of repeated core switching in systems using only a single current or a magnetic field remained unresolved since for rotating magnetic fields or currents two perpendicular fields or currents with a phase-shift of $\pi/2$ are required.

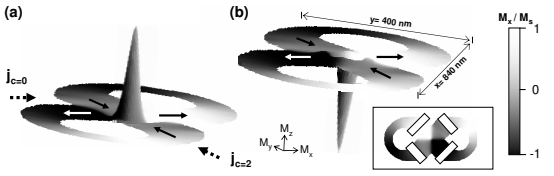

FIG. 1: Simulated magnetization configurations in ∞-shaped elements for (a) positive and (b) negative antivortex core polarization. The dotted arrows in (a) depict the directions of the exciting current at which the c-value of the antivortex is zero or two. The solid black and white arrows indicate the direction of the in-plane magnetization. The height denotes the z-component of the magnetization. The inset illustrates a plain view of the antivortex with four current contacts.

Here we show that isolated AVs can be used to store data. AV cores can be switched by a combination of alternating electrical currents and magnetic fields depending on the combination of the AV's in-plane and out-of-plane magnetization. In comparison to other storage concepts using magnetic vortex core switching, the AV random access memory (AVRAM) with an antivortex shown in Fig. 1 does not require an external strip line and a phase synchronization between electrical current and magnetic field,[19] or a phase synchronization between electrical currents applied simultaneously from perpendicular directions,[8] because the Oersted field is generated along with the current. The electrode contact geometry and thus the inhomogeneous current densities can be tailored so as to provide the required Oer-

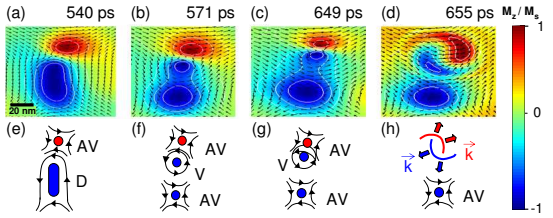

FIG. 2: (a)-(d) Micromagnetic simulations and (e)-(h) sketches of the different stages of simultaneous current- and field induced AV-core switching. (a), (e) A region of inverted out-of-plane magnetization (dip) is formed. (b), (f) The dip (D) decays into a new AV and a vortex of polarizations opposite to the original AV. (c), (g) The vortex and the original AV meet and (d), (h) annihilate shortly thereafter by emitting spin waves. The arrows in (h) denote the wave vectors of the spin waves.

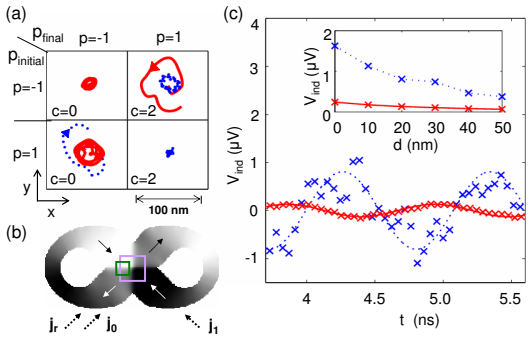

FIG. 3: Simulated write and read processes of AV cores. Red solid (blue dotted) lines and red (blue) crosses illustrate a negative (positive) core polarization $p = -1$ ($p = 1$). (a) The AV core with polarization p_{initial} is transformed into an AV with polarization p_{final} in dependence on the current direction described by the c-value. (b) The large square in the center of the antivortex element marks the area shown in (a), the small square marks the area of the inductive loop used to calculate the voltage signals in (c). The current direction for the read process is denoted by j_r, the current direction for the write process by j_0 and by j_1. (c) The crosses denote the voltage induced in a coil 20 nm above the sample's surface for $c = 0$, the fits represent the first harmonic of the antivortex gyration. The crosses in the inset show the maximum voltage for different distances between coil and sample, the lines are guides to the eyes.

sted field.[4] A writing mechanism is presented that does not require previous reading of the data[19] and inherently prevents repeated AV-core switching. A read-out scheme is presented that detects the AV's state by measuring the AV's gyration amplitude in response to low-amplitude excitation by alternating currents. The simulations were performed by using the Object Oriented Micromagnetic Framework (OOMMF)[20] extended by the spin-torque terms introduced by Zhang and Li.[21] To simulate the AV-core switching, an 840×400 nm^2 large and 50 nm thick ∞-shaped element (see Fig. 1) was excited by a spin-polarized current and its accompanying Oersted field perpendicular to the current. We assumed a homogeneous in-plane current density of amplitude $P \cdot j = 7.7 \cdot 10^{11}$ A/m^2 ($P \cdot j = 2.8 \cdot 10^{11}$ A/m^2), where P is the spin polarization, and a homogeneous in-plane magnetic field of $H = 20$ mT/μ_0($H = 7.9$ mT/μ_0) for the whole sample for the write (read) process.[26] The frequency of excitation for current and field was $\omega/2\pi = 914$ MHz, which is the resonance frequency of an AV in such an ∞-shaped-element as determined by a fit of the damped free relaxation.

The resonant excitation causes a growing AV gyration amplitude and thus AV velocity for the c-value $c = 0$ and the polarization $p = 1$. The gyrofield,[10] that points into the direction opposite to the polarization of the AV core grows and enlarges the halo-shaped 'dip' as shown in Fig. 2 (a), that normally surrounds the core isotropically.[22] This concentration of opposite out-of-plane magnetizations moves on an orbit close to the AV core on the inside of the AV orbit. The 'dip' splits into a vortex and an antivortex [see Fig. 2 (b)]. The new vortex moves towards the original antivortex and both annihilate by the formation of spin waves as shown in Fig. 2 (d), (h). A new antivortex of opposite polarization compared to the original antivortex remains.[7,14] Figure 3 (a) shows the trajectory of the AV core. Unlike in vortex switching, where repeated switching events have been observed due to long and strong field pulses,[23] we found that antivortices switch only once for simultaneous ac current- and field-excitation. Simulated ac current- and field-excitation of AVs with inverted polarization yielded AV gyration with much lower amplitude. Antivortex switching did not occur in this configuration. Instead, the current had to be injected from the direction with opposite c-value [see Fig. 1 (a)] to switch the AV back to its original polarization. Figure 3 shows the trajectories of AVs with negative and positive initial polarizations. This unexpected behavior is explained by the cp-dependent gyration amplitude and the concomitant cp-dependent AV velocity. Different directions of excitation represent a change of the c-value. The equation of motion for weakly damped systems at resonance in a field perpendicular to a current, as it is the case for Oersted fields accompanying currents traversing the elements, reads[15]

$$\begin{pmatrix} X \\ Y \end{pmatrix} = -\frac{e^{i\omega t}}{2\Gamma} \begin{pmatrix} 1 \\ ip \end{pmatrix} \left(v_j + v_H p e^{-\frac{i\pi}{2} cp} \right). \qquad (1)$$

Here Γ is the damping of the AV system and $v_j = b_j j$ is the velocity due to the current excitation with the current j and the coupling constant b_j between the current and the magnetization. In a magnetic field H, the AV velocity is $v_H = \gamma H l/2\pi$ with the characteristic lateral extension[16] l of the AV and the gyromagnetic ratio γ.

The amplitude of the AV-core gyration

$$r = r_0 \cdot \sqrt{\frac{v_H^2}{v_j^2} + 2p\frac{v_H}{v_j}\cos(\frac{c\pi}{2}) + 1}, \qquad (2)$$

is given in units of the gyration amplitude r_0 for current excitation alone. The maximum change occurs for opposite polarizations p at $c = 0$ or $c = 2$. Thus the current is best applied as shown in Fig. 1 (a). According to Eq. 2 we conclude that the cp-dependent field excitation causes a splitting $r_0\frac{|v_H \pm v_j|}{v_j}$ of the gyration amplitude for different polarizations or different directions of excitation. If the current excitation drives the AV close to the critical amplitude r_{crit} when core switching sets in, the additional velocity due to the Oersted field can facilitate or impede switching of the AV core. Oersted fields originating from alternating currents in permalloy elements were reported to contribute about 30% to the total force.[4] In this case the gyration amplitude of AVs where current and field support gyration is 2.5 times the gyration amplitude where the field acts against current excitation. Thus AV-core switching can serve as a robust writing mechanism for a data storage element. This holds true as long as the current density ensures that $r_0\frac{|v_H - v_j|}{v_j} < r_{\mathsf{crit}} < r_0\frac{|v_H + v_j|}{v_j}$.

A binary state $\zeta \in \{0, 1\}$ can now be defined by the magnetic configuration of an AV. If the sum of current and field excitation is sufficient to change the state once, then the suppressed gyration inhibits that the AV-core switches back. Note that for writing a bit the appropriate current direction has to be chosen, while the reading of the state can be realized always from the same direction. As illustrated in figure 3 (b) for writing the state $\zeta = 0$ ($\zeta = 1$) the current is applied in the direction as indicated by j_0 (j_1). For the read process the current is applied in the direction indicated by j_r, so that low gyration amplitudes represent a logical 'zero' and high gyration amplitudes represent a logical 'one'.

The read-out of the state has to be done with a lower current density so that the gyration amplitude stays below the critical radius $r_0\frac{|v_H + v_j|}{v_j} < r_{\mathsf{crit}}$ to avoid switching. The measurement of the gyration amplitudes could be realized by an inductive loop, which is positioned asymmetrically above the ∞-shaped sample to measure a non-vanishing change of the magnetic flux Φ. Different gyration amplitudes lead to varying amplitudes in the alternating magnetic flux. The amplitude of the induced voltage $V_{\mathsf{ind}} = -\frac{d}{dt}\Phi$ can then be detected to read the state ζ as illustrated in Fig. 3 (c). The time derivative of the magnetic flux $\Phi = \mu_0 \int_{\mathsf{loop}} H_z dS$ is calculated by the finite difference method. At an enhanced amplitude of antivortex gyration ($\zeta = 1$) the deviation of the inductive voltage from the sinusoidal line may be caused by transient spin waves, which decrease with time. Also anharmonic contributions to the confining potential might play a role at enhanced amplitudes. Very recently Kasai et al. demonstrated an alternative detection technique based on a magnetic tunnel junction.[24]

In conclusion micromagnetic simulations and an analytical model show how magnetic antivortex-core switching can be utilized in non-volatile storage elements. By a combination of spin-polarized currents and their accompanying Oersted fields, the switching is either favored or suppressed, depending on the state of the element. The time dependence of the magnetic flux of the gyrating antivortex can be employed to read out the binary data.

We thank Ulrich Merkt and Daniela Pfannkuche for valuable discussions and encouragement. Financial support by the Deutsche Forschungsgemeinschaft via the Graduiertenkolleg 1286 "Functional metal-semiconductor hybrid systems" and via the SFB 668 "Magnetismus vom Einzelatom zur Nanostruktur" is gratefully acknowledged.

[1] S.-B. Choe, Y. Acremann, A. Scholl, A. Bauer, A. Doran, J. Stöhr, and H. A. Padmore, Science **304**, 420 (2004).
[2] S. Kasai, Y. Nakatani, K. Kobayashi, H. Kohno, and T. Ono, Phys. Rev. Lett. **97**, 107204 (2006).
[3] B. Krüger, A. Drews, M. Bolte, U. Merkt, D. Pfannkuche, and G. Meier, Phys. Rev. B **76**, 224426 (2007).
[4] M. Bolte, G. Meier, B. Krüger, A. Drews, R. Eiselt, L. Bocklage, S. Bohlens, T. Tyliszczak, A. Vansteenkiste, K. W. Chou, A. Puzic, H. Stoll, Phys. Rev. Lett. **100**, 176601 (2008).
[5] K. Y. Guslienko and V. Novosad, J. Appl. Phys. **96**, 4451 (2004).
[6] A. Wachowiak, J. Wiebe, M. Bode, O. Pietzsch, M. Morgenstern, and R. Wiesendanger, Science **298**, 577 (2002).
[7] B. Van Waeyenberge, A. Puzic, H. Stoll, K. W. Chou, T. Tylisczak, R. Hertel, M. Fähnle, H. Brückl, K. Rott, G. Reiss, I. Neudecker, D. Weiss, G. Schütz, Nature **444**, 461 (2006).
[8] S.-K. Kim, K.-S. Lee, Y.-S. Yu, and Y.-S. Choi, Appl. Phys. Lett. **92**, 0022509 (2008).
[9] S.-K. Kim, Y.-S. Choi, K.-S. Lee, K. Y. Guslienko, and D.-E. Jeong, Appl. Phys. Lett. **91**, 082506 (2007).
[10] K. Y. Guslienko, K.-S. Lee, and S.-K. Kim, Phys. Rev. Lett. **100**, 027203 (2008).
[11] K. Shigeto, T. Okuno, K. Mibu, T. Shinjo, and T. Ono, Appl. Phys. Lett. **80**, 4190 (2002).
[12] A. Neudert, J. McCord, R. Schäfer, and L. Schultz, Phys. Rev. B. **75**, 1724041 (2007).
[13] S.-K. Kim, K.-S. Lee, B.-W. Kang, K.-J. Lee, and J. Kortright, Appl. Phys. Lett. **86**, 052504 (2005).
[14] S. Gliga, M. Yan, R. Hertel, and C. M. Schneider, Phys. Rev. B **77**, 060404(R) (2008).
[15] A. Drews, B. Krüger, M. Bolte, and G. Meier, Phys. Rev. B **77**, 094413 (2008).
[16] B. Krüger, A. Drews, M. Bolte, U. Merkt, D. Pfannkuche, and G. Meier, J. Appl. Phys. **103**, 07A501 (2008).

The amplitude of the AV-core gyration

$$r = r_0 \cdot \sqrt{\frac{v_H^2}{v_j^2} + 2p\frac{v_H}{v_j}\cos(\frac{c\pi}{2}) + 1}, \qquad (2)$$

is given in units of the gyration amplitude r_0 for current excitation alone. The maximum change occurs for opposite polarizations p at $c = 0$ or $c = 2$. Thus the current is best applied as shown in Fig. 1 (a). According to Eq. 2 we conclude that the *cp*-dependent field excitation causes a splitting $r_0\frac{|v_H \pm v_j|}{v_j}$ of the gyration amplitude for different polarizations or different directions of excitation. If the current excitation drives the AV close to the critical amplitude r_{crit} when core switching sets in, the additional velocity due to the Oersted field can facilitate or impede switching of the AV core. Oersted fields originating from alternating currents in permalloy elements were reported to contribute about 30% to the total force.[4] In this case the gyration amplitude of AVs where current and field support gyration is 2.5 times the gyration amplitude where the field acts against current excitation. Thus AV-core switching can serve as a robust writing mechanism for a data storage element. This holds true as long as the current density ensures that $r_0\frac{|v_H - v_j|}{v_j} < r_{\mathsf{crit}} < r_0\frac{|v_H + v_j|}{v_j}$.

A binary state $\zeta \in \{0, 1\}$ can now be defined by the magnetic configuration of an AV. If the sum of current and field excitation is sufficient to change the state once, then the suppressed gyration inhibits that the AV-core switches back. Note that for writing a bit the appropriate current direction has to be chosen, while the reading of the state can be realized always from the same direction. As illustrated in figure 3 (b) for writing the state $\zeta = 0$ ($\zeta = 1$) the current is applied in the direction as indicated by j_0 (j_1). For the read process the current is applied in the direction indicated by j_r, so that low gyration amplitudes represent a logical 'zero' and high gyration amplitudes represent a logical 'one'.

The read-out of the state has to be done with a lower current density so that the gyration amplitude stays below the critical radius $r_0\frac{|v_H + v_j|}{v_j} < r_{\mathsf{crit}}$ to avoid switching. The measurement of the gyration amplitudes could be realized by an inductive loop, which is positioned asymmetrically above the ∞-shaped sample to measure a non-vanishing change of the magnetic flux Φ. Different gyration amplitudes lead to varying amplitudes in the alternating magnetic flux. The amplitude of the induced voltage $V_{\mathsf{ind}} = -\frac{d}{dt}\Phi$ can then be detected to read the state ζ as illustrated in Fig. 3 (c). The time derivative of the magnetic flux $\Phi = \mu_0 \int_{\mathsf{loop}} H_z dS$ is calculated by the finite difference method. At an enhanced amplitude of antivortex gyration ($\zeta = 1$) the deviation of the inductive voltage from the sinusoidal line may be caused by transient spin waves, which decrease with time. Also anharmonic contributions to the confining potential might play a role at enhanced amplitudes. Very recently Kasai et al. demonstrated an alternative detection technique based on a magnetic tunnel junction.[24]

In conclusion micromagnetic simulations and an analytical model show how magnetic antivortex-core switching can be utilized in non-volatile storage elements. By a combination of spin-polarized currents and their accompanying Oersted fields, the switching is either favored or suppressed, depending on the state of the element. The time dependence of the magnetic flux of the gyrating antivortex can be employed to read out the binary data.

We thank Ulrich Merkt and Daniela Pfannkuche for valuable discussions and encouragement. Financial support by the Deutsche Forschungsgemeinschaft via the Graduiertenkolleg 1286 "Functional metal-semiconductor hybrid systems" and via the SFB 668 "Magnetismus vom Einzelatom zur Nanostruktur" is gratefully acknowledged.

[1] S.-B. Choe, Y. Acremann, A. Scholl, A. Bauer, A. Doran, J. Stöhr, and H. A. Padmore, Science **304**, 420 (2004).
[2] S. Kasai, Y. Nakatani, K. Kobayashi, H. Kohno, and T. Ono, Phys. Rev. Lett. **97**, 107204 (2006).
[3] B. Krüger, A. Drews, M. Bolte, U. Merkt, D. Pfannkuche, and G. Meier, Phys. Rev. B **76**, 224426 (2007).
[4] M. Bolte, G. Meier, B. Krüger, A. Drews, R. Eiselt, L. Bocklage, S. Bohlens, T. Tyliszczak, A. Vansteenkiste, K. W. Chou, A. Puzic, H. Stoll, Phys. Rev. Lett. **100**, 176601 (2008).
[5] K. Y. Guslienko and V. Novosad, J. Appl. Phys. **96**, 4451 (2004).
[6] A. Wachowiak, J. Wiebe, M. Bode, O. Pietzsch, M. Morgenstern, and R. Wiesendanger, Science **298**, 577 (2002).
[7] B. Van Waeyenberge, A. Puzic, H. Stoll, K. W. Chou, T. Tylisczak, R. Hertel, M. Fähnle, H. Brückl, K. Rott, G. Reiss, I. Neudecker, D. Weiss, G. Schütz, Nature **444**, 461 (2006).
[8] S.-K. Kim, K.-S. Lee, Y.-S. Yu, and Y.-S. Choi, Appl. Phys. Lett. **92**, 0022509 (2008).
[9] S.-K. Kim, Y.-S. Choi, K.-S. Lee, K. Y. Guslienko, and D.-E. Jeong, Appl. Phys. Lett. **91**, 082506 (2007).
[10] K. Y. Guslienko, K.-S. Lee, and S.-K. Kim, Phys. Rev. Lett. **100**, 027203 (2008).
[11] K. Shigeto, T. Okuno, K. Mibu, T. Shinjo, and T. Ono, Appl. Phys. Lett. **80**, 4190 (2002).
[12] A. Neudert, J. McCord, R. Schäfer, and L. Schultz, Phys. Rev. B. **75**, 1724041 (2007).
[13] S.-K. Kim, K.-S. Lee, B.-W. Kang, K.-J. Lee, and J. Kortright, Appl. Phys. Lett. **86**, 052504 (2005).
[14] S. Gliga, M. Yan, R. Hertel, and C. M. Schneider, Phys. Rev. B **77**, 060404(R) (2008).
[15] A. Drews, B. Krüger, M. Bolte, and G. Meier, Phys. Rev. B **77**, 094413 (2008).
[16] B. Krüger, A. Drews, M. Bolte, U. Merkt, D. Pfannkuche, and G. Meier, J. Appl. Phys. **103**, 07A501 (2008).

6 Conclusion and Outlook

The dynamics of magnetic vortices and antivortices has been investigated by micromagnetic simulations and by an oscillator model. The investigations cover the whole range of vortex dynamics in soft magnetic permalloy from the linear up to the highly nonlinear regime of vortex creation and annihilation. In the following the most important results are summarized.

Excited vortices and antivortices perform a damped gyration. The gyration is caused by an interaction between the magnetization vectors in the vortex core and the demagnetization field of the nonequilibrium magnetization pattern. A gyroscopic force and a dissipative force can be derived from the gyroterm and the dissipation term of the Landau-Lifshitz-Gilbert equation. These forces act on the vortex core, which can be treated as a quasiparticle. The restoring force of vortex gyration results from the demagnetization fields of the nonequilibrium magnetization pattern. The demagnetization energy is expanded up to the second order in a Taylor series to describe the harmonic vortex gyration for small core displacements by a driven harmonic oscillator [P1], [P2], [P3], [P4]. The trajectories from the model are in good agreement with the trajectories from micromagnetic simulations. The resonance frequency and the damping of vortices depend on the thickness and the length of the samples. The sense of gyration is given by the product of winding number and polarization [P2], [P3]. For alternating excitations in the steady state the trajectories have an elliptical shape with an amplitude and a ratio of the semiaxes that depend on the exciting frequency. The amplitude has its maximum at the resonance frequency. For a rotating excitation the trajectories become circular. For a pulsed excitation the core is displaced by the pulse and afterwards it performs a damped gyration. For constant excitations the core gyrates around a new equilibrium position. The characteristic c-value for an antivortex is introduced in analogy to the chirality of a vortex to study magnetic-field excitations in detail [P3]. For excitations with spin-polarized currents the phase of core gyration depends on the polarization and only for magnetic field excitation additionally on the chirality in case of vortex gyration or on the c-value in case of antivortex gyration [P1, P3, P4]. Thus a superposition of magnetic-field and current excitations leads to a variation of the amplitude of gyration in dependence on the chirality or c-value [P3].

For large core displacements the demagnetization energy becomes quartic. A nonlinear oscillator model is derived by evaluating the demagnetization energy up to the fourth order. Higher orders are not necessary to consider as confirmed by micromagnetic

simulations. The larger the amplitude the stronger the shape of the trajectories approaches the shape of the sample geometry. The resonance frequency exhibits a blue-shift the amplitude shows a gap slightly above the resonance frequency.
In the highly nonlinear regime a so-called dip particle is formed next to the vortex core with an out-of-plane magnetization that points opposite to that of the core. At a critical velocity the dip particle splits into a vortex and an antivortex. The splitting process is the limit of nonlinear vortex gyration. In case of vortex core switching the antivortex annihilates with the original vortex and the new vortex core of opposite polarization compared to the one of the original core remains. At antivortex core switching the states possess opposite winding numbers compared to vortex-core switching. During the switching a Bloch point, a magnetic singularity, is formed. This singularity can be described quantitatively only by quantum mechanics, because of the strong variations of adjacent elementary spins in the Bloch point. Generally Bloch-point dynamics can be considered topologically.

Vortices and antivortices could be used in non-volatile storage devices. The product of polarization and winding number for rotating excitations or the polarization and the chirality or c-value for simultaneous magnetic-field and current excitations represent logical states. The logical state can be read out by the amplitude of gyration [P5], [P6].

During the studies open questions arose. It has already be shown that vortices in adjacent samples couple via their stray fields. If only one vortex is excited by a current a second vortex in an adjacent sample gyrates only due to the temporally varying stray field of the excited vortex. The coupling results in amplitudes of gyration that depend on the polarizations and chiralities of the vortices. A detailed investigation of the coupling phenomena has to be done. This is an important step for the description of strongly correlated vortices in double Landau patterns or of vortices and antivortices in cross-tie walls. Also the coupling of vortices in multilayers could be investigated.
Another topic for further studies is the origin of nonlinear vortex dynamics. The influence of the halo formation and the influence of the domain walls on the vortex trajectories have to be investigated. A complete description of the switching process is still an open problem. The analytical description of vortex-antivortex pair decoupling from the dip particle, the gyration of the vortex core and the antivortex core around their center point, and an analytical Heisenberg description of the Bloch point dynamics have to be done.
Electrical circuits and devices that are necessary to realize VRAMs and AVRAMs comprising switches could be simulated. These simulations would yield the required dimensions and numbers of devices in one storage cell.
The dynamics of vortices in ferromagnets with non-vanishing anisotropy energies could be considered, which are important for technical applications. The anisotropy leads to a different dependence between the sample's geometry and the formation and dimensions of vortices compared to permalloy.

7 Publications

P1 B. Krüger, A. Drews, M. Bolte, U. Merkt, D. Pfannkuche, and G. Meier, *"Harmonic oscillator model for current- and field-driven magnetic vortices"*, Phys. Rev. B **76**, 224426, 2007.

P2 B. Krüger, A. Drews, M. Bolte, U. Merkt, D. Pfannkuche, and G. Meier, *"Vortices and antivortices as harmonic oscillators"*, J. Appl. Phys. **103**, 07A501, 2008.

P3 A. Drews, B. Krüger, M. Bolte, and G. Meier, *"Current- and field-driven magnetic antivortices"*, Phys. Rev. B **77**, 094413, 2008.

P4 M. Bolte, G. Meier, B. Krüger, A. Drews, R. Eiselt, L. Bocklage, S. Bohlens, T. Tyliszczak, A. Vansteenkiste, B. Van Waeyenberge, K. W. Chou, A. Puzic, and H. Stoll, *"Time-Resolved X-Ray Microscopy of Spin-Torque-Induced Magnetic Vortex Gyration"*, Phys. Rev. Lett. **100**, 176601, 2008.

P5 S. Bohlens, B. Krüger, A. Drews, M. Bolte, G. Meier, and D. Pfannkuche, *"Current controlled random-access memory based on magnetic vortex handedness"*, Appl. Phys. Lett. **93**, 142508, 2008.

P6 A. Drews, B. Krüger, G. Meier, S. Bohlens, L. Bocklage, T. Matsuyama, and M. Bolte, *"Current- and field-driven magnetic antivortices for nonvolatile data storage"*, Appl. Phys. Lett. **94**, 062504, 2009.

Bibliography

[1] C. Kittel. Theory of the structure of ferromagnetic domains in films and small particles. *Phys. Rev.* **70**, 965, 1946.

[2] R. V. Coleman and G. G. Scott. Magnetic domain patterns on single-crystal iron whiskers. *Phys. Rev.* **107**, 1276, 1957.

[3] J. S. Smart. *Effective field theories of magnetism*. Saunders, Philadelphia & London, 1966.

[4] W. Pauli. Zur Quantenmechanik des magnetischen Elektrons. *Z. Phys.* **43**, 601, 1927.

[5] P. Weiss. L´hypothèse du chomp moléculaire et la propriété ferromagnétique. *J. Phys.* **6**, 661, 1907.

[6] F. Bloch. Zur Theorie des Austauschproblems und der Remanenzerscheinung der Ferromagnetika. *Z. Phys.* **74**, 295, 1932.

[7] H. Barkhausen. Zwei mit Hilfe der neuen Verstärker entdeckte Erscheinungen. *Phys. Z.* **20**, 401, 1919.

[8] C. Kittel. *Introduction to Solid State Physics*. Wiley, New York, 2004.

[9] *http://hyperphysics.phy-astr.gsu.edu/Hbase/solids/ferro.html*. 2008.

[10] R. P. Cowburn, D. K. Koltsov, A. O. Adeyeye, M. E. Welland, and D. M. Tricker. Single-domain circular nanomagnets. *Phys. Rev. Lett.* **5**, 1042, 1999.

[11] *http://www.philsciletters.org/3rd week June/Visualizing objects at 20nanometer scales fig 2.png*. 2009.

[12] S. Blundell. *Magnetism in Condensed Matter*. Oxford University Press, New York, 2001.

[13] W. Heisenberg. Zur Theorie des Ferromagnetismus. *Z. Phys.* **49**, 619, 1928.

[14] B. Krüger. *Current-Induced Domain-Wall Dynamics in Ferromagnetic Nanowires*. Diploma Thesis, Universität Hamburg, 2007.

[15] L. Landau and E. Lifshitz. On the theory of the dispersion of magnetic permeability in ferromagnetic bodies. *Phys. Z. Sowjetunion* **8**, 153, 1955.

[16] A. Hubert and R. Schäfer. *Magnetic Domains: The Analysis of Magnetic Microstructures*. Springer, New York, 2000.

[17] T. L. Gilbert. A Lagrangian Formulation of the Gyromagnetic Equation of the Magnetization Field. *Phys. Rev. Lett.* **100***,* 1243, 1955.

[18] T. L. Gilbert. A phenomenological theory of damping in ferromagnetic materials. *IEEE Trans. Magn.* **40***,* 9464, 2004.

[19] J. D. Jackson. *Classical Electrodynamics*. New York, Wiley, 1999.

[20] A. J. Newel. A generalization of the demagnetizating tensor for nonuniform magnetization. *J. Geograph. Phys.* **98***,* 9551, 1993.

[21] S. Zhang and Z. Li. Roles of nonequilibrium conduction electrons on the magnetization dynamics of ferromagnets. *Phys. Rev. Lett.* **93***,* 127204, 2004.

[22] L. Berger. Emission of spin waves by a magnetic multilayer traversed by a current. *Phys. Rev. B* **54**, 9353, 1996.

[23] M. J. Donahue and R. D. McMichael. *Exchange energy representations in computational micromagnetics.* National Institute of Standards and Technology, 2002.

[24] M. Bolte. *Analysis and conceptual developement of highly dimensional algorithms for performance optimization with regard to complex dynamics processes*. Diploma thesis, Universität Hamburg, 2004.

[25] *OOMMF User's Guide.* National Institute of Standards and Technology, 2002.

[26] W. H. Press. *Numerical Recipes: The Art of Scientific Computing*. Cambridge University Press, New York, 1992.

[27] A. Wachowiak, J. Wiebe, M. Bode, O. Pietsch, M. Morgenstern, and R. Wiesendanger. Direct observation of internal spin structure of magnetic vortex cores. *Science* **298***,* 557, 2002.

[28] K. Y. Guslienko, Y. Novosad, Y. Otani, H. Shima, and K. Fukamichi. Field-evolution of magnetic vortex state in ferromagnetic disks. *Appl. Phys. Lett.* **78***,* 3848, 2001.

[29] K. Shigeto, T. Okuno, K. Mibu, T. Shinjo, and T. Ono. Magnetic force microscopy observation of antivortex core with perpendicular magnetization in patterned thin film of permalloy. *Appl. Phys. Lett.* **80***,* 4190, 2002.

[30] M. Bolte, G. Meier, B. Krüger, A. Drews, R. Eiselt, L. Bocklage, S. Bohlens, T. Tyliszczak, A. Vansteenkiste, B. Van Waeyenberge, K. Wei Chou, A. Puzic, and H. Stoll. Time-resolved x-ray microscopy of spin-torque-induced magnetic vortex gyration. *Phys. Rev. Lett.* **100***,* 176601, 2008.

[31] M. Bolte, T. Kamionka, and B. Güde, private commmunication.

[32] A. Drews, B. Krüger, M. Bolte, and G. Meier. Current- and field-driven magnetic antivortices. *Phys. Rev. B* **77**, 094413, 2008.

[33] A. Aharoni. Magnetostatics of curling in a finite cylinder. *J. Appl. Phys.* **68**, 2892, 1990.

[34] N. A. Usov and S. E. Peschany. Magnetization curling in a fine cylindrical particle. *J. Magn. Magn. Mat.* **118**, 290, 1992.

[35] K. Y. Guslienko, Y. Novosad, Y. Otani, H. Shima, and K. Fukamichi. Stability of magnetic vortex in soft magnetic nano-sized circular cylinder. *J. Magn. Magn. Mat.* **242-245**, 1015, 2002.

[36] A. A. Thiele. Steady-state motion of magnetic domains. *Phys. Rev. Lett.* **30**, 230, 1973.

[37] A. Thiaville, Y. Nakatani, J. Miltat, and Y. Suzuki. Micromagnetic understanding of current-driven domain wall motion in patterned nanowires. *Europhys. Lett.* **69**, 990, 2005.

[38] B. Krüger, A. Drews, M. Bolte, U. Merkt, D. Pfannkuche, and G. Meier. Harmonic oscillator model for current- and field-driven magnetic vortices. *Phys. Rev. B* **76**, 224426, 2007.

[39] B. Krüger, A. Drews, M. Bolte, U. Merkt, D. Pfannkuche, and G. Meier. Vortices and antivortices as harmonic oscillators. *J. Appl. Phys.* **103**, 07A501, 2008.

[40] M. Curcic, B. Van Waeyenberge, A. Vansteenkiste, M. Weigand, V. Sackmann, H. Stoll, M. Fähnle, T. Tyliszczak, G. Woltersdorf, C. H. Back, and G. Schütz. Polarization selective magnetic vortex dynamics and core reversal in rotating magnetic fields. *Phys. Rev. Lett.* **101**, 197204, 2008.

[41] K.-S. Lee and S.-K. Kim. Two circular-rotational eigenmodes and their giant resonance asymmetry in vortex gyroscopic motion in soft magnetic nanodots. *Phys. Rev. B* **78**, 014405, 2008.

[42] V. Novosad, F. Y. Fradin, P. E. Roy, K. S. Buchanan, K. Yu Guslienko, and S. D. Bader. Magnetic vortex resonance in patterned ferromagnetic dots. *Phys. Rev. B.* **72**, 024455, 2005.

[43] S.-K. Kim, K.-S. Lee, Y.-S. Yu, and Y.-S. Choi. Reliable low-power control of ultrafast vortex-core switching with the selectivity in an array of vortex states by in-plane circular-rotational magnetic fields and spin-polarized currents. *Appl. Phys. Lett.* **92**, 022509, 2008.

[44] K. S. Buchanan, M. Grimsditch, F. Y. Fradin, S. D. Bader, and V. Novosad. Driven dynamics mode splitting of the magnetic vortex translational resonance. *Phys. Rev. Lett.* **99**, 267201, 2007.

[45] K.-S. Lee and S.-K. Kim. Gyrotropic linear and nonlinear motion of a magnetic vortex in soft magnetic nanodots. *Appl. Phys. Lett.* **91**, 132511, 2007.

[46] H. Stoll, private communication.

[47] K.-S. Lee, K. Y. Guslienko, J.-Y. Lee, and S.-K. Kim. Ultrafast vortex-core reversal dynamics in ferromagnetic nanodots. *Phys. Rev. B* **76**, 174410, 2007.

[48] R. Hertel, S. Gliga, M. Fähnle, and C. M. Schneider. Ultrafast nanomagnetic toggle switching. *Phys. Rev. Lett.* **98**, 117201, 2007.

[49] B. Van Waeyenberge, A. Puzic, H. Stoll, K. W. Chou, T. Tyliszczak, R. Hertel, M. Fähnle, H. Brückl, K. Rott, G. Reiss, I. Neudecker, D. Weiss, C. H. Back, and G. Schütz. Magnetic vortex core reversal by excitation with short bursts of an alternating field. *Nature* **444**, 7118, 2006.

[50] K. Guslienko, K.-S. Lee, and S.-K. Kim. Dynamic Origin of Vortex Core Switching in Soft Magnetic Nanodots. *Phys. Rev. Lett.* **100**, 27203, 2008.

[51] O. A. Tretiakov and O. Tchernyshyov. Vortices in thin ferromagnetic films and the skyrmion number. *Phys. Rev. B* **75**, 012408, 2007.

[52] A. Thiaville, J. M. Garcia, R. Dittrich, J. Miltat, and T. Schrefl. Micromagnetic study of Bloch-point mediated vortex core reversal. *Phys. Rev. B* **67**, 094410, 2003.

[53] R. Hertel and C. M. Schneider. Exchange explosions: Magnetization dynamics during vortex-antivortex annihilation. *Phys. Rev. Lett.* **97**, 177202, 2006.

[54] K. Yamada, S. Kasai, Y. Nakatani, K. Kobayashi, H. Kohno, A. Thiaville, and T. Ono. Electrical switching of the vortex core in a magnetic disk. *Nat. Mater.* **6**, 269, 2007.

[55] S.-K. Kim, Y.-S. Choi, K.-S. Lee, K. Y. Guslienko, and D. E. Jeong. Electrical-current-driven vortex-core reversal in soft magnetic nanodots. *Appl. Phys. Lett.* **91**, 082506, 2007.

[56] K. Mukasa, M. Sawamura, K. Sueoka, E. Hirota, R. Nakane, and M. Nakamura. United States Patent US 6,757,192 B2. 2004.

[57] T. Min, Y. Guo, and P. Wang. United States Patent US 7,072,208 B2. 2006.

[58] Y. Liu, S. Gliga, R. Hertel, and C. M. Schneider. Current-induced magnetic vortex core switching in a permalloy nanodisk. *Appl. Phys. Lett.* **91**, 112501, 2007.

[59] T. Kimura, Y. Otani, and J. Hamrle. Determination of magnetic vortex chirality using lateral spin-valve geometry. *Appl. Phys. Lett.***187***,* 172506, 2005.

[60] S. Kasai, K. Nakano, K. Kondou, N. Oshima, K. Kobayashi, and T. Ono. Three-terminal device based on the current-induced magnetic vortex dynamics with the magnetic tunnel junctions. *Appl. Phys. Expr.* **1***,* 091302, 2008.

[61] S. Bohlens, B. Krüger, A. Drews, M. Bolte, G. Meier, U. Merkt, and D. Pfannkuche. Current controlled random-access memory based on magnetic vortex handedness. *Appl. Phys. Lett.* **93***,* 142508, 2008.

[62] A. Drews, B. Krüger, G. Meier, S. Bohlens, L. Bocklage, T. Matsuyama, and M. Bolte. Current- and field-driven magnetic antivortices for nonvolatile data storage. *Appl. Phys. Lett.* **94***,* 062504, 2009.

8 Acknowledgments

Many people have contributed to this thesis. Especially I want to thank

- PD Dr. Guido Meier for reviewing this thesis, for the excellent supervision, for supporting my work, for valuable discussions, and for his great enthusiasm for physics which he carries to me and all his students.
- Prof. Dr. Dietmar Möller for reviewing this thesis, for the support, and genial conversations.
- Prof. Dr. Ulrich Merkt for enabling me to work on this interesting topic, the excellent supervision, the accurate reading of all my manuscripts, for supporting my work, for many valuable discussions, and his support for preparing this thesis.
- Dr. Markus Bolte for our cooperation, for his support, for interesting discussions, for the introduction into micromagnetism and micromagnetic simulations, for his enthusiasm.
- Benjamin Krüger for our cooperation, for his support, for his deep understanding of physics and his patience in explaining, for valuable discussions, for reading this thesis. I am still waiting for the Krüger functions or the Krüger theory ;-).
- Stellan Bohlens for our cooperation and interesting discussions concerning vortex dynamics and Oersted field calculations.
- Bernd Güde for the hints of presenting my results, his cooperativeness, and discussions about noval storage devices.
- Massoud Najafi for his cooperativeness and discussions about software engineering.
- Gunnar Selke for discussions about software engineering.
- Thomas Kamionka and Michael Martens for discussions about vortex dynamics and COMSOL simulations.
- Lars Bocklage, Dr. Toru Matsuyama, Jeannette Wulfhorst, Gesche Nahrwold, Peter Lendecke, Jan Jacob, Dr. Jan Scholtyssek, Judith Moser, and the whole group N for interesting discussions and the genial working atmosphere.
- Prof. Dr. Daniela Pfannkuche and the whole group KM for interesting discussions.

- the Deutsche Forschungsgesellschaft for the financal support via Graduiertenkolleg 1286 "Functional metal/semi-conductor hybrid systems".
- my parents and Jenny for their support.